INVESTIGATION INTO CHAR STRUCTURE USING RAMAN AND PETROGRAPHIC TECHNIQUES TO ASSESS COMBUSTION REACTIVITY

Name: Vongani Chabalala

MSc. (Chemistry)

University of the Witwatersrand, Johannesburg

Supervisors: Prof. Nicola Wagner (School of Chemical and Metallurgical Engineering)

Prof. Sanja Potgieter-Vermaak (School of Chemistry)

DECLARATION

This dissertation is submitted in fulfilment of the requirements for the degree of the Masters of Science (Chemistry) at the School of Chemistry of the University of the Witwatersrand.

I, Vongani Chabalala, hereby declare that the dissertation with the title: INVESTIGATION INTO CHAR STRUCTURE USING RAMAN AND PETROGRAPHIC TECHNIQUES TO ASSESS COMBUSTION REACTIVITY is my own work and has not been submitted at any other university.

Signed at Johannesburg on the day of …….. July 2010

……

V. Chabalala

ACKNOWLEDGEMENTS

The author wishes to acknowledge and deeply express his appreciation to the following people for their role during the course of the research project:

(1) Professor Nicola Wagner and Professor Sanja Potgieter-Vermaak for their guidance, encouragements and invaluable assistance throughout the research project.
(2) Every member from Coal and Carbon Research Group from University of the Witwatersrand for their support during the time of need and for their friendship they showed me during the course of the project.
(3) Coal and Carbon Research Group (Northwest University (Potchefstroom)) for helping with char preparations.
(4) My family, especially my parents, Samuel Chabalala and Phephu Chabalala, for the continuous encouragements, support, patience and support they have given me throughout my studies.
(5) Eskom (TESP program) for providing financial support for this project.
(6) All my friends for the moral support they showed during the course of my studies.

ABSTRACT

Coal petrography, micro Raman spectroscopy (MRS) and thermogravimetric analysis (TGA) were employed to obtain further inside into the evolution of char structure and its reactivity during heat treatment in the temperature range of 300-1400°C on inertinite-rich South African coals. The lack of publications particularly on South African coals, relating Raman spectroscopy to coal petrography and thermogravimetric analyses when investigating the evolution of char structure was a motivation for the study. A laboratory scale Packed Bed Balance Reactor (PBBR) was used to prepare coal char samples at various temperatures; that is 300, 600, 800 and 1000 °C. A drop tube furnace (DTF) was used to prepare chars at 1400°C. Raman spectra of coal and chars were measured on the first-order in the range 800-2000cm^{-1}. Characteristic bonds for amorphous carbons, G band (graphitic) and D band (disorder), were deconvoluted and curve fitted using the OPUS software. Three bands for coal particles were determined; that is the G band at ~1590-1603cm^{-1}, D1 band at ~1343-1355cm^{-1} and D3 band at ~1507-1557cm^{-1}. Four bands were determined for char particles; that is the G band at ~1590-1603cm^{-1}, D1 band at ~1343-1355cm^{-1}, D3 band at ~1507-1557cm^{-1} and D4 band at ~1200-1232cm^{-1}. All the bands were fitted with a mixture of Lorentzian and Gaussian functions except the D3 band for which only a Gaussian function was used. It was found that sp2-sp3 bonding (reactive sites/crystallites) occurred in dense chars (originating from inertinite particles) at the initial heat treatment temperature, and these sp2-sp3 bondings are known to be consumed later at high temperature. Earlier consumption of sp2-sp3 bonding was observed in porous chars, since they were vitrinitic in origin and contained more reactive sites. The D1 and G bandwidths showed a significant change with heat treatment, which was consistent with structural modification due to high temperatures. Reflectance measurements, that is: mean vitrinite reflectance (MVR) and mean total reflectance (MTR), showed an increase with heat treatment temperature. MVR and MTR were successfully correlated with Raman parameters (D1 and G bandwidth). MVR and MTR also showed a good correlation with combustion reactivity measured by TGA. Char morphology analyses were carried out petrographically by point counting for quantification and qualification purposes. The char morphology data showed a significant

increase in the amount of dense/solid chars as compared to the porous chars with an increase in temperature which is in-line with expectations from the inertinite-rich parent coal. Correlations between the D1 and G bandwidths and char morphology counts were carried out. An inverse of D1 and G bandwidth showed good correlation with the proportion of dense/solid and porous char. It was concluded from this study that the best correlations between Raman spectroscopy and coal petrography was through reflectance measurements, and the identified Raman D1 and G bandwidths. A good linear correlation was also found between Raman D1 and G bandwidths and combustion reactivity. These correlations confirm the strong connection between char structure and its reactivity and illustrate the advantage of Raman spectroscopy in conjunction with coal petrography with respect to other structural analyses. Therefore, the use of MRS and petrography on coal chars enhances the understanding of char structural evolution on a molecular level and may lead to enhanced understanding of pulverised fuel (pf) coal combustion.

TABLE OF CONTENTS PAGE

ABBREVIATIONS

Δ weight %	Change in weight percent
DTF	Drop Tube Furnace
FMR	Full Maceral Reflectance
FWHM	Full width at half maximum
Gt	Giga tones
%	Percentage
% vol	Percentage Volume
HTT	Heat treatment temperature
I_D	Intensity of the D band
I_G	Intensity of the G band
MRS	micro Raman Spectroscopy
Mt	Million tones
MVR	% Mean Vitrinite Reflectance
MTR	Mean total maceral reflectance
MW	Megawatts
mW	Milliwatts
m_{ASH}	Weight of the ash in the sample
m_o	Sample weight on a dry basis at initial (at time t=0 seconds/minutes)
m_t	Sample weight on a dry basis at time t
PBBR	Packed Bed Balance Reactor
$1/T_{20\%}$	Measure of reactivity at 20% conversion
$1/T_{50\%}$	Measure of reactivity at 50% conversion
RMS	Root mean square
RoV	Vitrinite Reflectance measurement
RoC	Coal maceral reflectance
Rr%	Reflectance in percentage
Stdev	Standard deviation
XRD	X-ray Diffraction
TGA	Thermogravimetric analysis

X Conversion

LIST OF FIGURES

LIST OF TABLES

LIST OF PUBLICATIONS (Conference proceedings)

Chabalala, V.P., Wagner, N., Potgieter-Vermaak, S., 2009. Investigation into the evolution of char structure using Raman spectroscopy in conjunction with coal petrography. Presented at the Fossil Fuel Foundation Annual Indaba, Johannesburg, South Africa, 11-12 March 2009.

Chabalala, V.P., Wagner, N., Potgieter-Vermaak, S., 2009. Investigation into the evolution of char structure using Raman spectroscopy in conjunction with coal petrography. Presented at the International Conference of Coal Science and Technology (ICCS&T), Cape Town, South Africa, 26-29 October 2009.

CHAPTER 1

1.1 Introduction

Coal dominates as South Africa's primary energy source and presently it provides about 79% of our country's primary energy needs. South Africa is known to be the world's sixth largest producer of coal, mining around 220 million tones per annum over a third of which is exported (DME, 2004). Because coal is abundant, and is the primary fossil fuel, it will continue to play an increasingly important role to meet the increasing demands for different forms of energy (electricity and liquid fuels). In the domestic market in South Africa coal is used in electricity generation (110Mt), petrochemical coal-to-liquids industry (41Mt), general industries (8Mt), the metallurgical industry (7Mt), and for domestic use (7Mt) (Falcon and Van der Riet, 2007). South Africa has approximately 75% of Africa's coal resources and consists of nineteen coalfields of which nine are currently producing (Wagner and Hlatswayo, 2005). Over 95% of South African coal reserves are bituminous, with about 2% being anthracite (Kershaw and Taylor, 1992). South African coals contain considerable amounts (up to 60%) of low reflecting inertinite, called 'reactive semifusinite' (Snyman and Botha, 1993; Hagelskamp and Snyman, 1988). South African Permian coals typically have minor liptinite content (less than 7% by volume) and high mineral matter content (up to 30%), in comparison to Northern Hemisphere Carboniferous coals (Kruszewska, 2003; Cairncross, 2001; Walker, 2000; Snyman and Botha, 1993).

Coal in South Africa is primarily used in combustion and gasification processes. For a better understanding of these processes, it is necessary to study coal structure and its derivatives (char and coke); because the structure of coal can have an influence on its performance in coal conversion processes (combustion and gasification). An understanding of coal and char structure can assist with predicting and controlling these processes. In this chapter, the need for the investigation into the evolution of char structure and its reactivity during combustion is motivated.

1.2 Background and motivation

Since the 1950's, South African coals were mined and then beneficiated. The high value products are used in the production of high-value export grade blend-coking coals and high grade steam coal. The lower grade coals are used as feedstocks in combustion and gasification plants. This has resulted in a reduction of good quality coal available to the inland market, and local consumers are obliged to use lower-grade high-ash coal, either in the form of middlings arising from beneficiation or lower quality run of mine seams. Southern African coals are characteristically rich in minerals, relatively difficult to beneficiate, and variable in rank (maturity) with high inertinite contents and hence low combustion efficiency when compared to world coals (Falcon and Ham, 1988). This presents a challenge to the coal-based industries (power and liquid fuels) as run of mine quality of the coal reserves continue to decrease in the South African region. In parallel, the increasing environmental constraints being imposed on users of coal provides further challenges to coal conversion. These factors have led to challenges being experienced by local coal users; coals of different type and grade to that which the boiler or gasifier plant was originally designed are introduced into the process. Under such conditions poor combustion or gasification performance often results. This is manifested at times by poor ignition, irregular flames and flameouts, delayed heat transfer, high carbon carry-overs, overall inefficient combustion and ash deposits of various types (Falcon and Ham, 1988; Lee and Lau, 1985).

The greatest utilization of coal lies with coal combustion for power generation. Coals for combustion are assessed for ignition and burnout characteristics. The combustion behaviour depends on the characteristics of the coal and also on the operating conditions of the boiler (temperature, heating rate, oxygen concentration, etc.) (Alonso *et al*. 2001b). There are two distinct stages in the combustion of pulverised fuel (Pyatenko *et al*. 1992; Bailey, 1989; Bend *et al*. 1989; Sadakata *et al*. 1989; Tsai and Scaroni, 1987; Gromulski and Sieurin, 1983). The first stage is pyrolysis, which is the rapid release of volatiles and their combustion. The second stage is char combustion. The performance of a particular

coal in a furnace therefore depends on how it reacts in the stages of pyrolysis and char combustion (Cloke and Lester, 1994).

In order to reduce problems encountered in coal utilization, various tests and analyses are conducted on coals and their resulted chars. These include: proximate analysis, ultimate analysis, coal petrography, mineral analysis, calorific value, swelling index, physical tests, thermogravimetric analyses tests, and drop tube furnace tests (DTF). There are many results reported in literature on the characterization of South African coals and their resulted chars using some of these tests (Falcon and Ham, 1988; Falcon, 1986; Falcon and Snyman, 1986). The structure of coal and char can be characterised with the help of advanced techniques including X-ray diffraction (XRD), high-resolution transmission electron microscopy (HRTEM), and Raman spectroscopy. Raman spectroscopy is a powerful technique, because it is sensitive not only to the crystalline structure but also to the molecular and amorphous structures of samples. It has been widely employed to characterise almost all carbonaceous materials (Yoshiba *et al*. 2006; Quirico *et al*. 2005; Sadezky *et al*. 2005; Beyssac *et al*. 2003; Zerda *et al*. 2000; Ferrari and Robertson, 2000; Cuesta *et al*. 1998; Jawhari *et al*. 1995; Cuesta *et al*. 1994; Green *et al*. 1983; Rouzaud *et al*. 1983; Tuinstra and Koenig, 1970). More recently, it has also been applied to analyse coal char structure, which was further correlated with char reactivity (Li *et al*. 2006; Sekine *et al*. 2006; Zaida *et al*. 2006; Sekine *et al*. 2005; Bar-ziv *et al*. 2000; Livneh *et al*. 2000; Doorn *et al*. 1990), also discussed in a recent review article (Potgieter-Vermaak *et al*. 2010). Raman spectroscopic analysis can provide insight into char structure, the effect of heat treatment on the structure evolution, and consequently on char reactivity. There are a limited number of publications in the literature relating Raman spectroscopy to coal petrography and thermogravimetric analyses when investigating the evolution of char structure, and none on South African coals. Amongst them, none of these publications was found relating Raman spectroscopy directly to coal petrography and thermogravimetric analyses. The need for a detailed investigation into the evolution of char structure and its reactivity was considered important and was chosen as the subject for this research. The purpose of the research was to consider char structure formation and its reactivity during coal conversion via

Raman spectroscopy and coal petrography. A pulverised Witbank coal sample was pyrolysed under various treatment temperatures (300-1000°C) to generate char samples, which were examined using Raman spectroscopy, petrography and thermogravimetric analyses. The study aims to improve the knowledge and understanding of combustion properties, and may assist in predicting combustion performance of coal, thus aiding in the design and maintenance of combustion boilers, and may help to maximise burning efficiency and assist in reducing carbon particle emission from coal utilities.

1.3 Research questions

A number of authors (Senneca *et al*. 2004, Feng *et al*. 2002, Sharma *et al*. 2001, Shim *et al*. 2000, Russell *et al*. 1999) propose that the understanding of char structural change during heat treatment is essential for theoretical description of char reactivity evolution during coal combustion and gasification. Hence, the following research questions were derived:

(a) Would the use of Raman spectroscopy in conjunction with petrography enable a better understanding of the behaviour of char during combustion?
(b) Would the combination of petrography and Raman spectroscopy assist in solving problems associated with coal utilization including suitability for combustion, gasification and liquefaction?

And since Sheng (2007) showed good correlation between combustion reactivity (TGA) and Raman spectroscopy (Raman ratios):

(c) Would TGA results (to assess the combustion reactivity) correlate with ratio's of the obtained Raman bands, and would there be any correlation with the petrographic results?

1.4 Aims of the investigation

The aims of the research project are as follows:

(a) To investigate the evolution of char structure and char reactivity using Raman spectroscopy in conjunction with coal petrography and thermo-gravimetric analysis (TGA) of pulverised coal samples.

(b) To gain an understanding of char structure formation at a molecular level to enhance understanding of coal combustion.

1.5 Objectives of the investigation

(a) Parent coal will be characterised using different techniques, namely: proximate analysis, coal petrography, X-ray diffraction, micro Raman spectroscopy, and thermogravimetric analysis.

(b) Then coal will be charred to different temperatures (300ºC-1000ºC), and the resultant chars will be analysed using the same techniques outlined above (1.5 (a)).

(c) An additional set of char samples produced at 1400ºC will be obtained to get an indication of the behaviour of coal at this temperature.

1.6 Hypothesis

The hypotheses to be addressed during the course of the research investigation are:

(a) Petrographic analysis (char morphology and reflectance) can be correlated with Raman bands or ratio's of Raman bands.

(b) Char reactivity (determined by thermo gravimetric analysis) can be correlated with Raman bands or ratio's of Raman bands.

1.7 Scope of the dissertation

The dissertation is summarised as follows:

Chapter 1: Introduction which has four sections, i.e. background and motivation, research questions, aims and objectives of the investigation and scope of the dissertation.

Chapter 2: Literature review.

Chapter 3: Experimental methodology followed during the investigation.

Chapter 4: Results and discussion.

Chapter 5: Conclusion and recommendations.

CHAPTER 2

Literature review

In this chapter, a literature review concerning the detailed characterisation of coal and chars using different techniques such as coal petrography, Raman spectroscopy, powder X-ray diffraction (PXRD) and thermogravimetric analysis is provided. Section 2.1 gives a general introduction to South African Witbank coals; Section 2.2 describes the petrographic properties of coal; Section 2.3 describes coal conversion; Section 2.4 describes the facilities used to prepare chars (for example DTF and PBBR); PXRD is discussed in Section 2.5; Section 2.6 discusses the Raman spectroscopy; TGA is discussed in Section 2.7; and the chapter is concluded by a brief summary of different techniques used to characterise coal and char (Section 2.8).

2.1 General introduction to South African Witbank coals.

The South Africa Witbank Basin contains approximately 16.2Gt of *in situ* coal (Snyman and Botha, 1993) out of the 60Gt found in the Permian Karoo Basin of South Africa (Cadle *et al*. 1993; Smith and Whittaker, 1986). Most of the Witbank coal occurs as part of the Vryheid Formation (Cairncross *et al*. 1988). The Vryheid formation is in the cratonic Witbank Basin and was deposited on a glacially incised topography forming part of the Permian Ecca Group, resting either directly on pre-Karoo strata or on Permo-Carboniferous Dwyka glacial sediments (Cairncross and Cadle, 1988). South African Permian coals from the Witbank Basin frequently have high a inertinite content (Boshoff *et al*. 1991), as illustrated in Table 2.1. Inertinite formation is thought to be the product of fungal activity, cold climatic conditions and atmospheric exposure of peat resulting in oxidation (Cadle *et al*. 1993; Snyman and Botha, 1993). The Witbank coals also have minor liptinite content (less than 7% by volume) and high mineral matter content (up to 30% by volume) (Kruszewska, 2003; Cairncross, 2001; Walker, 2000; Snyman and Botha, 1993).

Table 2.1: The calculated average ash-free maceral composition of 34 mines samples from the Witbank Coalfield; data calculated from Boshoff *et al*. (1991)

Maceral group	Average Witbank coal (% by volume)
Vitrinite	27.9 ± 12.2
Liptinite	4.2 ± 1.2
Inertinite	67.9 ± 12.3

When comparing the Witbank coalfield to some of the other South African coalfields such as the Highveld and Waterberg coalfields, it is found that the inertinite contents are comparable (approximately 60-80%) (Wagner and Hlatshwayo, 2005). Vitrinite is the dominant maceral (up to 90% by volume) in the upper zone of the Waterberg coals, decreasing with depth of formation, with 60% inertinite at the base of the formation (Faure *et al*. 1996).

2.2 Properties of coal

2.2.1 Coal petrography

Coal petrography is the study of the microscopic organic and inorganic constituents in coal and the degree of metamorphosis (or rank). It has become a major tool in evaluation and assessment procedures and is often an integral part of the testing during the exploration, mining, beneficiation, marketing and utilization phases in the coal industry (Berry, 1981; Zimmerman, 1979; Steyn and Smith, 1977; Smith, 1972a, 1972b; Brown *et al*. 1971; Taylor *et al*. 1967; Schapiro and Gray, 1964; Francis, 1961). Microscopically, coal is composed of a number of discrete organic constituents termed macerals, which are analogous to their inorganic counterparts, minerals. There are three main maceral groups, namely: vitrinite, liptinite and inertinite. It might be expected that the inertinite would be less reactive during combustion than the other fractions. However, although this may be true for a single coal, not all inertinites are inert and not all vitrinites are reactive. For a maceral to be classed as reactive, it must exhibit thermoplasticity during pyrolysis and char formation; hence if ‘inerts’ are to be considered as reactive, some degree of structural alteration must be shown to have occurred. Low-reflecting inertinite (termed

reactive semi-fusinite) is the most likely sub-maceral in which plasticity would be observed during combustion (Thomas *et al*. 1991), although medium-reflecting inertinite can also undergo the same degree of plastic deformation. When determining the proportions of macerals in a coal, a point count system is used and a volume % maceral composition is obtained.

Reflectance is one of the most important analyses in coal petrography, and it can be performed on vitrinite particles or on total macerals. The reflectance is a measure of the state of coalification based on a scale correlating from brown coal to anthracite; this progression shows an increase in value with carbon content (Berkowitz, 1985). The maceral vitrinite (specifically telovitrinite) is selected as a reference material as its reflectance increases uniformly with the coalification process. The mean vitrinite reflectance (MVR) value is a very reliable parameter because it is independent of the vitrinite content and the grade of the coal, but dependent on the carbon/hydrogen and carbon/oxygen ratios and the volatile matter, and is commonly used as a rank indicator (Cloke and Lester, 1994). A total maceral reflectance/mean total reflectance (MTR) can also be measured on coal samples with readings taken on all organic components: liptinite, vitrinite and inertinite (Tang *et al*. 2005a, 2005b; O'Brien *et al*. 2003; Benfell, 2001). It has been suggested by Tang *et al*. (2005a); Cloke and Lester (1994) that the MVR value can be an accurate parameter for predicting combustion behaviour. Tang *et al*. (2005a, 2005b) and O'Brien *et al*. (2003) proposed a full maceral reflectance (FMR) parameter defined as the summation of each reflectance value multiplied by its frequency derived from the full reflectogram, thus incorporating both rank and maceral composition. FMR has more advantages over MVR, because it provides the information for whole coal, instead of just vitrinite information (Tang *et al*. 2005b).

The reflectance and type of macerals present in the parent coal have an effect on char properties. Thus the reflectance has an effect on the combustion and gasification reactivity (Mendez *et al*. 2003; Alonso *et al*. 2001a; Rosenberg *et al*. 1996a, 1996b; Hurt *et al*. 1995; Cloke and Lester, 1994; Crelling *et al*. 1992; Bailey *et al*. 1990; Oka *et al*. 1987; Jones *et al*. 1985a, 1985b).

Petrographic analyses, including maceral, microlithotype, mineral groups, and rank by vitrinite reflectance, allow for the characterisation and classification of coal in terms of type, grade and rank for the determination of technical behaviour and utilisation potentials of the materials. Petrography plays an important role in determining char morphology, because an understanding of the type of macerals present in the coal can enable the prediction of the type of char morphology from that particular coal. Most workers (Bengtsson, 1987; Skorupska, 1987; Jones *et al*. 1985a, 1985b; Nandi *et al*. 1977) have concentrated upon the influence of petrographic composition in determining specific char morphology. Investigations into the relative behaviour of vitrinite and inertinite macerals of a specific rank range has led some workers to conclude that specific char morphologies were generated from specific macerals (for examples cenosphere from vitrinite, honeycomb structures or dense particles from inertinite-rich particles) during pyrolysis or combustion (Skoruspka *et al*. 1987; Jones *et al*. 1985a, 1985b; Nandi *et al*. 1977).

2.3 Coal conversion

2.3.1 Coal combustion and char formation.

The greatest utilization of coal lies with coal combustion. Coals are assessed for ignition and burnout characteristics when determining suitability for combustion. Coal combustion involves the generation of thermal energy as a result of oxidation of the combustible constituents of coal in the presence of heat. The process is a series of reactions in which oxidation and heat generation lead to devolatilization of the organic matter. Combustion behaviour depends on the characteristics of the parent coal and also on the operating conditions of the boiler or furnace (temperature, heating rate, oxygen concentration, etc.) (Alonso *et al*. 2001a). There are two distinct stages in the combustion of pulverised fuel as identified by most workers (Bend *et al*. 1989; Sadakata *et al*. 1989). The first stage is pyrolysis; that is rapid release of volatiles and their combustion (Pyatenko *et al*. 1992; Bailey, 1989; Tsai and Scaroni, 1987; Gromulski and Sieurin,

1983). The second stage is char combustion. During the pyrolitic stage, tar and gases escape, leaving solid carbon-rich residues known as char which is then oxidised and consumed until, at elevated temperatures, no organic residues remain at all (Falcon and Ham, 1988). The performance of a particular coal in a furnace therefore depends on how it reacts in the stages of pyrolysis and char combustion (Cloke and Lester, 1994). Much research has been carried out into the link between maceral types and combustion behaviour (Cloke and Lester, 1994), and the overall conclusion from the literature is that the combustion behaviour of a coal is not always related to the basic maceral composition as the behaviour of vitrinite varies with its reflectance (generally referred to as 'rank') (Bengtsson, 1986; Jones *et al*. 1985b). The reflectance of inertinite is known to affect the combustion behaviour of the coal as well as that of the vitrinite (Diessel and Wolff-Fischer, 1987; Shibaoka, 1969). Jones *et al*. (1985a, 1985b) suggested that both rank and maceral composition contribute to the morphology of the char. Shibaoke *et al*. (1985) suggested that the morphology of chars generated from vitrinite during devolatilization mostly depends on the coal rank, and that some type of inertinites, which are usually considered to have poor combustibility, might have as good combustibility as vitrinites.

The evolution of char structure during coal pyrolysis mainly depends on coal petrography, rank of the coal and pyrolysis conditions (Tang *et al*. 2005a), and it also depends on the particle size and the temperature of the char formation (Bengtsson, 1987). Major components of coal char are fixed carbon and ash. Generally, in pulverised coal combustion/gasification technology, the existence of ash reduces the heating value and corrodes the internal surfaces in boilers or furnaces (Qui *et al*. 1999; Reifenstein *et al*. 1999).

2.3.2 Char morphology

The morphology of char is determined by changes occurring during pyrolysis, and the types of char present affect the overall combustion efficiency (Oka *et al*. 1987). Char morphology, that is shape, size, thickness and porosity, has significant effects on coal combustion (Tang *et al*. 2005a, 2005b). Subjective quantitative analysis of char products

has generally taken preference to actual objective quantification of their characteristics. Poor repeatability between laboratories world-wide is partly due to the common practice of using self-defined analysis techniques, which are tailored to suit the type of samples that are under analysis. Char analysis is essentially a non-standardised technique (Bailey *et al*. 1990; Shibaoka *et al*. 1989), where the operator creates a series of different char classes based on the characteristics of the sample that are considered to be most important.

Numerous research groups have attempted a microscopic description of different structural types of char particles (Bailey *et al*. 1990; Jones *et al*. 1985a, 1985b; Shibaoka *et al*. 1985; Lightman and Street, 1968). Lightman and Street (1968) was the first to investigate the morphology of pyrolyzed char from a drop tube furnace (DTF) with a Scanning Electron Microscope (SEM) and an optical microscope, and four types of char were distinguished. It is well known that the porosity of most vitrinite-derived char decreases with increasing rank, and most inertinite-derived chars are initially less porous than the vitrinite-derived char. However, the difference decreases with the increase of rank (Tang *et al*. 2005a, 2005b). The higher the temperature the more thick-walled are the char particles formed. Networks are present in chars from lower rank coals which are related to coal aromaticity, and increase with coal rank (Cloke and Lester, 1994). Bend *et al*. (1992) also examined vitrinite-rich coal of increasing rank and found that low rank coals generated multi-chambered and optical isotropic chars and that with increasing rank, hollow single-chambered optical anisotropic chars are formed. Some vitrinites are non-reactive, such as pseudo-vitrinite with a high reflectance (Cloke and Lester, 1994; Bengtsson, 1987). Thomas *et al*. (1993a, 1993b) and Rosenberg *et al*. (1996); report that the structure of char particles mainly depends on the individual maceral compositions of the parent coal particles. Bailey *et al*. (1990) correlated the formation of eleven different char types with coal microlithotypes and Bend *et al*. (1991) related content of vitrinite-rich microlithotypes with porosity of chars formed under different conditions. O'Brien *et al*. (2003) successfully correlated the full maceral reflectance parameter (FMR) with coal chemical properties (proximate and ultimate) while Tang *et al*. (2005b) correlated this parameter with porosity for coals with pure macerals only. Tang *et al*. (2005b) estimated char reactivity kinetics from a coal reflectogramme and thermogravimetric analyser

experimental results, and related the pre-exponential factor (Arrhenius equation) with FMR parameter with application to particularly chars derived from inertinite rich coals.

Figure 2.1 shows the microscopic representation of different types of char and their descriptions are given in Table 2.2 (Cloke and Lester, 1994). Whilst there may be several different descriptions for a specific char type, there is some degree of consistency between the literatures reported in Table 2.2. For the purpose of this project, the terminology as proposed by Falcon and Wagner (1995, 1994), Wagner (1998) and Bailey (1990) will be applied.

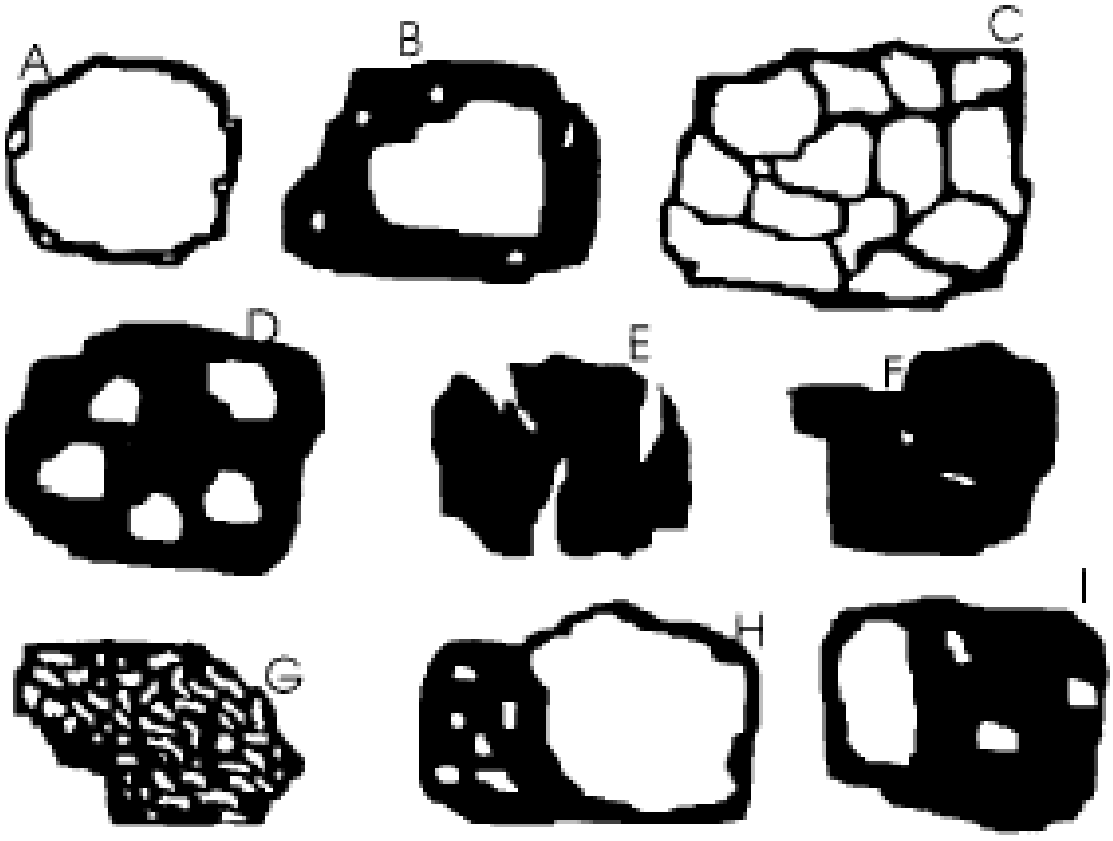

Figure 2.1: Diagrammatic representation of char types as discussed in Table 2.2 (Cloke and Lester, 1994)

Table 2.2: Char classification systems adapted from Cloke and Lester (1994) and expanded.

	A	**B**	**C**	**D**	**E**	**F**	**G**	**H**	**I**
Wagner (1998)	thin walled cenosphere	thick walled cenosphere	thin walled honeycomb	thick walled honeycomb	dense	dense/ solid	fusinoid	mixed (banded, granular)	-
Crelling (1992)	cenosphere	cenosphere	honeycomb	-	unfused char	unfused char	unfused char	-	-
Bailey (1990)	tenuisphere	crassisphere	tenuinetwork	mesosphere	inertoid	solid	fusinoid	mixed dense	mixed dense
Shibaoka (1989)	plastic	plastic	plastic	-	open solid	solid char	open solid	mixed	mixed
Phong-Anant (1989)	cenosphere	cenosphere	network honeycomb	solid	solid	solid	solid	solid	solid
Young (1987)	thin walled	thick walled	network	honeycomb	solid disrupted	unfused disrupted skeleton	unfused	solid	solid
Oka et al (1987)	thin walled balloon	thick walled balloon	network	-	unfused block	unfused	skeleton	-	-
Jones et al. (1985)	cenosphere	-	honeycomb	-	unfused	unfused	unfused	unfused	-
Lightman (1968)	thinwalled cenosphere	thickwalled ceneosphere	lacy cenosphere	solid	solid	solid	solid	solid	-

2.3.3 Char structure

Coal chars are composed of pseudo-graphitic building blocks (Walker and Mahajan, 1978). They contain nanometer crystalline domains (graphene layers) that grow due to heat treatment (Emmerich, 1995). In coal chars, particularly those prepared at low temperature, the carbon crystallites are small in size and poorly aligned because of cross linking. The edge site and various imperfections in the carbon structure (including single bonded "dangling" carbons) are thought to be the "active sites" during gas reactions. It was observed that annealing-induced structural rearrangement of graphene layers is induced by heat treatment (Emmerich, 1995), affecting the char reactivity and hence its lifetime in a reactor (Senneca *et al*. 2005, 1998; Salatino *et al*. 1999; Davis *et al*. 1995; Suuberg, 1990). Coal char is a highly disordered carbonaceous material that has a short-range order polycrystalline structure (Sharma *et al*. 2001; Shim *et al*. 2000; Davis *et al*. 1995). Hence the understanding of its structural change during heat treatment is essential for its (char) theoretical description of reactivity evolution during coal combustion and gasification, which has been the subject of many research efforts (Senneca *et al*. 2004; Feng *et al*. 2002; Sharma *et al*. 2001; Shim *et al*. 2000; Russell *et al*. 1999).

A frequently applied technique for following the changes in the structure of carbonaceous materials with heat treatment is by optical properties, one of the most useful of which is maximum reflectance. The increase in maximum reflectance for heat treatment temperatures up to about 1000°C for coal chars has been well established (Goodarzi, 1984; Murchison, 1978; Goodarzi and Murchison, 1972; de Vries *et al*. 1968; Ghosh, 1968; Chandra and Bond, 1956). It is attributed to increasing anisotropy resulting from changing mutual orientation of the aromatic layers (Rouzaud *et al*. 1983). It has been suggested (Rouzaud *et al*. 1983) that changes in optical properties are brought about by changing mutual orientation of the polyaromatic molecules.

Carbonaceous materials like coal and char structure are often characterised by maceral analysis or reflectance measurements which are often subjective in nature and do not distinguish atomic level differences of different carbon types. Recently, advanced

analytical tools such as the X-ray diffraction (XRD) or Raman spectroscopy are being developed to characterise carbon structure of different carbonaceous materials including coal, char and their high temperature derivatives. The former gives the crystalline structure and the latter gives the bonding structure. Therefore, by comparing the XRD and Raman analysis of an identical sample, a deeper insight of the coal and char carbon structure can be developed (Kawakami *et al*. 2006; Lu *et al*. 2001). Recently Sheng (2007) showed that the evolution of char structure under heat treatment can be characterised by Raman spectroscopy, in particular, band area ratios, where it was shown that the increase in heat treatment on the char had led to the increase of its structural order. Good correlations were also found between the combustion reactivity (determined by TGA) and the Raman ratios. The correlations were independent on the coal types and heat treatment conditions. In this investigation the main techniques applied will be petrography, PXRD, Raman spectroscopy and TGA.

2.3.4 Char reactivity

The major factors which control the reactivity of carbonaceous solids to O_2, CO_2, H_2O, and H_2 are known (Walker *et al*. 1959). They are: (1) concentration of active sites, (2) presence of inorganic impurities which could act as catalysts, and (3) diffusion limitations on how rapid the reactive gas can reach active sites. Char reactivity have been investigated by numerous researchers. The rank of the parent coal (Koba and Ida, 1980; Linares-Solano *et al*. 1979; Tomita *et al*. 1977; Hippo and Walker, 1975; Jenkins *et al*. 1973), the heat treatment temperature (Koba and Ida 1980; Hippo *et al*. 1979; Linares-Solano *et al*. 1979; Tomita *et al*. 1977; Hippo and Walker 1975; Jenkins *et al*. 1973), the heating rate (Radovic *et al*. 1983; Ashu *et al*. 1978), and the presence of inorganic impurities (Radovic *et al*. 1983; Hippo *et al*. 1979; Ashu *et al*. 1978; Soledade *et al*. 1978; Jenkins *et al*. 1973; Patrick and Shaw, 1972), have been found to affect char reactivity.

The results for pyrolysis of chars generated over 1000°C indicate that the higher the temperatures and heating rates, the lower the reactivity of the chars. This is attributed to the increased devolatilization rates, enhanced thermal annealing and decreased

concentration of active sites (Russell *et al*. 1999; Davis *et al*. 1995). Most of the studies have considered the influence of the characteristics of the parent coal (rank and maceral composition) in the structure and reactivity of chars (Cai *et al*. 1998; Thomas *et al*. 1993a, 1993b; Bend *et al*. 1992; Bailey *et al*. 1990). General trends of decreasing char reactivity with the increase of the rank of the parent coal have been obtained at both low and high temperatures, although some deviations of the general trend were also reported (Khan, 1987; Smith, 1978). The results are somewhat contradictory when dealing with inertinite-rich coal chars, which show generally lower intrinsic reactivity than the vitrinite-rich chars of similar rank in thermogravimetric experiences, but comparable to higher performances in industrial boilers or DTF experiments (Davini *et al*. 1996; Morgan *et al*. 1986).

Structural changes of char induced by heat treatment (Senneca *et al*. 1998; Davis *et al*. 1995; Radovic *et al*. 1983) are known to have an important role on its reactivity. In many studies, char reactivity is represented by the density of active sites on the internal surface, and this is often assumed to be constant during reaction. It has been assumed that the main effect of heat treatment is the reduction of the internal surface area at a constant reactive surface area fraction (Bhatia and Perlmutter, 1980; Gavalas, 1980; Lewis and Simons, 1979; Petersen, 1957). A significant change in the density of active sites during conversion is well documented (Radovic *et al*. 1983; Laurendeau, 1978). Several studies (Weiss and Bar-Ziv, 1993; Hurt *et al*. 1988) reported shrinkage of the highly porous char, which was also attributed to changes in the density of active sites. Kantorovich and Bar-Ziv (1998; 1994) modeled the reactivity of coal char and showed the mutual influence of reactivity and pore structure. They showed a monotonic increase of the intrinsic reaction rate during conversion, which is consistent with the increase in edge-to-basal-plane carbon atom ratio. Thermal conductivity was used as a mean to detect changes in pore structure, showing significant changes with reactivity (Zhang *et al*. 1998; Kantorovich and Bar-Ziv, 1997).

Snow *et al*. (1960) studied the influence of hydrogen content on the oxidation of carbon black and observed that the higher the hydrogen content, the higher the reactivity

(Jenkins *et al*. 1973; Snow *et al*. 1960). Further, they noted that the C/H ratio of the residue increased sharply with increasing burn-off of the sample, suggesting that the hydrogen was being preferentially oxidised relatively to carbon. Walker and co-workers (Linares-Solano *et al*. 1979; Hippo and Walker, 1975; Jenkins *et al*. 1973) have shown that the reactivity of coal char to air, CO_2, and steam is strongly dependent upon the rank of coal from which the char is produced and mineral matter composition. The differences in reactivity of coal chars are attributed to three factors. The low-rank chars have: (1) a higher concentration of active carbon sites, (2) better site utilization because of a greater concentration of feeder pores, and (3) impurities of higher specific catalytic activity than the higher-rank coal chars. Comparison of reactivity of low- and high-temperature chars shows that the low-temperature chars exhibit higher reactivity than either the parent coals or the high-temperature chars (Khan, 1987). The char reflectance measurements indicate that the low temperature chars are carbon-poorer than their high temperature counterparts, and contain high amounts of residual H and heteroatoms, which could be responsible for their higher intrinsic reactivity (Alonso *et al*. 2001a).

2.4 Drop Tube Furnace

The drop tube furnace (DTF) is a laboratory-scale test instrument that empirically simulates the combustion environment of a pulverised-fuel (p.f) boiler furnace. Good correlations have been reported between predicted and actual boiler combustion efficiencies based on the standard DTF char test at 3% oxygen (Van der Riet, 1995; Smoog, 1992). This instrument (DTF) allows for the identification of ignition and burnout characteristics of pulverised coal, by measuring the combustible matter content of a sample taken at a specific point. A DTF can be used to prepare pyrolysis chars, since it can reproduce the conditions experienced by coal in the initial stages of combustion (Lester and Cloke, 1999). Work has been published (Lester *et al*. 1995) which shows the similarity between the characteristics of chars produced in the DTF, with char samples from the same coal taken from the first port of a 1MW combustion test facility. With such a short residence time the pyrolysis stage should have produced an intermediate char that has begun to experience the first stage of combustion. One set of samples used in this

investigation was prepared in a DTF. Others char samples were prepared using a packed bed balanced reactor (PBBR).

2.5 Powder X-ray diffraction

Powder X-ray diffraction (PXRD) is one of the traditional methods of investigating carbons (Fischbach, 1971; Ergun, 1968; Ruland, 1968). The intensity of the diffracted X-rays is measured as a function of the diffraction angle 2θ and the orientation of the specimen. It allows the direct measurement of the inter-layer spacing and stack height, and some measurements of layer diameter. PXRD can provide average measurements from a relatively large sample, and can be used to follow the graphitization process (Marchand, 1986; Mering and Maire, 1960; Pinnick, 1952). It is a non-destructive and well established technique with good reproducibility. PXRD uses a relatively large amount of sample and collects most of the intensity scattered from the examined sample. Therefore the properties yielded represent an average for the sample rather than the local properties. This is very important to a material like coal, which is inherently heterogeneous.

PXRD is one of the techniques applied to determine the coal structure (Alvarez *et al*. 1998; Farrell *et al*. 1998; Iwashita and Inagaki, 1993; Lin and Guet, 1990; Radovic *et al*. 1983; Blayden *et al*. 1944) which yet to be fully understood due to its complexity and heterogeneity. The main feature of the PXRD pattern of coal is the appearance of the peak similar to that of graphite at the position (002), which is the peak at around 26.5° in 2θ; and a peak at the position (10), which is a peak at around 45° in 2θ (Lu *et al*. 2001, 2000). The coal contains a short-range graphite-like structure to a small degree and this is evident by the positions at the (002) and (10) bands that correspond to the position of graphite bands (Van Niekerk *et al*. 2008). A gamma band can be observed on the left-hand side of the (002) band and represent the aliphatic side chains that are attached to the crystalline carbon (aromatic carbon) (Lu *et al*. 2001, 2000). It is generally accepted that coals contain small regions of stacks of aligned aromatic ring structures (Hirsch, 1954) which approximate the structure of graphite. Size, perfection and concentration are different for different coals and change on heating (Schoening, 1983).

2.6 Raman spectroscopy

Raman spectroscopy is a well established technique for studying the vibration of the molecules in their electronic ground state and can provide information relating to the molecular structure of the samples. It is concerned with the change in frequency associated with the inelastic scattering of photons by lattice vibration phonons in solids and can be used as a lattice dynamic probe. Inelastic scattering means that the frequency of photons in monochromatic light changes upon interaction with a sample. Photons of the laser light are absorbed by the sample and then reemitted. Frequency of the reemitted photons is shifted up or down in comparison with original monochromatic frequency, which is called the Raman effect. The frequency shifts observed for the scattered light are due to the interaction of incident photons with vibrating molecules. Frequency shifts provide information about vibrational, rotational and other low frequency transitions in molecules. The frequency shifts depend on the molecular structure of the scattering media and can be regarded as unique fingerprints that can be used to characterise materials and to obtain information about local molecular orientation.

The Raman effect occurs when light impinges upon a molecule and interacts with the electron cloud and the bonds of that molecule. As the electromagnetic radiation wave interacts with the matter, the electron orbits within the constituent molecules are perturbed periodically with the same frequency (ν_0) as the electric field of the incident wave. The oscillation or perturbation of the electron cloud results in a periodic separation of charge within the molecules, which is called an induced dipole moment. For the spontaneous Raman effect, a photon excites the molecule from the ground state to a virtual energy state. The oscillating induced dipole moment is manifest as a source of electromagnetic radiation, thereby resulting in scattered light. When the molecule relaxes it emits a photon and returns to a different rotational or vibrational state. The difference in energy between the original state and this new state leads to a shift in the emitted photon's frequency away from the excitation wavelength.
If the final vibrational state of the molecule is more energetic than the initial state, then the emitted photon will be shifted to a lower frequency in order for the total energy of the

system to remain balanced. This shift in frequency is designated as a Stokes shift. If the final vibrational state is less energetic than the initial state, then the emitted photon will be shifted to a higher frequency, and this is designated as an Anti-Stokes shift. Raman scattering is an example of inelastic scattering because of the energy transfer between the photons and the molecules during their interaction.

A change in the molecular polarization potential or amount of deformation of the electron cloud with respect to the vibrational coordinate is required for a molecule to exhibit a Raman effect. The amount of the polarizability change will determine the Raman scattering intensity. The pattern of shifted frequencies is determined by the rotational and vibrational states of the sample.

The Raman spectra of coal were first published by Tuinstra and Koenig (1970) and Friedel and Karlson (1971) and reported the two broad bands in the regions 1575-1620cm^{-1} and 1355-1380cm^{-1}, called the G (graphitic) and D1 (disorder) bands. Tuinstra and Koenig (1970) suggested that the 1575cm^{-1} band could be assigned to the E_{2g} graphite mode with D^4_{6h} crystal symmetry, and the band at ~1370cm^{-1} to the A_{1g} mode forbidden in a hexagonal lattice and activated when symmetry rules are relaxed as a result of boundary discontinuities. Tuinstra and Koenig (1970) related the ratio I_{D1}/I_G to the average graphite domain dimension, La. Numerous papers have been published since the pioneering work of Tuinstra and Koenig (1970) on the deconvolution of the G and D bands and its consequent assignment, of which an elegant review, specifically addressing coal Raman analyses has been published recently (Potgieter-Vermaak *et al*. 2010). The following paragraph highlights some of the findings, but is by no means a comprehensive overview of the published results, and the reader is referred to the review paper for further reading. Friedal and Carlson (1971) debated the origin of the band at 1580cm^{-1} by investigating IR absorption and Raman scattering of very finely ground graphite (C-C bond broken), coal and carbon black and suggested that the bands at 1580cm^{-1} and 1350cm^{-1} most likely arose from graphitic structures and not from aromatic (Cannon and Sutherland, 1955) or conjugated carbonyls (Brown, 1955), as has been suggested earlier. Tsu e*t al*. (1977) speculated that the 1370cm^{-1} band (disordered induced) could be explained by phonon dispersion of graphite and postulated a typical cluster size for a coal

molecule in the order of 65-72 'Å. Additional "disorder bands" are found at 1250cm^{-1} (D4 band) and 1450cm^{-1} (D3 band). These disorder-induced bands (D bands) are activated due to finite size effects and structural defects such as: presence of in-plane substitutional hereroatoms, grain boundaries, vacancies or other defects. All of those affect the crystalline symmetry (Brown *et al*. 2001). Another disorder band can also be found at 1620cm^{-1} (Jawhari *et al*. 1995; Li and Lannin, 1992; Dillon *et al*. 1984; Lespade *et al*. 1984). A 1150cm^{-1} band (D4 band) was found and is apparently associated with sp3 bonding (Basca *et al*. 1993), or with mixed sp2-sp3 bonding (Schwan *et al*. 1996), which has been proposed as the location of active sites in carbons (Livneh *et al*. 2000). Vidano and Fischbach (1981) mention that, although the Raman active band at 1580cm^{-1} for the in-plane E_{2g} mode has been assigned, the assignment of the observed bands at intermediate wave numbers (1100-1700cm^{-1}) remained controversial. These show that there is still a discrepancy on where the Raman spectrum originates, it depends on the type of material being analysed.

Apart from literature focusing on the characterization of the Raman spectrum of coals and other amorphous carbonaceous materials, Raman bands and their corresponding ratios have also been used to explain various phenomena pertaining to the degree of order in the amorphous C structure, graphitization, char reactivity and many more. Raman spectroscopy has been used to study carbonaceous materials and follows the graphitization process (Lespade *et al*. 1984; Rouzaud *et al*. 1983; Lespade *et al*. 1982). During the graphitization process, D-bands tend to disappear, and the Raman spectrum progressively transforms, becoming closer and closer to the graphite spectrum. The change in frequency, relative intensity, and widths of the bands have been observed by several authors and correlated with the degree of graphitization (Zaida *et al*. 2007). Studies on Raman spectra of wide range of carbonaceous materials have revealed frequency shifts and changes in relative intensities and bandwidths which can be used for structural characterization (Dillon *et al*. 1984; Green *et al*. 1983; Lespade *et al*. 1982; Vidano and Fischbach, 1978; Nakamizo *et al*. 1974; Nathan *et al*. 1974; Solin and Kobliska, 1974; Tuinstra and Koenig, 1970). Various workers have tried to correlate Raman spectral parameters with the data provided by other characterization techniques.

The most useful of these is the crystallite diameter (La), as measured by PXRD, for various carbonaceous materials. The findings of these studies (Lespade *et al*. 1982; Nakamizo *et al*. 1974; Nathan *et al*. 1974; Solin and Kobliska, 1974; Tuinstra and Koenig, 1970) were not all consistent with each other, probably because most workers have concentrated on measuring Raman band intensity ratios. These are difficult to measure accurately due to the presence of overlapping bands, and comparison between experiments carried out on different instruments may not be valid. Although no consistent quantitative interpretation of the Raman spectra emerged from these earlier studies, there was general agreement that the intensity of the D-band, relative to the G band, decreases as La increases.

Raman spectral properties, such as the intensity ratio of the D1 band and G band and the full width at half maximum (FWHM) of the G band, have been proved to have good correlations with the degree of carbon structural order (Yoshida *et al*. 2006; Cuesta *et al*. 1998; Green *et al*. 1983; Tuinstra and Koenig, 1970). Van Doorn *et al*. (1990) employed Raman spectroscopy to determine the degree of ordering in various carbonaceous materials including coal, activated carbon, soot, and correlated it with their oxidation reactivity measured by temperature programmed oxidation. They found a linear relationship between the peak position of the G band and the maximum oxidation temperature. Bar-ziv *et al*. (2000) developed the approach of applying Raman to characterise synthetic, coal and cellulose chars. They found fairly good correlations between the first-order and the second-order Raman spectral parameters and the gasification reactivity towards air and carbon dioxide. The full width at half maximum (FWHM) intensity of the G band is known to reflect the surface crystallinity of carbon material (Katagiri, 1996). The reduction of G band FWHM results from increasing structural order through the carbon network as a consequence of increasing the thermal maturity. Previous studies of G band reduction of Raman spectra of coals and kerogens (Beny-Bassez and Rouzaud, 1985) have observed that the G band FWHM can be correlated to vitrinite reflectance measurements (%RoV). Johnson *et al*. (1986) studied the characterization of coal char, and found that powder X-ray diffraction and Raman spectroscopy do not correlate with the reflectance measurements.

2.7 Thermogravimetric analysis

Thermogravimetric analysis (TGA), the monitoring of sample weight loss as a function of temperature, has been shown to be an effective tool for studying coal combustion behaviour (Cumming, 1984; Cumming and McLaughlin, 1982; Smith *et al*. 1981; Wagoner and Duzy, 1976; Wagoner and Winegartner, 1973). The TGA based techniques are accepted as a standard method in assessing the combustion reactivity (Unsworth *et al*. 1991). They fall into two categories: (1) isothermal, where the sample is maintained at a constant temperature and (2) non-isothermal, where the sample is heated at a constant rate. The most common parameter of char reactivity, derived from isothermal TGA measurements, is the time taken to reach 50% of the original sample weight. It can be used for linear ranking of char reactivity (Tang *et al*. 2005a, 2005b). The non-isothermal approach has the great advantage of being able to achieve complete conversion, and hence characterizations of char with a very wide range of reactivity using the same short heating program. However, the reactivity measured does not mean intrinsic reactivity, particularly at higher temperature when the oxygen diffusion plays an important role (Tang *et al*. 2005a, 2005b).

TGA is commonly used to measure the chemical reactivity of a char. Precautions such as using low temperature; small sample weight and small particle size are usually taken in TGA experiments to eliminate the influence of molecular diffusion on the measured reactivity. The rate parameters thereby measured are assumed to reflect the overall influence of the physicochemical properties of the char such as the pore size distribution, the number and nature of active sites, and catalytic effects of inorganic impurities. TGA reactivity data, therefore, is not only important in predicting coal ignition and char burn-out behaviour but also in providing insight into the nature and structure of the chars (Tsai and Scaroni, 1987).

Most of the studies on char reactivity have made an extensive use of TGA techniques in order to determine the intrinsic reactivity of the material for their use in the modelling of char combustion under the various combustion regimes described in the literature (Alonso *et al*. 1999; Alvarez *et al*. 1998; Smith *et al*. 1993). These procedures do not

pretend to reproduce the conditions prevailing in the boiler but allow the monitoring of the reactions under well-controlled conditions and yield kinetic parameters which can be extrapolated to the higher temperature systems such as DTF and even full scale power plants (Borrego *et al*. 1997; Thomas *et al*. 1993a, 1993b). Previous TGA studies have shown coal combustion to be influenced by rank (Smith *et al*. 1981), the surface area available (Ghetti, 1985) and even differences on whole coal maceral content (Morgan *et al*. 1986; Crelling *et al*. 1988; White *et al*. 1989). Char combustion reactivity can be measured using thermogravimetric analyzer (TGA). In order to study the reactivity of coal and chars, TGA data can be collected from a Perkin-Elmer TGA analyser in flowing oxygen gas at 34ml/min. The shape of the TGA curve can give useful information about the presence of carbonaceous materials such as amorphous carbon. The strong influence of heat treatment on char reactivity can be shown in TGA, which was also reported by Radovic *et al*. (1998), and Jones and Thrower (1991).

2.8 Summary

In this research, pulverised coal sample from Witbank coalfield is pyrolysed under various heat treatment conditions to generate char samples. The coal and chars samples are subjected to: (1) petrography for reflectance measurement and for quantification and qualification purposes, (2) PXRD to confirm the presence of graphite in the samples, (3) Raman spectroscopy for microcrystalline structure analysis, and (4) TGA for reactivity determination. The objective is to apply these techniques to characterise the evolution of coal char microstructure and its reactivity from South African Witbank coal treated at various heat treatment temperatures, and to probe the correlation between these techniques. Therefore, by comparing the results obtained from these analyses, a deeper insight of the coal and char carbon structure can be developed.

CHAPTER 3

Experimental

3.1 Introduction

This chapter describes the methods involved in the preparation of the parent coal to produce chars prior to characterisation analyses. The different sections address the origin of the parent coal sample (Section 3.2), preparation of chars (Section 3.3), proximate analysis on coal and chars (Section 3.4), sample preparation in Section 3.5, and the analytical techniques used for the analyses and characterisation of the char samples (Sections 3.6-3.8). The aim of this chapter is to highlight the methods used to prepare coal and char and to give the operation procedures of the techniques used to characterise them (coal and char) such as the operation procedures of coal petrography, Raman spectroscopy, PXRD and TGA.

3.2 Origin and preparation of the coal sample

The parent coal sample originates from the South African Witbank coal field. Coal from this region is mainly utilised as a power station feedstock by Eskom, for the production of synthetic petroleum products (Sasol), and it is also exported to Europe and Asia mainly for steam generation. Approximately 10kg of parent coal sample was mixed thoroughly on a clean concrete floor by transferring the coal from one point to another by shovel. The mixed coal sample was divided into four quarters. The opposite quarters were rejected, and the retained quarters were mixed again. The process was repeated until the required amount of material (2kg) has been reached. A representative coal sample was crushed using a ring roller mill to -850µm passing sieve and retained on the 450µm screen. This was done to effectively minimise the amount of fine particles. The resulting representative sample was used to prepare the blocks for petrographic analyses. A representative coal sample (firstly ground and thoroughly mixed) was pulverised in the laboratory by screening to below 150µm. From this population the following analyses

were performed on the raw coal: Proximate analysis (moisture, ash, volatile matter, fixed carbon) as well as petrographic analyses (using reflected polarised light microscopy and oil objective lens) were conducted to determine the coal properties. In addition, Raman spectroscopy and XRD were performed to probe the molecular structure of the coal. This same portion of the original 10kg sample was then used to produce the packed bed balance reactor char samples (up to a temperature of 1000°C) and the char structure, morphology and reactivity were investigated by Raman spectroscopy, petrography, XRD and TGA. Due to in-house furnace temperature limitations, four char samples were obtained from Eskom. These four samples were all prepared at different times, from different populations by utilising a pilot plant operating a drop tube furnace (DTF) at 1400°C, at Eskom. Their parent coals were known to originate from the Witbank coal field as well.

3.3 Char preparation

A Packed Bed Balanced Reactor (PBBR) was used to prepare char samples at different temperatures (300ºC, 600ºC, 800ºC and 1000ºC) using the pulverised coal sample (Witbank coal) via a pyrolysis process (Figure 3.1). Facilities located at the University of North-West (Potchefstroom campus) were used.
The method used for the char preparation consisted of the following:

a) Approximately 40g of pulverised coal (<150µm) was loaded into the reactor and introduced into the furnace.
b) The sample was equilibrated at ambient temperature and pressure in a nitrogen atmosphere.
c) The sample was heated at a constant heating rate of 15ºCmin^{-1} to 300ºC/ 600ºC/800ºC or 1000ºC to obtain the char sample.
d) The sample was held isothermally at the target temperature for 60min to ensure that all the volatiles were driven off.
e) The resultant char sample was then cooled to ambient temperature under nitrogen flow and placed in a closed plastic bag.

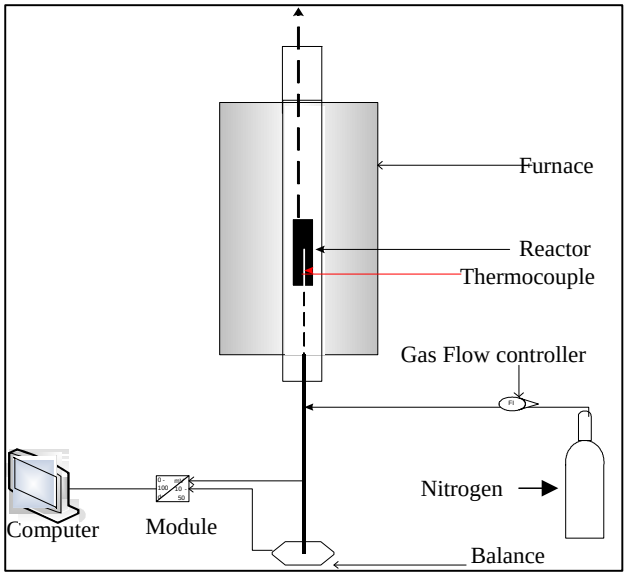

Figure 3.1: Schematic representation of PBBR used to prepare chars.

Due to inability to prepare the char samples (above 1000°C) in-house, Eskom provided the four samples obtained from a drop tube furnace (DTF) charred at 1400ºC in order to get an indication/snapshot of the behaviour of coal samples charred at that particular temperature (1400ºC). The four DTF char samples were prepared from the four separate coal samples, all slightly different from PBBR parent coal sample, but known to originate from Witbank coal field. The operation procedure of DTF can be found in Wagner (2008), and its description is also covered in Chapter 2 (Section 2.4). The four DTF char samples were collected and graded into <38µm and 38 - 75µm. The >75µm DTF char samples could no be obtained from the supplier. The four DTF char samples were prepared for analyses.

3.4 Proximate analysis on coal and chars

Proximate analysis of the parent coal and chars was performed using an in-house TGA method similar to the method of Jones *et al*. (1999). Samples (~15mg) were heated under nitrogen at 50°C/min to 110°C and held to constant weight for 3s, before being heated at

the same rate to 900°C and again held to constant weight for 3s. This yielded the moisture and volatile matter contents. Air (oxygen) was then introduced to the TGA furnace, and the sample burned to constant weight, so that the ash and fixed carbon contents were determined. The name of the TGA was Perkin-Elmer TGA instrument which uses Pyris software. The equipment is located in School of Chemical and Metallurgical Engineering in University of the Witwatersrand. Refer to Appendix 'A' and Figure A.1 for more details.

3.5 Samples preparation for microscopic analysis

The parent coal and char samples were prepared for microscopic examination in accordance with the ISO Standard 7404-2, (1985), and also followed the procedure given in Oka *et al*. (1987): 100-200mg of char particles were poured into a plastic mold, followed by mixture of epoxy resin and hardener, which were then mixed together and left overnight to harden at room temperature. The mounted coal and char samples were polished using a Struers Tegraforce polisher with an application of alumina (Al_2O_3) powder in the final stage of polishing. The mounted coal and char blocks were examined microscopically in reflected light with oil immersion using a Leica DMP 4500 reflected light polarising microscope. The samples were prepared in the School of Chemical and Metallurgical engineering in University of the Witwatersrand.

The coal and char blocks prepared were microscopically analysed using petrography and Raman spectroscopy. The petrographic microscopy is located in the School of Chemical and Metallurgical engineering, and Raman spectroscopy is located in School of chemistry, both techniques are in University of the Witwatersrand

3.6 Petrographic analysis

3.6.1 Reflectance analysis

Coal rank was determined on the polished block surface of the parent coal using a petrographic microscope with a polarised light attached and a sensitive photometer. This

microscope was also used to determine the reflectance analysis on chars. The analyses are conducted using a Leica DMP 4500 reflected light polarising microscope equipped with an oil objective lens of X50 magnification. The microscope is interfaced with a J and M spectroscopic system where by reflectance values are obtained via a fibre optic cable. A computer collects and processes the data via MSP software. The microscope is calibrated using glass reflectance standards with known reflectance reading (0.431, 0.906, 1.728 and 3.240 %RoV). Rank determination was conducted through vitrinite random reflectance and through total maceral reflectance measurements in order to establish the parent coal maturity for all macerals. These were carried out in accordance with ISO Standard 7404-5, (1994). 100 readings were taken on the vitrinite particles. 100 readings were also taken on the total maceral reflectance count on the parent coal sample, as well as on the char particles derived from the parent coal sample. These were averaged to obtain a mean vitrinite reflectance (%MVR) and mean total reflectance (%MTR) values, and ranges of readings and standard deviations were also recorded.

3.6.2 Maceral group analysis and char morphology

Petrographically, coal maceral and char morphological analyses were conducted and categorised using reflected light microscopy to determine their morphology and porosity. For the parent coal sample, the group macerals were quantified by a 500-point count technique, following the ISO 7404-3 (1994) method and the reactive macerals were identified according to the method of Smith *et al*. (1983) for South African coals.

Char morphology classifications were conducted following the work done by Wagner (1998) and Bailey *et al*. (1990) as shown in Table 3.1. The char classification was conducted in order to compare the char morphologies with the original feed coal (parent coal). In order to examine the population of the categorised chars, each char group on the sample block was counted using a point counter, following the ISO 7404-3 (1994) method, and up to 500 points were also recorded proportionately per sample. The analysis of each block was repeated three times to confirm the results.

Table 3.1: Char morphology classification (Wagner, 1998 and Bailey *et al*., 1990)

Char type	**Shape**	**Pore volume**	**Vesicles**		**Pore shape**	**Wall thickness**
			Primary	Secondary		
Thin walled cenosphere (Tenuisphere)	Spheroidal	>80%	1-3	common	spheroidal	<5µm
Thick walled cenosphere (Crassisphere)	spheroidal	60-90%	1-5	common	spheroidal	>5µm
Thin walled honeycomb (Tenuinetwork)	spheroidal, elongate or irregular	60-90%	-	many	Spheroidal to elongate and subparallel	<5µm
Thick walled honeycomb (Mesosphere)	spheroidal, elongate or irregular	40-60%	-	>3	Spheroidal to elongate and subparallel	>5µm
Mixed porous	spheroidal to irregular	>50%	-	-	variable	variable
Mixed dense	rectangular to irregular	<50%	-	-	variable	variable
Dense/solid	rectangular to irregular	<5%	-	-	-	Solid
Fusinoid	irregular	<5%	-	-	Inherited cellular porosity	solid
Mineroid/ Carbominerite	Spheroidal to rectangular	-	-	-	-	Mineral >50%

The char morphology system outlined in Table 3.1 is based on the physical properties that determine char reactivity. There are three major types of materials encountered in the samples. The first is porous material, which contains vesicles produced by degassing and shows evidence of fusion, while the second is dense material containing few or no pores and often resembling fusinite, semi-fusinite, macrinite or inertodetrinite macerals. The third type of material consists of minerals.

3.6.3 Micro Raman spectroscopy (MRS)

MRS was undertaken to determine the structural characterization of the coal and char particles using a micro Raman spectrometer (Senterra, Bruker) located in School of Chemistry, University of the Witwatersrand. This instrument consists of a microscope with a Raman spectrometer having spectrographic dispersion and multichannel detection. A 50X objective was used to focus the excitation laser beams (532 and 785nm exciting lines of a spectra Nd-YAG lasers) on the particle. This can be used to obtain insight into coal and char structure and, the effect of heat treatment on the char structure evolution and consequently on the char reactivity, can be addressed.

MRS operation can be described as summarised in Figure 3.2. An optical beam produced by a continuous-wave Nd-YAG laser enters a microscope and is directed onto an objective that focuses it to a 50 X 1000μm spot on the sample surface. The incident light interacts with the sample and the consequent Raman scattering generated from a surface layer is collected with a 180° configuration. The Raman photons emitted from the illuminated spot (~4-5μm) are collected by the same microscope objective (50X) and sent to spectrometer. The spectrometer comprises of foremonochromator that selects the spectral range. The spectral information is sent to the multi-channel detector (CCD) and the data is saved in a computer.

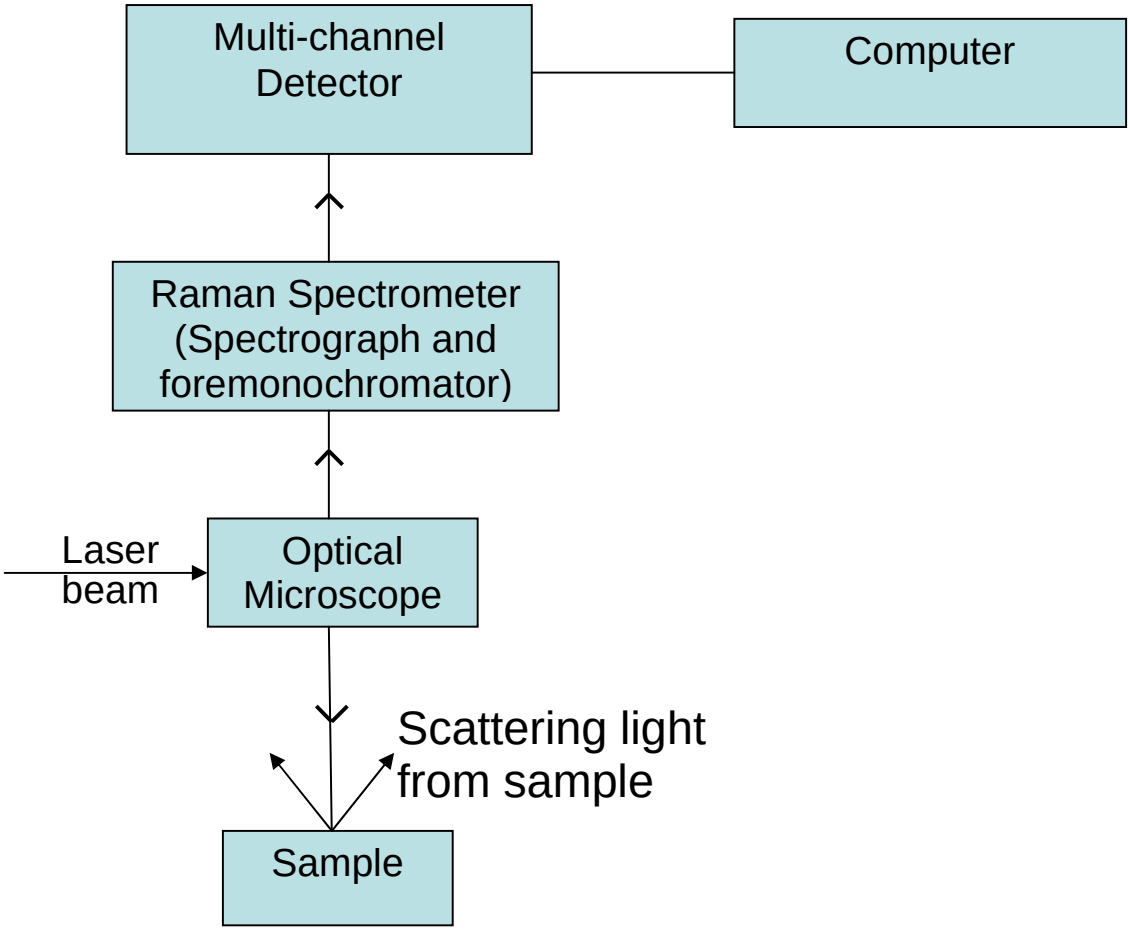

Figure 3.2: A schematic diagram of the micro Raman spectroscopy (MRS).

Raman spectra of coal and char particles were taken using a 50X objective and a 532nm Nd-YAG laser beam. The spectra were recorded at ~3-5cm^{-1} resolution. The laser power at the sample surface was controlled at about 2mW to avoid laser damage. The laser spot diameter on the sample was about 4-5µm, much larger than the size of carbon micro-crystallites in the coal/chars. Therefore, the Raman spectroscopy provided average information of a large number of randomly distributed micro-crystallites. Approximately 30-50 different particles were randomly chosen from the polished coal and char blocks, and analysed. The spectra were recorded in the range 800-2000cm^{-1}, covering the first-order bands, and the acquisition time for each spectrum was 60s.

3.7 Powder X-ray diffraction (PXRD)

PXRD was conducted to determine the graphitic nature of the parent coal as well as the resultant chars. The coal and char samples were pressed firmly into the sampler holder before analysis using the Philips PW 1830 diffractometer located in School of Chemical and Metallurgical Engineering, University of the Witwatersrand. The Powder X-ray diffractometer was operated at 40kV and 40mA for 45min, over a range of °2θ from 0° to 80º, and a step size of 0.04. The High Score Plus software was used for data identification and interpretation.

3.8 Char reactivity

Char combustion reactivity was measured using a Perkin-Elmer TGA instrument located in School of Chemical and Metallurgical Engineering, University of the Witwatersrand. The measurement was performed under non-isothermal conditions following the procedure of Shim and Hurt (2000). A 5-15mg sample char was placed in the TGA pan and heated from room temperature at 7ºC/min to 105°C and held for 30min to remove any moisture. It was then heated at 7ºC/min to 950°C and held for 10min for a complete burnout. The reaction gas used was oxygen, and reaction was conducted in flowing oxygen at 34mL/min flow rate. Figure 3.3 shows the summary of the determination of char combustion reactivity using TGA.

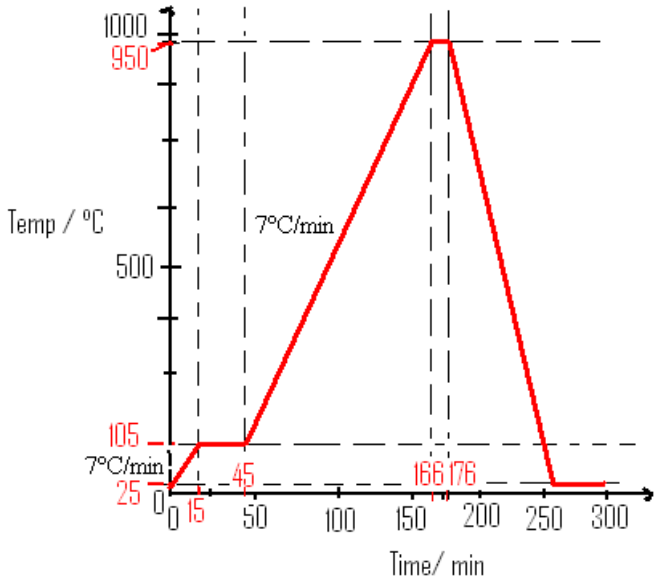

Figure 3.3: Schematic representation of determination of char combustion reactivity using TGA.

3.9 Summary

In this chapter the methodology applied to this research investigation was introduced. Figure 3.4 provides a flow chart that summarises the methodology outlined above.

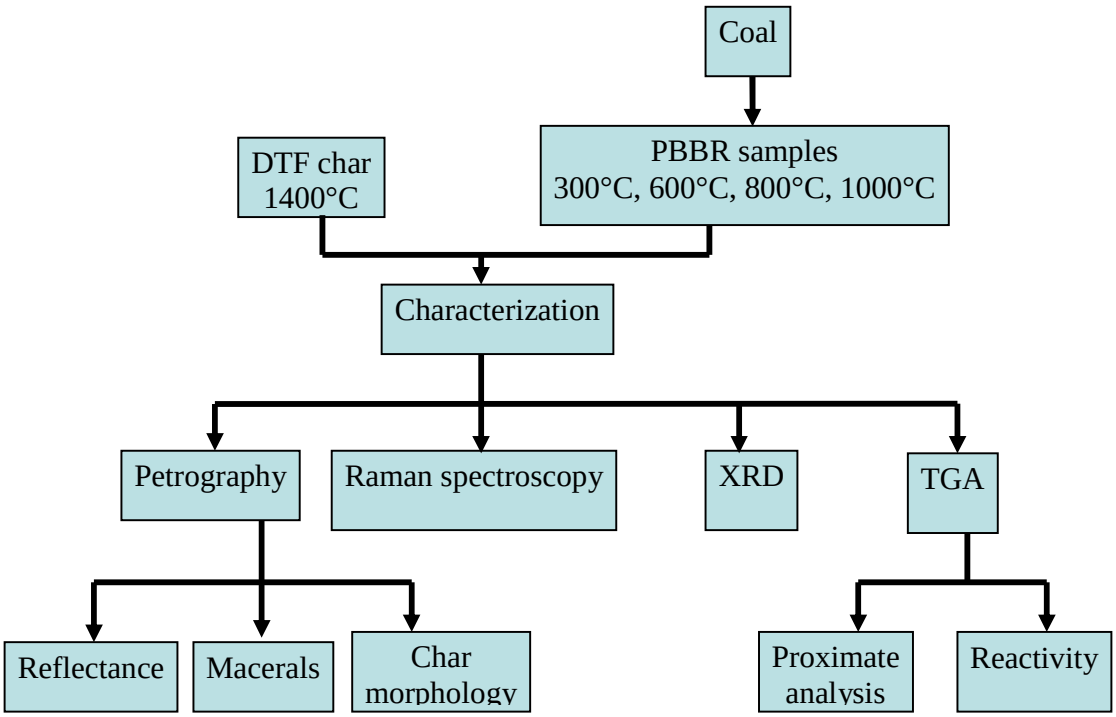

Figure 3.4: The flow chart summary of the research methodology.

CHAPTER 4

Results and discussion

4.1 Introduction

In this chapter, the experimental results from the investigation into the evolution of char structure at different temperatures (300, 600, 800, 1000, and 1400°C) and char reactivity are presented. Samples charred at 300-1000°C were made in the packed bed balance reactor (PBBR), and correspond to the same sub-set of samples, prepared as described in Section 3.2 from parent coal from the Witbank coalfield. Samples 1-4 charred at 1400°C were made in a drop tube furnace (DTF) from different parent coal populations than those used in the PBBR, but also originating from Witbank coal field. The experiments were conducted using techniques including coal petrography, powder X-ray diffraction (PXRD), micro Raman spectroscopy (MRS), as well as thermogravimetric analysis. The objective of this chapter is to: 1) provide quantitative information concerning the detailed morphological composition of coal and char. 2) provide insight of the char structure (crystallinity and molecular) and the effect of heat treatment on the structural evolution; 3) provide information concerning the reactivity behaviour of the char; and 4) make comparison between the different techniques to determine the correlations.

Proximate analyses are discussed in Section 4.2. This is followed by the petrographic results which include reflectance measurements and qualitative and quantitative compositional information (detailed morphological composition), these are presented in Section 4.3. PXRD results are discussed in Section 4.4 which confirms the presence of graphite (graphitic ordering) in coal and chars. Raman spectroscopic results are discussed in Section 4.5. The reactivity of coal and char is illustrated in Section 4.6. The chapter is concluded by drawing correlations between petrography, Raman spectroscopy and thermogravimetric analysis in Section 4.7.

4.2 Proximate analyses

4.2.1 Proximate analyses on coal and chars prepared using PBBR

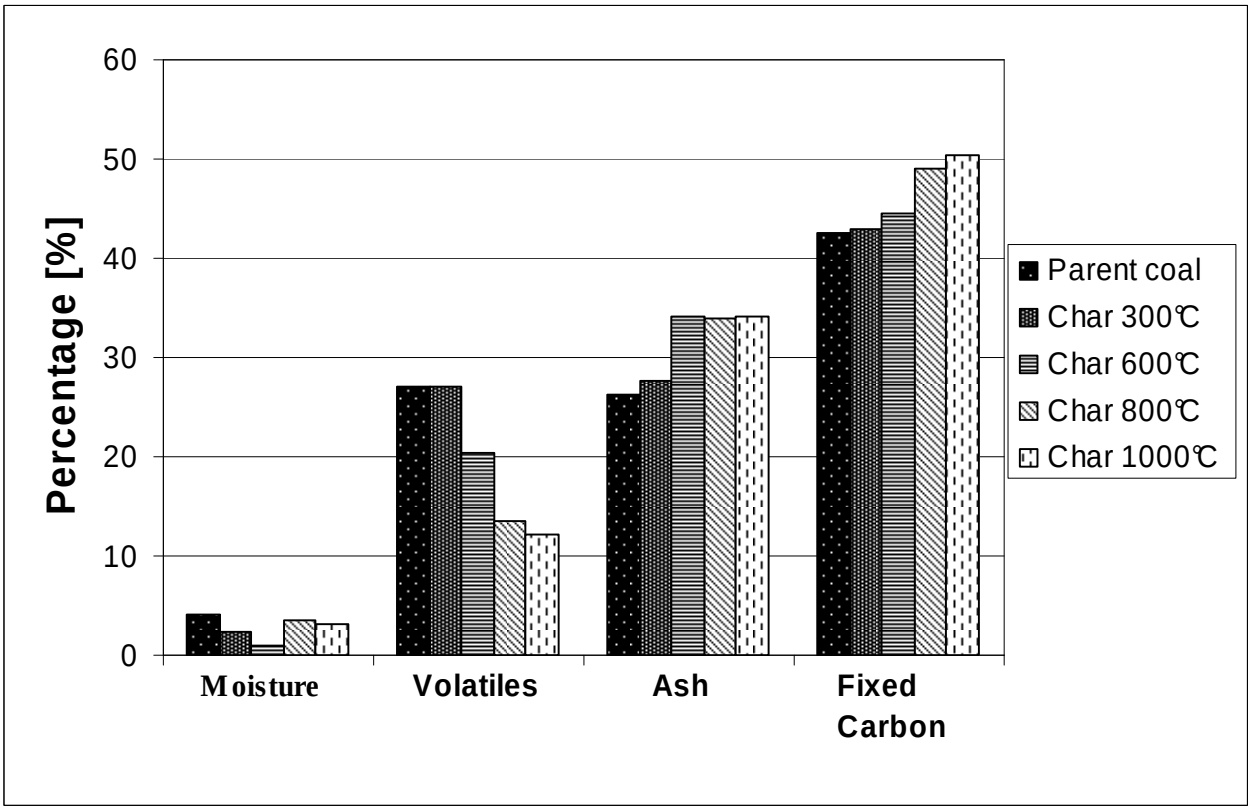

Figure 4.1: Comparison of proximate analysis on coal and chars derived from the PBBR (air dried).

The results of proximate analyses on coal and the resulted chars at different temperatures are presented in Figure 4.1. The percentage components (moisture, volatile matter, ash and fixed carbon) were calculated as illustrated in Appendix A. It can be seen that the volatile matter in the samples decreases with an increase in charring temperature (from 27% in the parent coal to 12.3% in char 1000°C), and correspondingly the percentage fixed carbon increases from 42.5% for parent coal (air dry) to 50.4% at 1000°C. This is in agreement with results obtained by Falcon and Ham (1988). The fact that some volatile matter remained indicates that these chars did not achieve complete conversion. The trend of the variations in the value of volatile matter and fixed carbon in the coal and chars are as anticipated, as the trend is similar to values reported by Fuwape (1996);

Buekens and Schoeters (1987); Jenkins *et al*. (1973); Brocksiepe (1971) and Hoffman and Fitz (1968). An anomaly was noted on the samples charred at 800°C and 1000°C, where an increase of moisture was observed. This could be attributed to the increase in the surface area as approaching the high charring temperature. Repeated runs produced the same results.

4.2.2 Proximate analyses on chars prepared using DTF

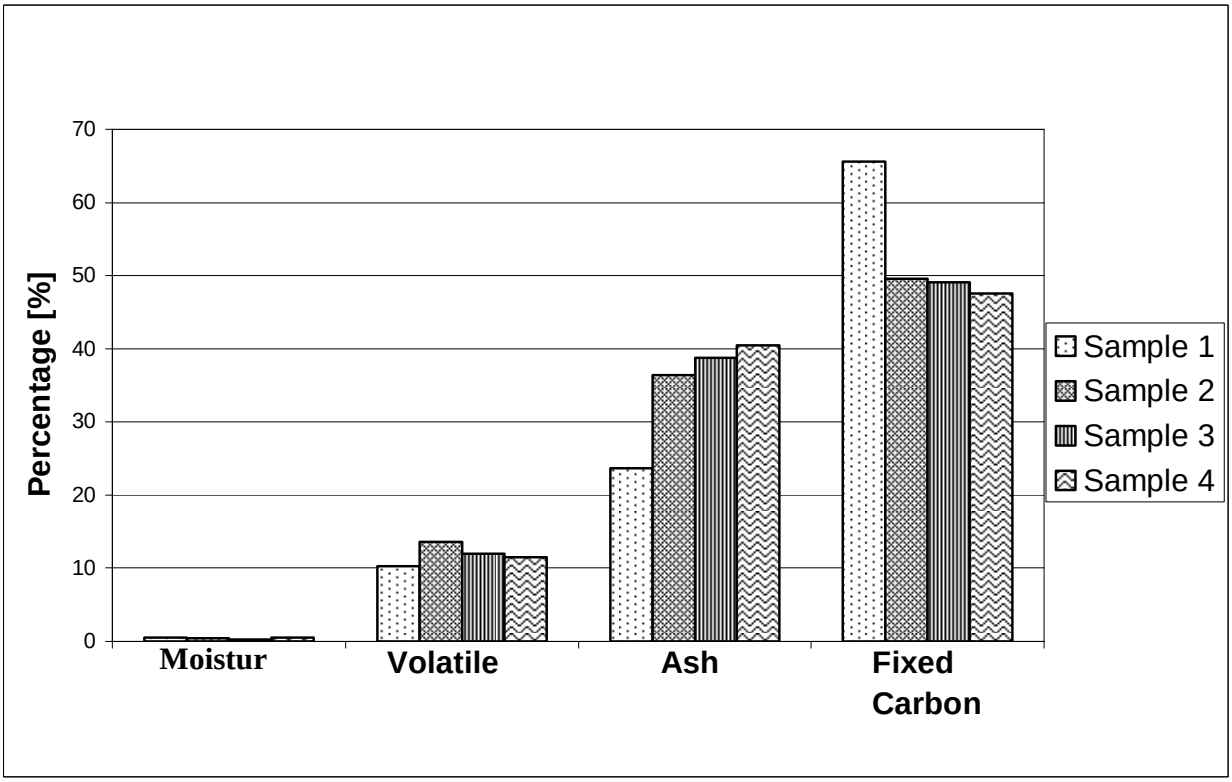

Figure 4.2: Comparison of proximate analysis on drop tube furnace (DTF) chars (air dried).

The four char samples (charred at 1400°C) in a DTF vary in terms of the proximate analysis data (Figure 4.2). Following the trend of the values of volatile matter and fixed carbon obtained from PBBR chars, it was expected that the four DTF chars would have less volatile matter and higher fixed carbon as compared to the PBBR chars due to the higher temperature that the coal was exposed to. However, this was not as different as anticipated, with approximately 10% volatile matter remaining in the DTF chars. The

proximate analysis reveal a difference between the DTF chars, with sample 1 having much lower ash content (23.6%), and therefore a higher fixed carbon content (65.6%). This sample (sample 1) might have a totally different parent coal as compared to the other three DTF samples.

4.3 Petrographic analysis

The section contains reflectance properties (Section 4.3.1), which include both mean vitrinite reflectance (MVR) and mean total maceral reflectance (MTR); maceral analysis (including minerals) on parent coal (Section 4.3.2); and char morphology analysis (Section 4.3.3).

4.3.1 Reflectance analyses

As outlined in Section 3.6.1, Reflectance measurements were performed on the parent coal and char samples using vitrinite as a reference material (determination of mean vitrinite reflectance (MVR) and mean total maceral reflectance (MTR) analysis. The results are presented in Table 4.1 and the histograms are located in Appendix B.1 (Figure B.1 and B.2). The parent coal has RoV of 0.59% and a mean total reflectance or RoC of 1.09% (Table 4.1).

Figure 4.3 shows the results from MVR analysis on the PBBR. It can be seen that the MVR increases with heat treatment temperature, which agrees with previous work (Goodarzi, 1984; Murchison, 1978; Goodarzi and Murchison, 1972; de Vries *et al*. 1968; Ghosh, 1968; Chandra and Bond, 1956). The increase in MVR could be attributed to increasing anisotropy resulting from changing mutual orientation of the aromatic layers (Rouzaud *et al*. 1983). MVR was determined on vitrinite particle and on char components clearly recognisable as originating from vitrinites in the parent coal, which is isotropic porous char.

Table 4.1: The table of Mean Vitrinite Reflectance (MVR / %), Mean Total reflectance (MTR /%).

Sample name	Reflectance [%]	
	MVR	**MTR**
Parent coal	0.59	1.09
Char 300°C	0.62	1.12
Char 600°C	1.60	2.69
Char 800°C	4.06	4.75
Char 1000°C	5.38	6.05

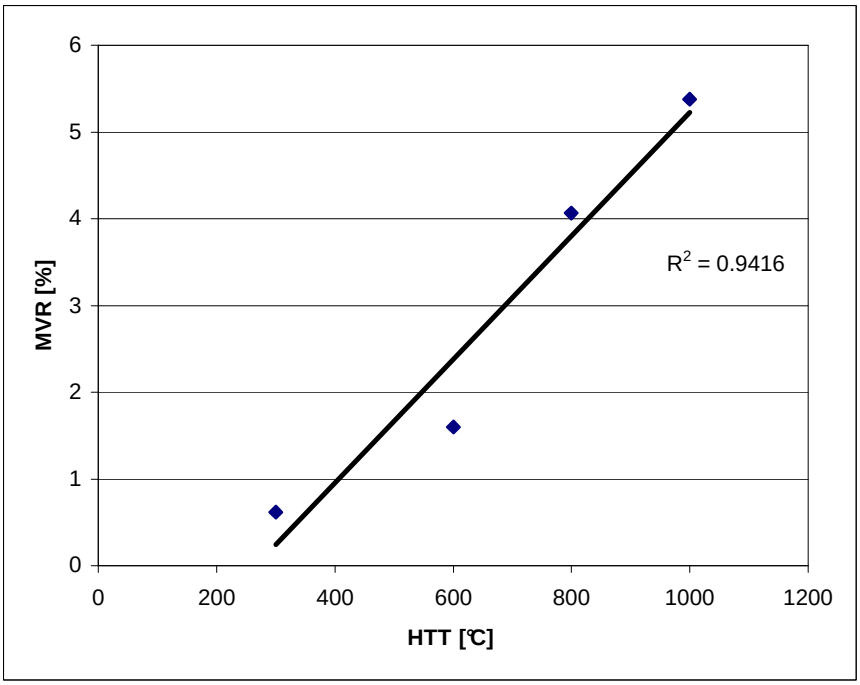

Figure 4.3: Variation of mean vitrinite reflectance (MVR) with heat treatment temperature.

Figure 4.4 shows results from mean total maceral reflectance (MTR) experiments. It was also found that MTR increases with heat treatment temperature. The extent of the change in MTR as a result of the different charring temperatures was determined in all coal macerals and their resultant char components. Very significant shifts were displayed in

the levels and ranges of MTR in the char samples compared to those shown by the original coal (Table 4.1).

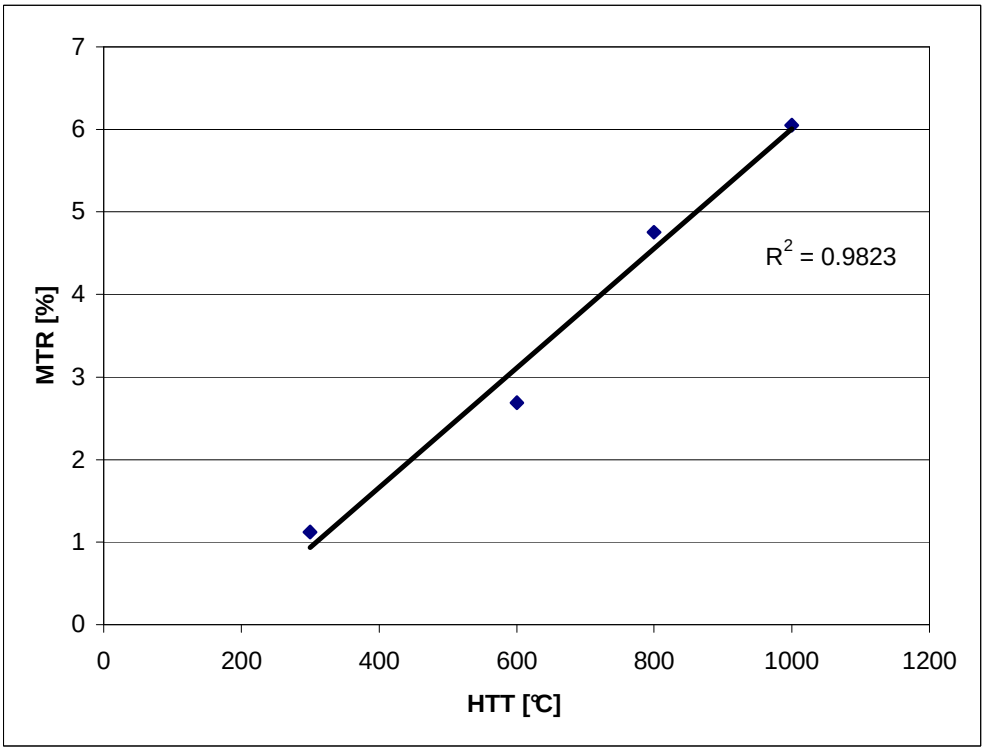

Figure 4.4: Variation of mean total maceral reflectance (MTR) with heat treatment temperature.

4.3.2 Maceral group analysis on parent coal and chars.

Table 4.2: Maceral group analysis (including minerals)

Particle type		**Percentage (by volume)**	
Maceral & mineral groups	**Maceral subgroups**	**%**	**Total (%)**
Vitrinite	Telovitrinite	22.4	22.4
Inertinite	Fusinite	5.4	54.0
	Reactive semi-fusinite	6.8	
	Inert semi-fusinite	8.0	
	Inertodetrinite	33.8	
Liptinite		1.6	1.6
Minerals			22.0

Results obtained from the maceral group analysis on the parent coal show that the coal is rich in inertinite particles (54.0%), with a low vitrinite content (22.4%) and very low liptinite content (1.6%), which is typical of Witbank coals. Two categories of minerals were identified in the parent coal sample, namely: those associated with organics (carbominerite) and those liberated such as pyrite, clay, quartz and carbonate minerals. The overall amount of mineral matter determined petrographically is 22% (Table 4.2). This implies that the coal is likely to have a moderate to high ash content, which is a clearly evident from the values of percentage ash presented in Figure 4.1 (26-34%). Examples of maceral types described in Table 4.2 are shown in Figure B.3 in Appendices section (Appendix B). The petrographic composition of parent coal of DTF chars could not be presented, as the DTF char's parent coal could not be obtained from Eskom.

Results obtained from PBBR char samples show the effect of temperature on carbon conversion as illustrated in Table 4.3 below.

Table 4.3: Coal maceral analysis on parent coal and PBBR char samples (% by volume).

Coal maceral group	**Parent coal**	**Char300°C**	**Char600°C**	**Char800°C**	**Char1000°C**
Vitrinite	22.4	21.4	3.6	0	0
Liptinite	1.6	0.8	0	0	0
Inertinite	54.0	53.8	23.4	13.6	0
Minerals	22.0	24.0	8.4	8.0	7.8
Total char by difference	0	0	64.6	78.4	92.2

The sample charred at 300°C showed no observable conversion on a maceral basis, since almost the same percentages were found in terms of maceral composition relative to the parent coal (Table 4.3). According to Bengtsson (1986), liptinite is likely to alter at lower temperature compared to the other maceral groups, and indeed a lower value was obtained at 300°C. However this is also within the range of reproducibility/repeatability. At 600°C no liptinite was recorded, because at lower temperatures (300 and 600°C), liptinite liquefies and vaporises, forcing holes in the surface of the softened particle (Bengtsson, 1986). Hence, liptinite is significant only in the pyrolysis stage and does not contribute significantly to the char combustion stage. As anticipated, there was a marked reduction of macerals as charring temperature increases as the organic matter is converted to chars. By 1000°C, no coal macerals were observed, meaning that all macerals were converted into chars. The proportion of minerals showed a decrease with an increase in temperature, as the minerals may have turned to a glass-like amorphous phase; such minerals cannot be identified or quantified petrographically. Other minerals showed alteration to ash and were not included in the maceral count.

4.3.3 Char morphological analysis

Table 3.1 in Chapter 3 summarises the char morphology classification followed in the study, which follows the work conducted by Wagner (1998) and Bailey *et al*. (1990). The types of char formed depend on the parent coal macerals and microlithotypes, coal rank, particle size and temperature of char formation (Cloke and Lester, 1994). Char morphologies obtained from Witbank coal are illustrated in Figures 4.5, 4.6 and 4.7; and are divided into three categories: 1) porous particles, 2) dense particles and 3) carbomineroid/mineroid particles respectively.

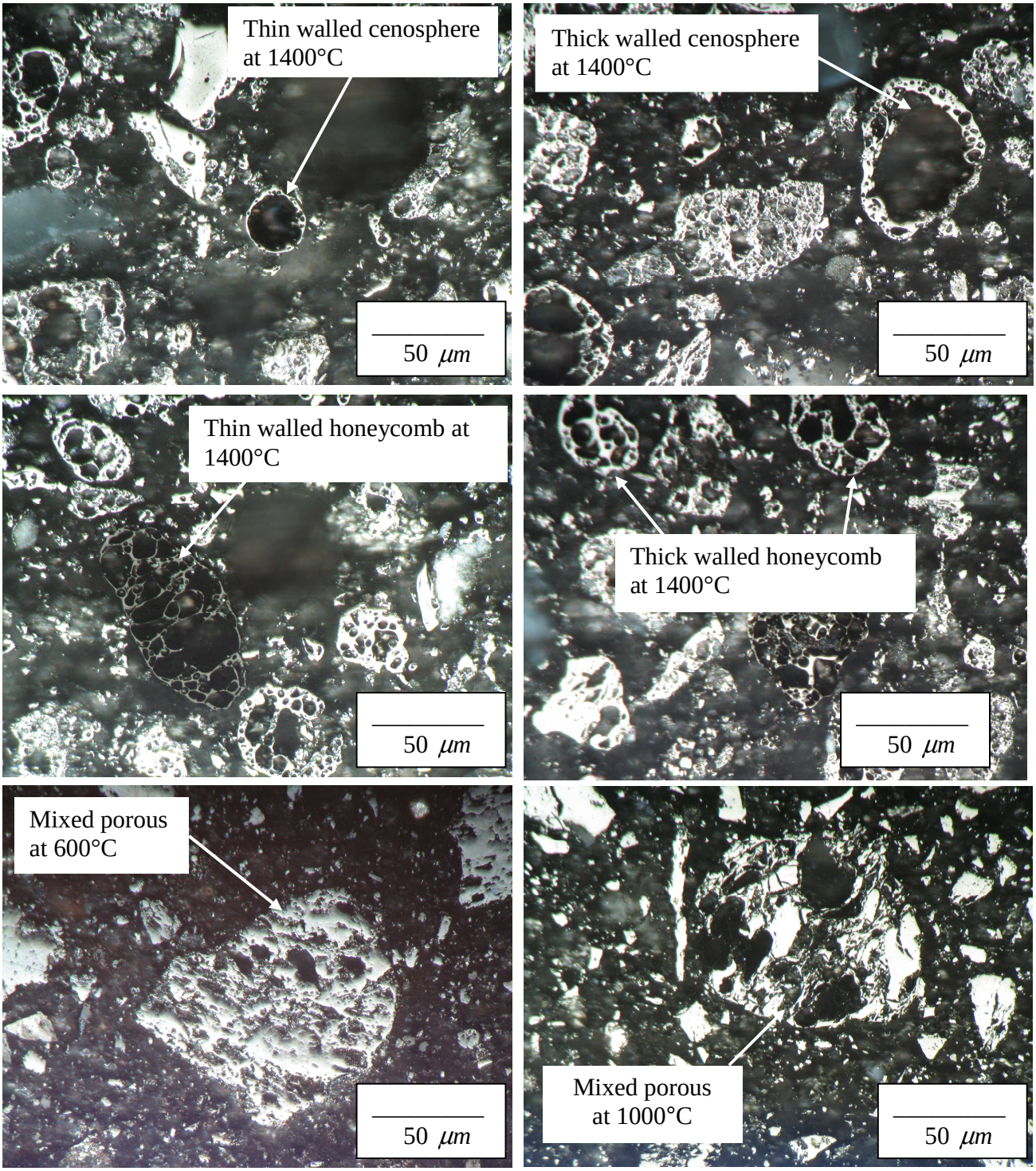

Figure 4.5: Examples of porous char particles (oil immersion lense, X500, reflected light).

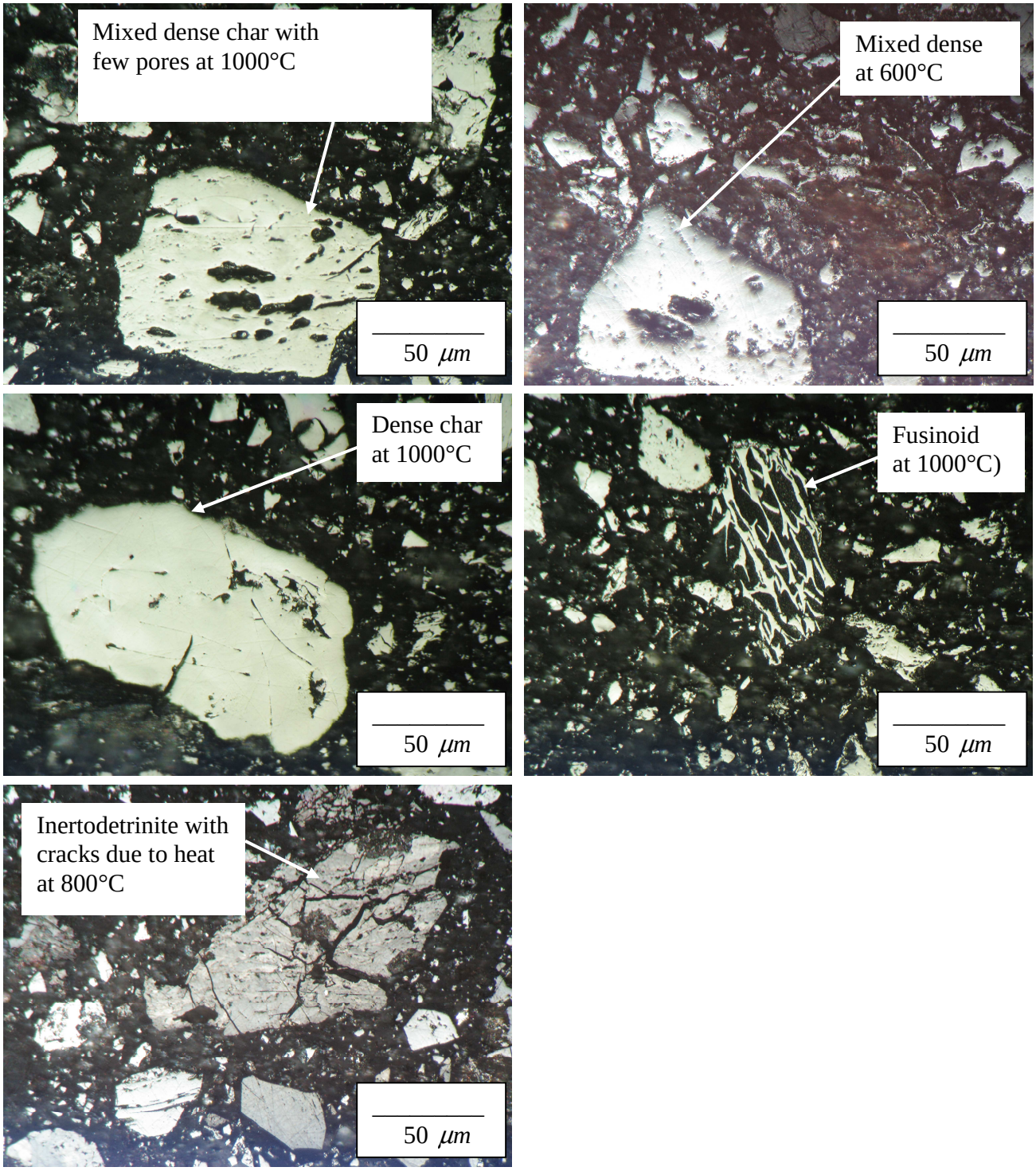

Figure 4.6: Examples of dense char particles (oil immersion lense, X500, reflected light).

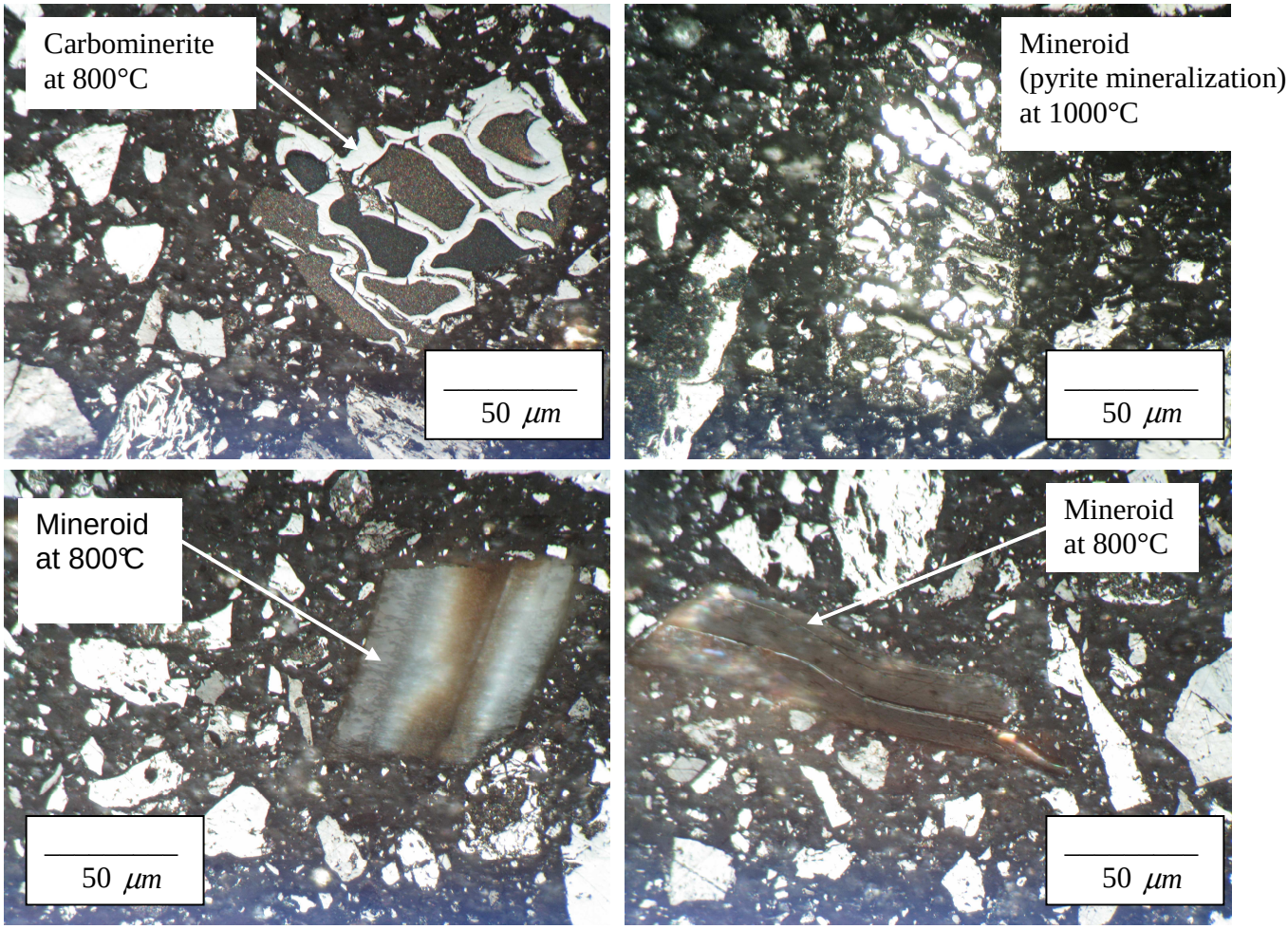

Figure 4.7: Examples of mineroid/mineral associated with organics (carbominerites), (oil immersion lense, X500, reflected light).

Table 4.4: Char morphology analysis

Char morphology		PBBR chars (% by vol)[1]				DTF chars (% by vol)			
Main groups	**Subgroups**	**Char 300°C**	**Char 600°C**	**Char 800°C**	**Char 1000°C**	**Sample 1**	**Sample 2**	**Sample 3**	**Sample 4**
Porous	Thin walled cenosphere	0	0.6	1.4	1	2.1	0.7	0.2	2.2
	Thick walled cenosphere	0	0	0	0	3.2	2.8	0.8	2.8
	Thin walled honeycomb	0	0	0	0	2.2	3.5	0.6	1.0
	Thick walled honeycomb	0	0	0	0	3.1	1.4	2.2	1.6
	Mixed porous	0	3.4	5	7.6	31.2	45.8	40.8	30.0
Total		**0**	**4.0**	**6.4**	**8.6**	**41.8**	**54.2**	**44.6**	**37.6**
Dense	Mixed dense	0	18.4	22.2	38	29.3	30.4	38.0	24.0
	Dense/solid	0	35.4	44.8	41	23.9	4.8	9.0	32.4
	Fusinoid	0	2.2	0.4	1.8	1.8	1.1	1.4	0.8
Total		**0**	**56.0**	**67.4**	**80.8**	**55.0**	**36.3**	**48.4**	**57.2**
Mineral	Mineroid	**0**	**4.6**	**4.6**	**2.8**	**3.2**	**9.5**	**7.0**	**5.2**

[1] The PBBR char ≠100% as the difference is due to the coal particles as per Table 4.3

The types of char studied in this research are summarised in Table 4.4. These include char formed in the PBBR and the DTF. These chars are divided into two main groups; that is porous particles (reactive char) and dense particles (less reactive char). Results obtained from the PBBR chars showed that an increase in temperature lead to an increase in the amount of char formed. This was observed as the amount of dense particles were found to be 80.8% at 1000°C as compared to 0% at 300°C and the amount of porous particles were found to be 8.6% at 1000°C as compared to 0% at 300°C (Table 4.4) as also shown by the graphs below (Figure 4.9 and 4.8, respectively).

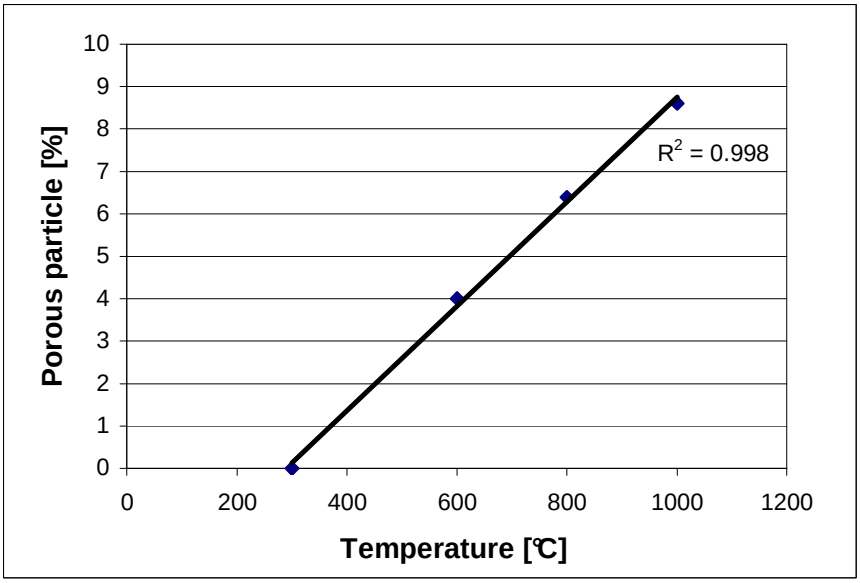

Figure 4.8: Effect of temperature in the evolution of porous char particle.

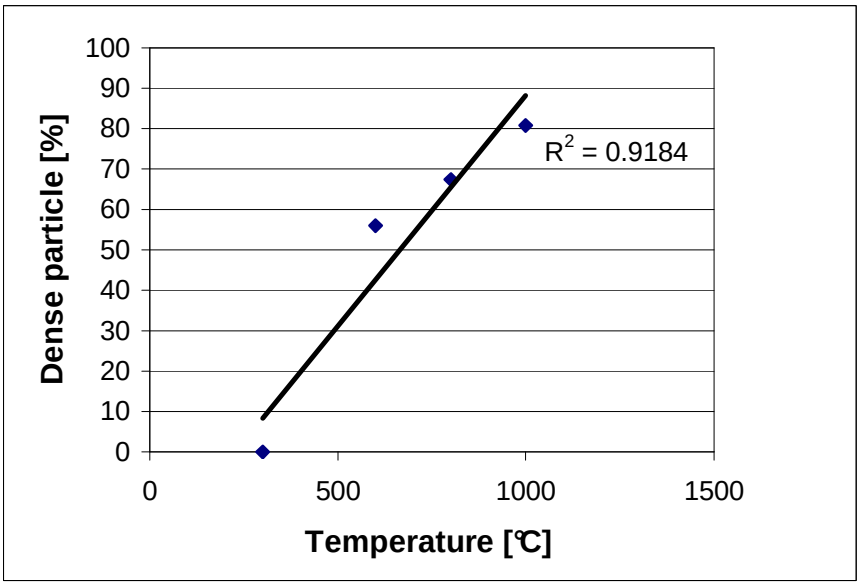

Figure 4.9: Effect of temperature in the evolution of dense char particle.

The two straight line graphs above (Figure 4.8 and 4.9) show that increasing the charring temperature leads to an increase in the amount of char particles due to the conversion from parent coal. Such trends were also observed by Everson *et al*. (2008), studying the properties of high ash char particles from inertinite-rich coal, where a large fraction of char at high charring temperature (900°C) was quantified as compared to charring temperature at 700°C.

The DTF chars showed some differences in terms of their char morphologies. As expected, the four DTF char samples did not originate from the same population. As compared with the PBBR chars, all four DTF char samples were dominated by dense particles (36.3-57.2%), but also showed to have high percentage of porous chars (37.6-54.2%), which was not observed in PBBR chars. Such difference might be attributed to the different petrographic composition (macerals composition) of the parent coals from which the chars prepared in the two reactors (PBBR and DTF) were derived (Table 4.4).

4.4 Powder X-ray diffraction (PXRD) analysis

4.4.1 PXRD results on parent coal and chars

PXRD is discussed in Section 3.7. Figures 4.10 and 4.11 show some PXRD results obtained from the parent coal and char samples. The (002) reflection observed on coal and chars corresponds to the spacing of aromatic layers (Lu *et al*. 2001). It was found that the parent coal contained a short-range graphite-like structure to a small degree and this was evident by the position at the (002) band that corresponds to the position of graphite band. Gamma bands were observed on the left-hand side of the (002) band (Figure 4.10), and represent the aliphatic side chains that are attached to the crystalline carbon (aromatic carbon) (Lu *et al*. 2000, 2001). The gamma band tends to disappear as the heat treatment temperature increases up to 1000°C (Schoening, 1983). The sharpening of the peaks with heat treatment temperature in Figure 4.10 clearly shows the development of structural order (Schoening, 1983). Schoening (1983) associated the peak at about 20° in 2θ (a-peak) as a two dimensional reflection arising from graphite-like atomic order within single plane, and the same peak (at 20° in 2θ) was also observed in a DTF chars as shown in Figure 4.11 and was labelled as ‘a-peak’. The graphite-like band can be associated with the G band (crystalline band) at ~1580cm^{-1} (Tuinstra and Koenig, 1970) which was found in micro Raman spectroscopy (MRS) as discussed in Section 4.5. The other compositions (gamma bands) might be associated with the disorder in the structure of coal and char. This confirms that charring eliminates some of the disorder in the structure which is associated with gamma bands.

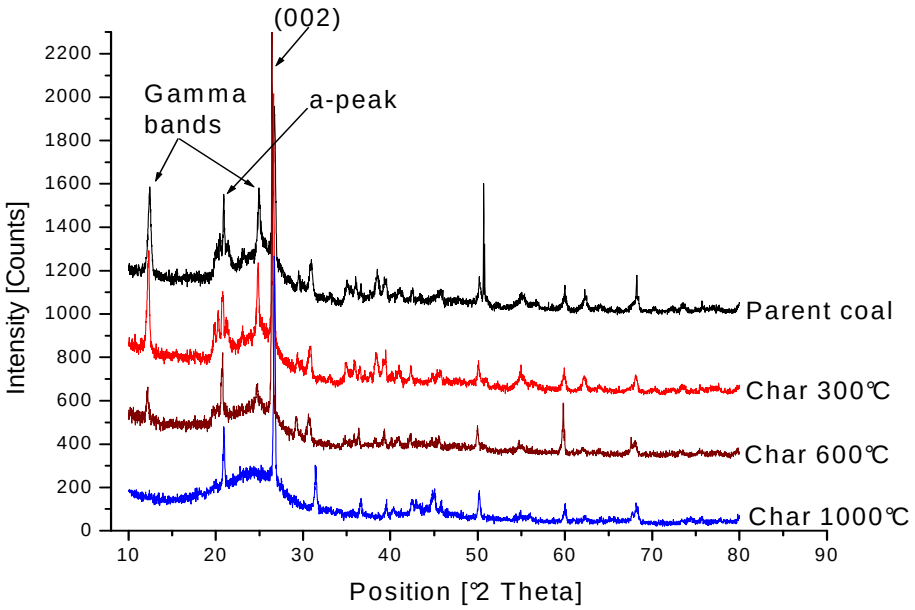

Figure 4.10: Summary on PXRD spectra of parent coal and the resultant chars (PBBR chars)[2]

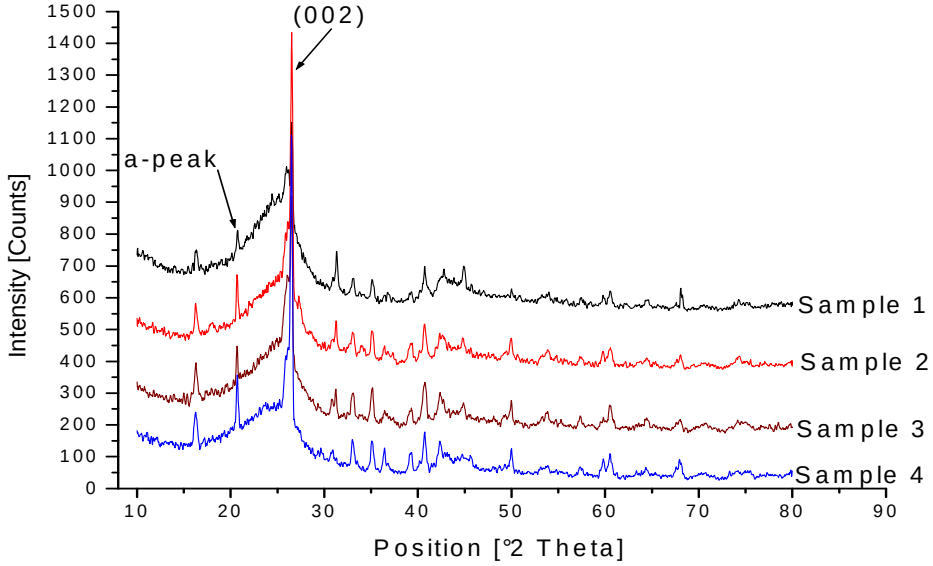

Figure 4.11: Summary on PXRD spectra of DTF chars prepared at 1400°C.[3]

[2; 3] Spectra in Figure 4.10 and 4.11 have been offset on the y-axis for clarity.

4.5 Raman spectroscopic analysis

Figure 4.12 below shows a summary of spectra generated from the coal and the char samples at different temperatures, which shows a decrease in the bandwidths with the increase in temperature.

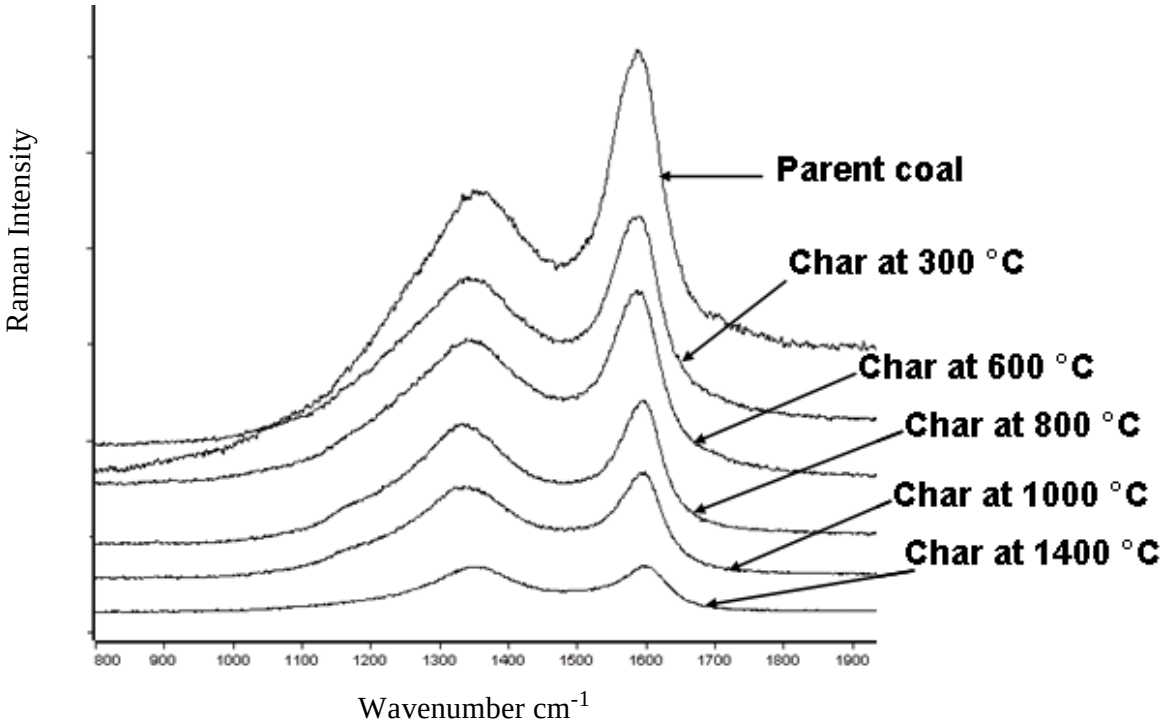

Figure 4.12: Raman spectra generated from parent coal and different char samples[4].

In order to improve the accuracy in the determination of spectroscopic parameters such as peak position, bandwidth, line shape (i.e., Lorentzian, Gaussian or a mixture of both) and band intensity, each spectrum was subjected to curve fitting using curve fitting software in OPUS. From the curve fitting program, mathematical fitting procedures/models were set up following the procedures outlined in Sadezky *et al*. (2005), Dippel *et al*. (1999), Jawhari *et al*. (1995), Cuesta *et al*. (1994), and Nistor *et al*. (1994), as summarised in Table 4.5 below.

---

[4] Spectra in Figure 4.12 have been offset on the y-axis for clarity and the Raman intensity is referred as arbitrary units.

Table 4.5: Band combinations tested for curve fitting of first-order Raman spectra of coal [I (Cuesta *et al*. 1994); II (Jawhari *et al*. 1995) and III] and char particles [IV (Dippel *et al*. 1999); V; VI; VII; VIII] in this work and earlier studies (initial position; line shape: L = Lorentzian, G = Gaussian and L+G = mixture of Lorentzian and Gaussian).

Band	**Initial position**	**I**	**II**	**III**	**IV**	**V**	**VI**	**VII**	**VIII**
G	1592	L	L	100% L+G	L	L	L	L	100% L+G
D1	1350	L	L	100% L+G	L	L	L	L	100% L+G
D2	1620	-	-	-	-	L	L	-	-
D3	1530	L	G	G	L	L	G	G	G
D4	1180	-	-	-	L	L	L	L	100% L+G

The models above were used to fit all the spectra obtained from the coal or char samples. Band fitting combinations I, II and III were tested for the parent coal sample; and IV, V, VI, VII, and VIII combinations tested for curve fitting the char spectra. The best fittings were found through combination III (for coal) and combination VIII (for chars). The reason for not including the D4 band (originating from sp3/ sp2-sp3 bonded carbon) on the curve fitting of coal spectra in the adjusted deconvolution was because Raman spectra detected in the sample had no obvious trace of graphitic microcrystallinity (Nistor *et al*. 1994). The parameters such as peak position, intensity, width, integral, and shape were obtained for each coal/char particle analysed. Multiple spectra (~50 spectra) were obtained from the parent coal and from each char sample. The average values as well as the standard deviations of the Raman structural parameters were then obtained from each sample. Figure 4.13 shows some typical curve fitted spectra measured at different temperatures. The ratios of the intensity of the D bands to the intensity of the G band (I_{D4}/I_G, I_{D1}/I_G, I_{D3}/I_{D3}) will be discussed, followed by discussion on the D and G bandwidths, as well as G band position. The word “mixture” labeled in Figure 4.14, 4.15,

4.16, 4.17, 4.18 and 4.19 refers to all the chars together without differentiating between dense and porous.

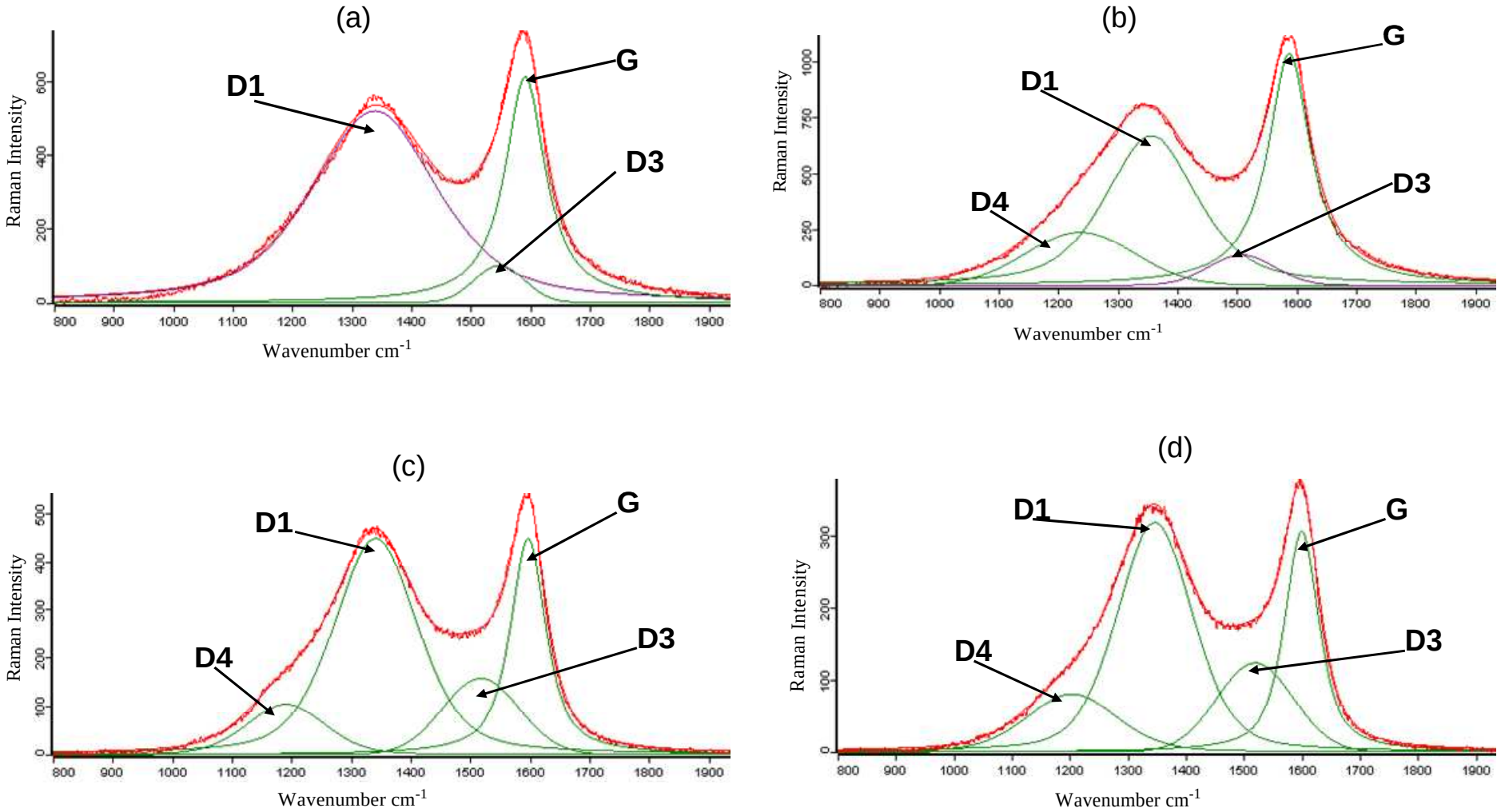

Figure 4.13: First order region Raman spectra of coal and the resultant chars, (a) Parent coal and char 300°C spectrum overlapping, (b) char600°C spectrum, (c) char 800°C spectrum, (d) char 1000°C and char 1400°C spectrum overlapping[5].

[5] The vertical scales differ and done so that the spectra are clear.

The summarised results of the curve fitted spectra shown above (Figure 4.13) are presented in Tables 4.6 and 4.7 below. The complete data are available in Appendix C. The spectra of parent coal and of the sample charred at 300°C displayed the same deconvolution (Figure 4.13a). The spectra of the sample charred at 1000°C and 1400°C also displayed the same deconvolution (Figure 4.13d). It was observed that the spectra obtained from the same sample were different for different macerals. This was attributed to the heterogeneity of coal particles within a sample.

Table 4.6: Summarised results from micro Raman Spectroscopy (MRS) in PBBR chars.

Sample and Raman bands	Band position (cm^{-1})				Intensity ratios	Full width at Half maximum (cm^{-1})	Integral	RMS error	Stdev RMS error
	Lowest-highest		Average/ mean	Standard deviations					
					I_D/I_G				
Parent coal									
D1	1345	1359	1352 ± 3	5.3	0.96 ± 0.04	281 ± 8	160703	8.63	1.80
D3	1555	1566	1559 ± 2	3.9	0.32 ± 0.06	91 ± 1	13606		
G	1593	1595	1594 ± 1	0.8		87 ± 2	64503		
Char 300°C									
D1	1342	1359	1348 ± 3	7.6	0.91 ± 0.05	270 ± 6	181943	10.58	2.50
D3	1554	1561	1556 ± 2	3.2	0.27 ± 0.03	93 ± 4	14005		
G	1593	1595	1594 ± 1	0.9		84 ± 3	75066		
Char 600°C									
D4	1199	1281	1238 ± 8	5.3	0.23 ± 0.03	189 ± 21	56265	11.07	0.10
D1	1335	1364	1351 ± 3	3.5	0.80 ± 0.12	176 ± 4	184467		
D3	1505	1478	1529 ± 22	27.8	0.22 ± 0.06	135 ± 7	21255		
G	1587	1594	1591 ± 1	1.6		82 ± 2	111452		
Char 800°C									
D4	1206	1208	1207 ± 7	0.5	0.24 ± 0	165 ± 12	34497	7.31	0.01
D1	1343	1344	1343 ± 2	0.3	0.85 ± 0.09	161 ± 4	126014		
D3	1510	1510	1510 ± 7	0.2	0.29 ± 0.04	154 ± 11	31979		
G	1596	1596	1596 ± 1	0.1		72 ± 5	80514		
Char 1000°C									
D4	1200	1202	1200 ± 4	0.6	0.24 ± 0	183 ± 14	15737	3.01	0.05
D1	1348	1350	1349 ± 3	0.1	1.12 ± 0.01	157 ± 3	66631		
D3	1527	1531	1528 ± 1	0.9	0.42 ± 0	157 ± 1	21247		
G	1601	1602	1602 ± 0	0.2		70 ± 1	29935		

Table 4.7: Summarised results from micro Raman Spectroscopy (MRS) in DTF chars.

Sample and Raman bands	Band position (cm^{-1})				Intensity ratios	Full width at Half maximum (cm^{-1})	Integral	RMS error	Stdev RMS error
	Lowest-highest		Average/ mean	Standard deviations					
Sample 1					I_D/I_G				
Char 1400°C									
D4	1206	1239	1216 ± 3	7.3	0.18 ± 0	222 ± 9	6590	2.17	0.10
D1	1353	1356	1355 ± 9	0.8	1.20 ± 0	156 ± 1	37046		
D3	1527	1539	1533 ± 2	1.8	0.38 ± 0.01	153 ± 3	8679		
G	1602	1605	1603 ± 0	0.3		75 ± 4	14170		
Sample 2									
Char 1400°C									
D4	1211	1273	1230 ± 1	13.0	0.21 ± 0	240 ± 7	9817	2.27	0.10
D1	1352	1356	1354 ± 5	0.9	1.21 ± 0	152 ± 2	41988		
D3	1535	1539	1537 ± 7	1.0	0.42 ± 0	153 ± 1	10904		
G	1602	1604	1603 ± 1	0.3		73 ± 1	15943		
Sample 3									
Char 1400°C									
D4	1205	1234	1217 ± 4	8.0	0.21 ± 0.02	228 ± 10	8490	2.17	0.02
D1	1353	1356	1355 ± 6	0.9	1.25 ± 0	154 ± 1	39155		
D3	1537	1539	1538 ± 3	0.01	0.46 ± 0	162 ± 3	11259		
G	1603	1604	1604 ± 0	0.01		73 ± 1	14199		
Sample 4									
Char 1400°C									
D4	1201	1222	1211 ± 3	9.9	0.20 ± 0	221 ± 5	6303	2.08	0.07
D1	1355	1357	1356 ± 7	0.2	1.28 ± 0	161 ± 3	35111		
D3	1539	1542	1540 ± 2	0.3	0.48 ± 0	161 ± 1	9529		
G	1603	1605	1604 ± 0	0.5		74 ± 2	11706		

The effect of heat treatment temperature to some Raman spectroscopic parameters such as intensity ratios of D1, D3 and D4 band to the G band, D1 and G bandwidths and G band position is discussed below.

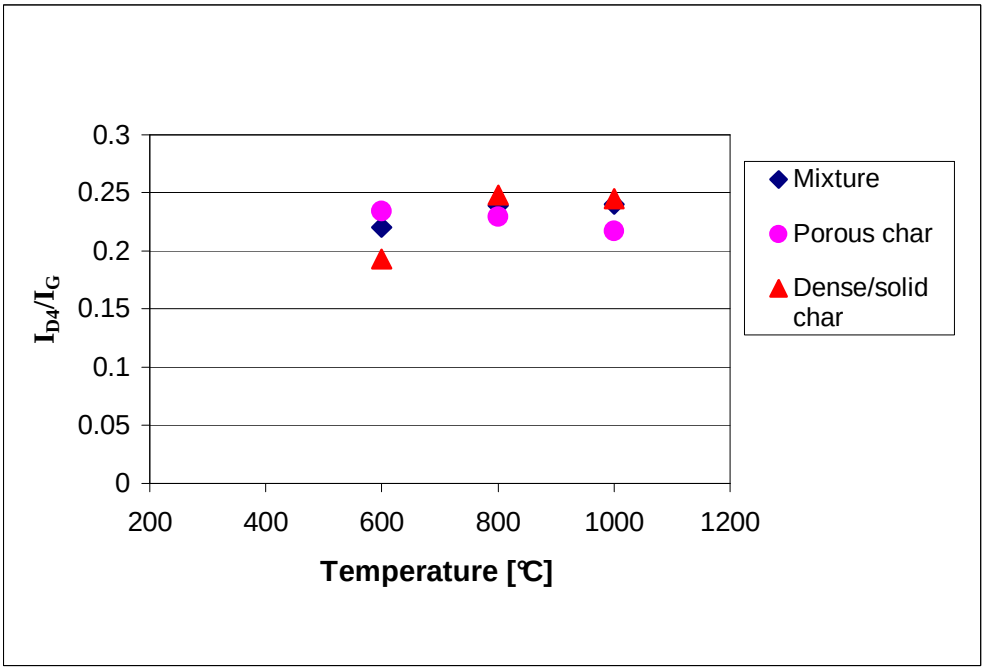

Figure 4.14: First-order intensity ratio (I_{D4}/I_G) versus heat treatment temperature of chars[6].

Figure 4.14 shows the relationship between I_{D4}/I_G and heat treatment temperature. The interpretation of the ratio (I_{D4}/I_G) is attributed to the abundance of sp3 (Schwan *et al*. 1996) or sp2-sp3 sites (Basca *et al*. 1993) and would imply an association with the concentration of active carbon sites (Livneh *et al*. 2000). From such an interpretation it is expected that this ratio should decrease monotonically with temperature, because annealing decreases the number of active sites. This was only proven true when considering the porous chars derived from vitrinite particles. In contrast, this ratio was seen to increase up to ~950°C when considering dense chars (derived from inertinite particles) and the whole char mixture (overall mixture). With a further increase in temperature, above 950°C, a monotonic decrease in the ratio was observed, as expected

[6] "Mixture" labeled in Figure 4.14, 4.15, 4.16, 4.17, 4.18, and 4.19 refers to all the chars together without differentiating between dense and porous.

(Zaida *et al*. 2007). The initial increase in this intensity ratio can be attributed to the preferential creation of sp2-sp3 bonding by annealing very small crystallites. Above 950°C there is a consumption of sp2-sp3 bonds by further annealing and I_{D4}/I_G ratio decreases (Zaida *et al*. 2007). Dense/solid chars show the same trend as the overall mixture which could indicate that the parent coal could be dominated by inertinite macerals, as confirmed petrographically in Section 4.3 (Table 4.2).

The difference in the behaviour of the chars originating from the two macerals (inertinite and vitrinite) as shown in Figure 4.14 could be due to their different organic structural composition, since the inertinite-rich coal is more aromatic and more polycondensed (indicated by a higher bridgehead carbon content) than vitrinite-rich coal. The inertinite-rich coal is structurally more ordered, with a high degree of crystalline stacking (Van Niekerk *et al*., 2008). At 300°C, no chars were obtained as the sample only contained unheated coal macerals and hence the points of the figures begin at 600°C. In conclusion, it could be noted that reflectance shows the change earlier than morphology.

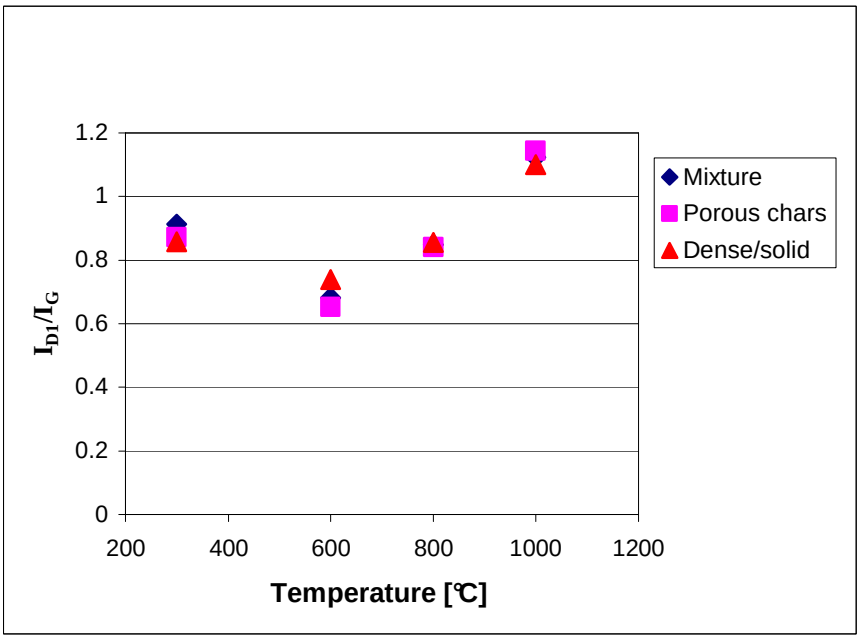

Figure 4.15: First-order intensity ratio (I_{D1}/I_G) versus heat treatment temperature of chars.

Figure 4.15 shows that the I_{D1}/I_G ratio cannot be used blindly to quantitatively characterise the degree of disorder in the carbon material as suggested by Tuinstra and Koenig (1970). It was expected that this ratio would decrease monotonically with temperature, which was observed only in the range from parent coal up to char 600°C. However, there was an increase in the ratio (I_{D1}/I_G) from char 600°C upwards. It may be said that the initial decrease in I_{D1}/I_G was observed purely because coal/char has extremely complex structure at the molecular level up to about 600°C because of the remaining atomic groups containing H or O as shown by Yamauchi and Kurimoto (2003). The value of root mean square (RMS) error/standard deviation obtained from curve fitted spectra was quite high, ranging between 8.63 on parent coal to 13.81 at 600°C (Table 4.6) and could indicate largely differing structures. The I_{D1}/I_G ratios reported in open literature are widely inconsistent, since these (I_{D1}/I_G) are difficult to measure correctly due to strongly overlapping bands (Sheng, 2007; Zaida *et al*. 2007; Zaida *et al*. 2006; Yamauchi and Kurimoto, 2003; Johnson *et al*. 1986; Green *et al*.1983). Therefore trends of the intensity ratios of D band to the G band (I_{D1}/I_G) with increase in heat treatment temperature are also inconsistent.

Work done on magnetron sputtered carbon films at temperatures varying from 30-450°C by Cho *et al*. (1992) led them to an assumption that at the initial stage of annealing, the increase of the number of graphitic clusters and their degree of crystallinity takes place without changing their size. Above 600°C, there was an increase on the I_{D1}/I_G ratio for the char samples. Such behaviour has also been observed by Livneh *et al*. (2000). They speculated that below a certain size the crystallites are "invisible" to the Raman effect. Initially, the crystallites of the char are too small to effectively couple with the incident/incoming laser beam, and thus contribute little to the Raman spectrum. Upon high temperature the crystallites grow in size, and thus begin to contribute to the Raman spectrum, causing the ratio I_{D1}/I_G to decrease. Similar behaviour of the intensity ratio (I_{D1}/I_G) has also been observed when considering the individual particles, for example, porous chars derived from vitrinite particles and dense/solid chars derived from inertinite particles.

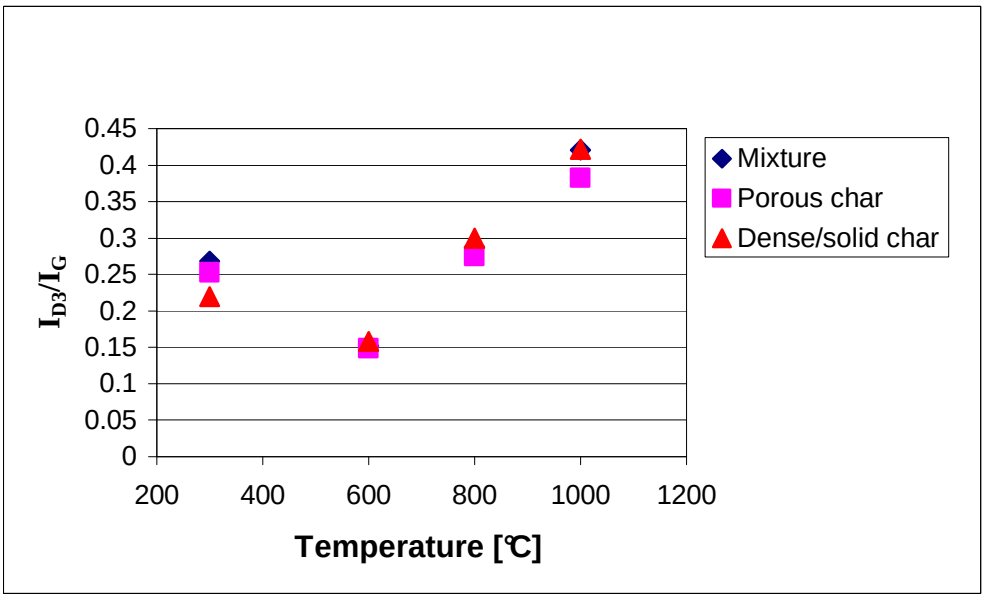

Figure 4.16: First-order intensity ratio (I_{D3}/I_G) versus heat treatment temperature of chars.

Figure 4.16 shows the relationship between I_{D3}/I_G and heat treatment temperature. The decrease could be assigned to a decrease in disordered C or the increase of graphitic character. From 600°C upwards, the behaviour was similar to that of the D1 (I_{D1}/I_G) band.

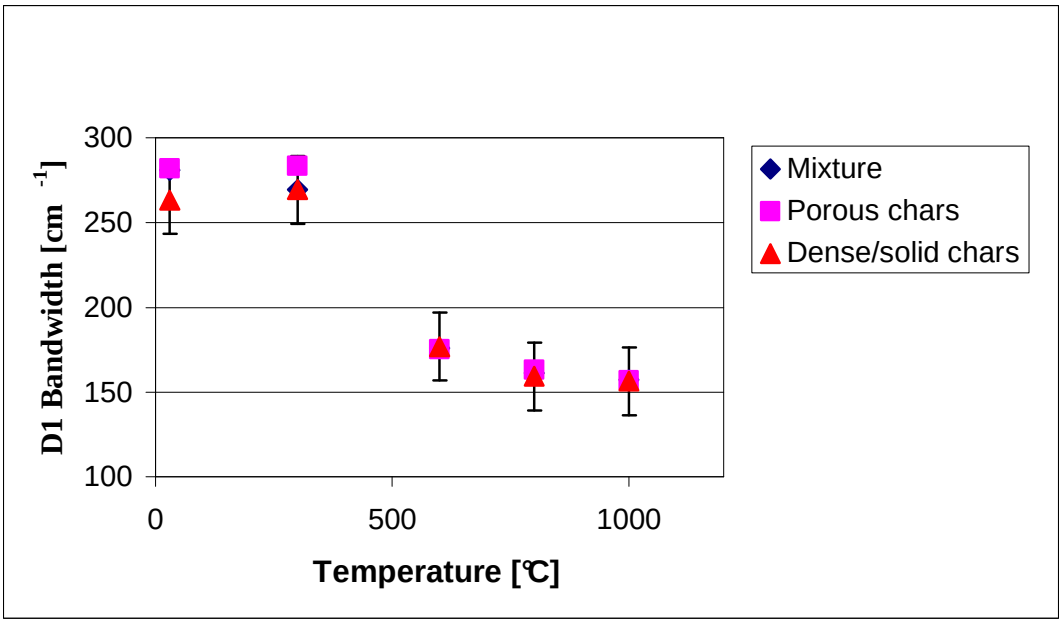

Figure 4.17: First-order bandwidth of D1 band versus heat treatment temperature of chars.

Figure 4.17 shows that the D1 bandwidth decreases with increase heat treatment temperature. This agrees well with the graph of D bandwidth versus heat treatment temperature reported previously (Johnson *et al*. 1986; Green *et al*. 1983), but the difference is not that significant as the error bars indicate.

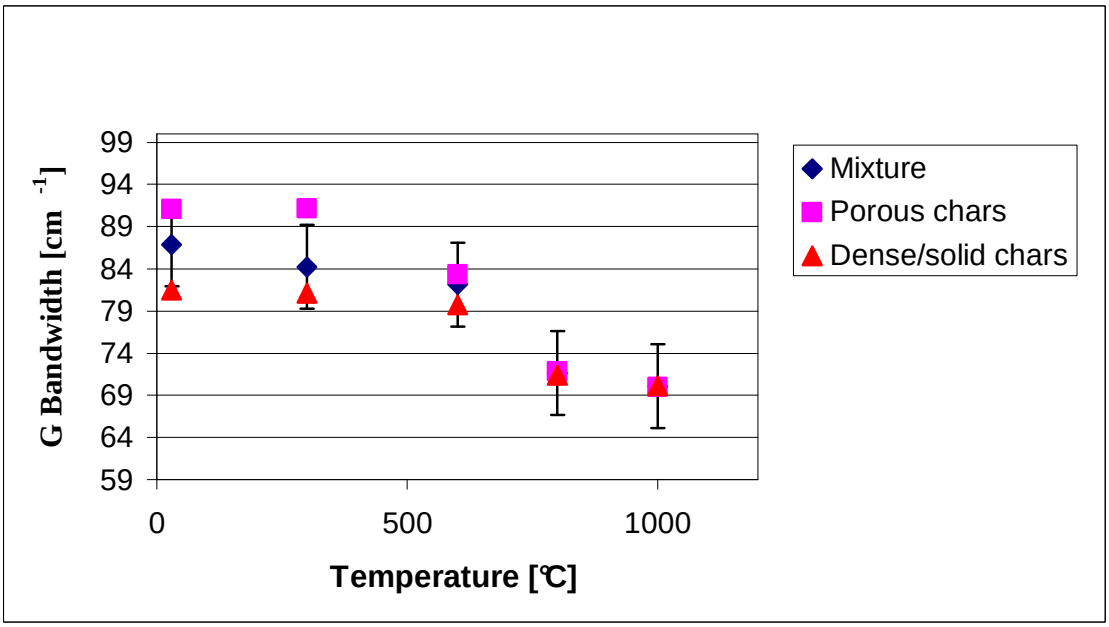

Figure 4.18: First-order bandwidth of G band versus heat treatment temperature of chars.

Figure 4.18 shows that the G bandwidth decreases with increase in heat treatment temperature from parent coal up to chars at 1000°C. As expected, this could be caused by annealing which makes the graphene layers larger and hence, a decrease of G bandwidth was seen (Zaida *et al*. 2006; Bar-Ziv *et al*. 2000; Green *et al*. 1983). These results confirm that the G band is related to the crystalline component in carbons. The observed decrease of G bandwidth with increasing heat treatment temperature is consistent with what has been reported in the literature (Zaida *et al*. 2006; Bar-Ziv *et al*. 2000; Green *et al*. 1983).

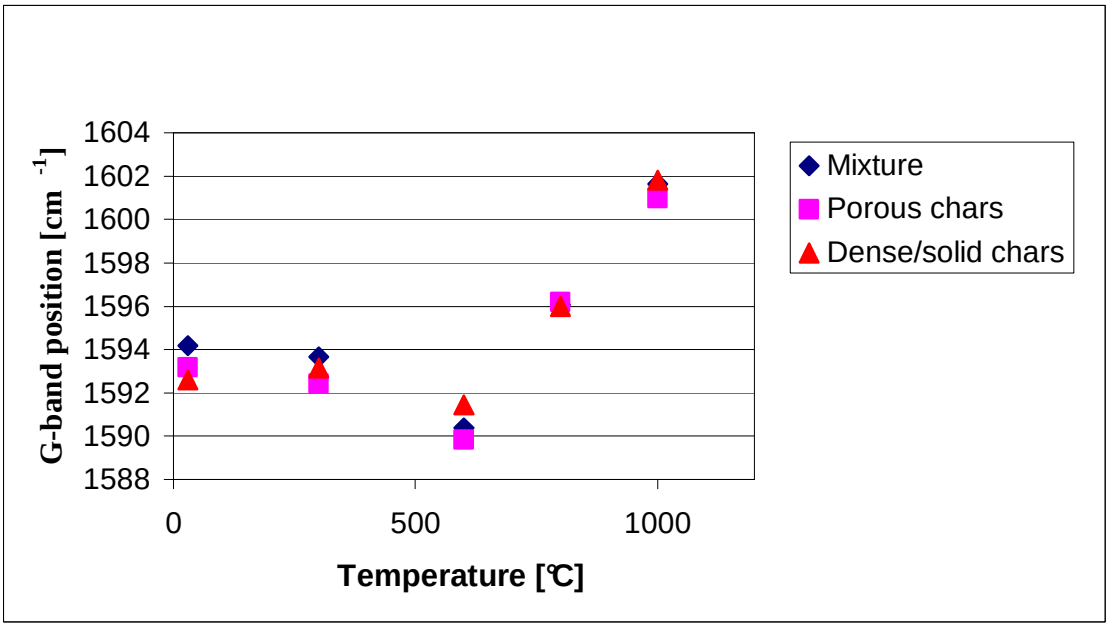

Figure 4.19: G-band position versus heat treatment temperature of chars.

It was found (Tables 4.6 and 4.7) that the variations of the bands positions (D band positions) with the heat treatment temperature were not significant, which might be attributed to the experimental errors and the strong overlapping of the bands. It was reported by Robertson (1986) that an increase of order in carbonaceous materials was reflected by an increase in the frequency of the G mode as well as a decrease of its bandwidth (Figure 4.18 and 4.19). Figure 4.19 shows that there was a slight decrease in G band's position up to 600°C, which could be explained by the "invisibility" to the Raman effect of the very small crystallites. This might also be possible due to the fact that the D2 mode, which usually appears at about 1620cm^{-1} as a shoulder, was not observed and probably interferes with the G mode, thus complicating the interpretation (Jawhari *et al*. 1995). Further annealing makes the graphene layer larger (which indicates lower degree of band-angle disorder) and hence an increase was seen, as expected (from 600°C upwards).

4.5.1 Conclusions

MRS proves to be a useful technique for obtaining information on the crystalline and molecular structure of coal and chars. Raman parameters such as intensity ratio of D band relative to G band (I_D/I_G), D and G bandwidths, G-band position were used to determine the insight of the char structure and the effect of heat treatment on the structural evolution of char. The results obtained from I_D/I_G in the range from coal up to char 600°C showed a decline in the intensity ratio with an increase in temperature, which could be attributed to the coal/char having extremely complex structure at the molecular level up to about 600°C because of the remaining atomic groups containing H or O. Above 600°C, the intensity ratio of I_{D1}/I_G started to increase, which showed the increase in the size of the crystallites.

It was found that sp2-sp3 bonding (reactive sites/crystallites) was created in dense chars (originating from inertinite particles), indicated by the increase in I_{D4}/I_G ratio with an initial heat treatment temperature and these sp2-sp3 bondings were known to be consumed later at high temperature. These could be because inertinite particles are carbon-rich, creating sp2-sp3 bonding by annealing aromatic structures. Earlier consumption of sp2-sp3 bonding (indicated by decrease in I_{D4}/I_G ratio) was observed in porous chars from the start, because they were vitrinitic in origin and contained more reactive sites (more oxygen-rich and easier consumption of Sp2-Sp3 bonding from the start). From the D and G bandwidth results, it was found that the parent coal bands (D and G band) were relatively broad, indicating that its crystallite size was too small to couple with the Raman laser. But as the annealing temperature increased, the bandwidths seemed to decrease which was consistent with the removal of disorder and the increasing dominance of crystallites. The results obtained show the usefulness of MRS technique on characterizing coal and char structure, and confirm the results of the other researchers in this field (Sheng 2007; Zaida *et al*. 2007; Zaida *et al*. 2006; Yamauchi and Kurimoto, 2003; Bar-Ziv *et al*. 2000; Livneh *et al*. 2000; Schwan *et al*. 1996; Basca *et al*. 1993; Johnson *et al*. 1986; Green *et al*. 1983; Tuinstra and Koenig, 1970).

4.6 Reactivity on coal and chars

Char combustion reactivity was measured using thermogravimetric analyzer (TGA) as discussed in Section 3.8. The shape of the TGA curve can give useful information about the presence of carbonaceous materials such as amorphous carbon. In order to study the reactivity of coal and chars, TGA data were collected from a Perkin-Elmer TGA analyser in flowing oxygen gas at 34ml/min. and the results are presented in Figure 4.20. This figure shows a strong influence of heat treatment on char reactivity. This is also reported by Radovic *et al*. (1998) and Jones and Thrower (1991).

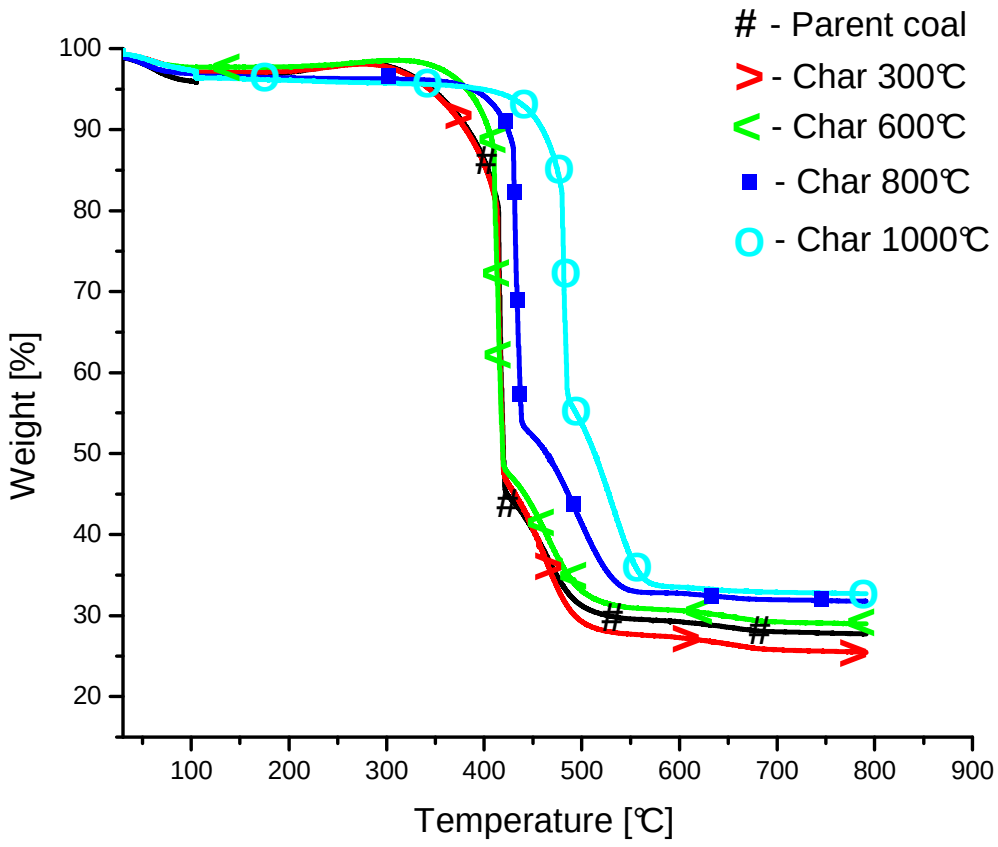

Figure 4.20: TGA results of parent coal and the resultant chars formed at different temperatures (300-1000°C).

All samples showed similar oxidation behaviour with weight loss stage at different temperatures (Figure 4.20). Decomposition of coal and chars was observed in the temperature range 350-550°C. Generally, this account for most of the weight loss of approximately 70%. The results show that as charring temperature increases, chars become more stable due to the increase in loss of carbon.

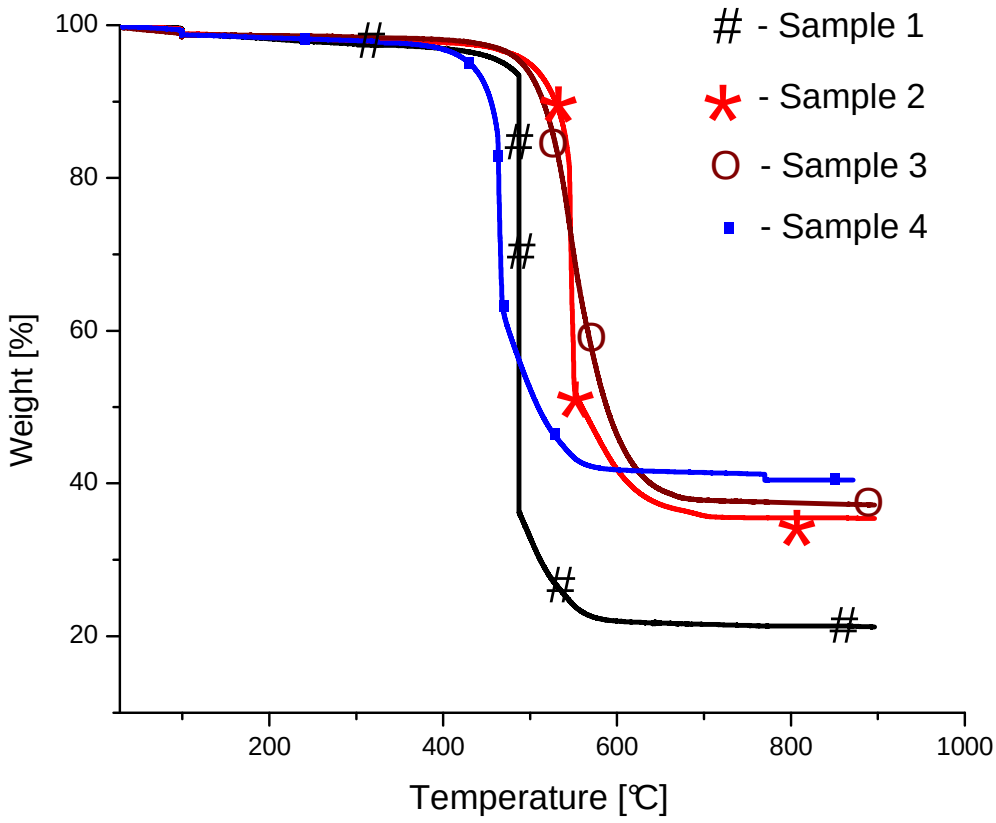

Figure 4.21: TGA results of DTF chars formed at 1400°C.

The four DTF chars show a difference in their reactivities (Figure 4.21). Sample 4 shows decomposition earlier as compared to the other three DTF samples. This could be due to the high mineral matter which acts as a catalyst during the reaction. This is confirmed by high percentage ash (40.5%) in Sample 4 obtained from proximate analysis (Figure 4.2). The four DTF results are relatively consistent with proximate analysis data presented in

Section 4.2 (Figure 4.2) in terms of ash contents, which increases from 23.6% (Sample 1) up to 40.5% (Sample 4).

4.6.1 Conversion

The coal and char conversion at any time t was calculated from equation 1 below.

$$X = \frac{m_0 - m_t}{m_0 - m_{ASH}} X\,100\,\% \qquad (1)$$

Where m_0 and m_t are the sample weights on a dry basis at initial and time t, respectively, and m_{ASH} is the weight of the ash in the sample.

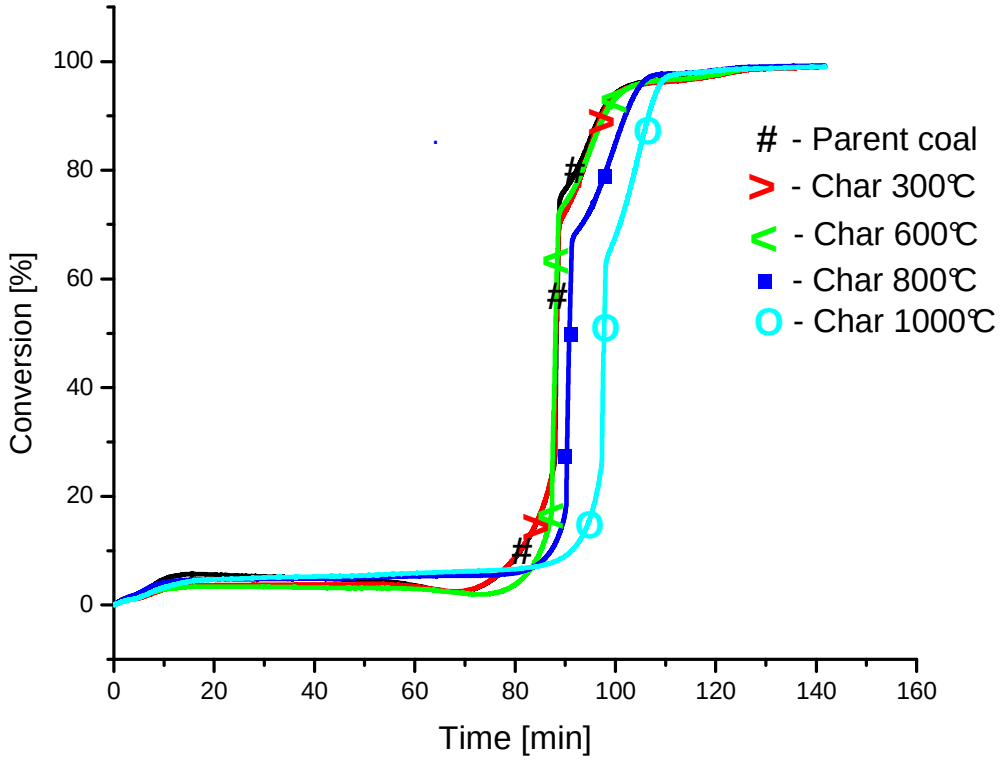

Figure 4.22: Conversion of parent coal and the resultant char versus time.

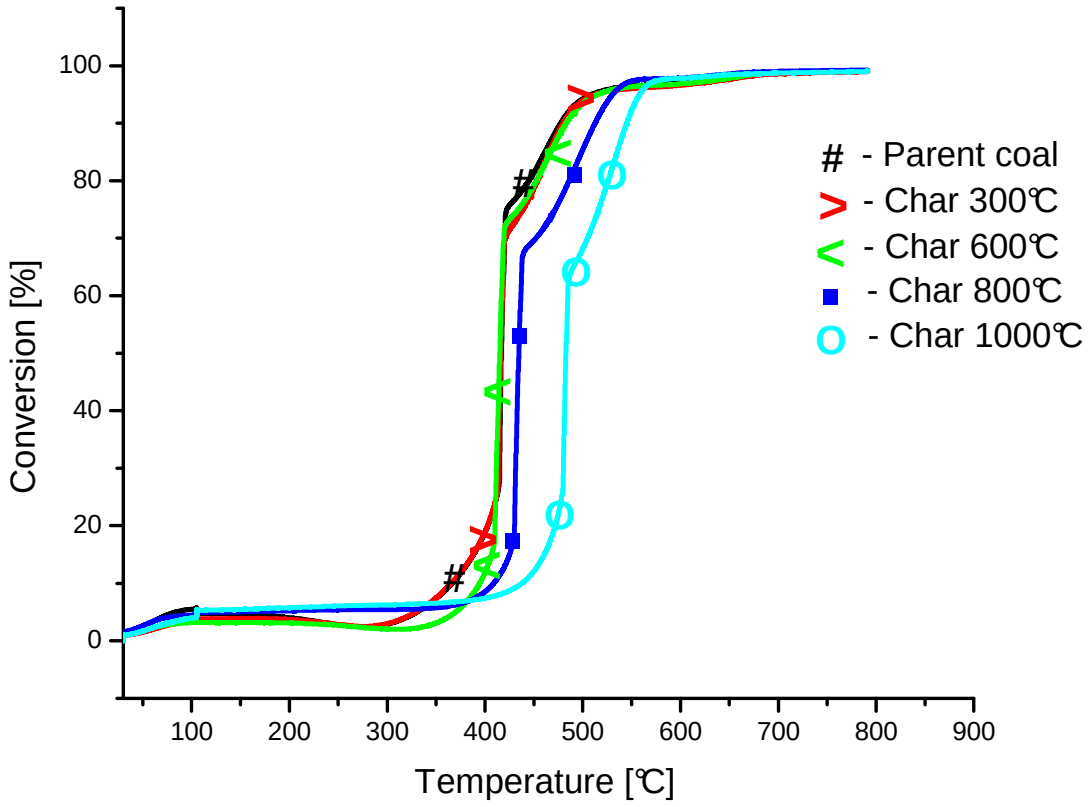

Figure 4.23: Conversion of parent coal and the resultant char at: 300-1000°C.

Combustion reactivity determination was attempted through 20% ($T_{20\%}$) and 50% ($T_{50\%}$) conversion following the procedure outlined in Zaida *et al*. (2007) and Sheng (2007). The results are presented in Appendix D. The results from 20% conversion ($T_{20\%}$) did not show good consistency. It was found that combustion reactivity of coal and chars could be measured with the help of sample temperature at 50% conversion ($T_{50\%}$). The value of $1/T_{50\%}$ was a good measure of the reactivity of the chars, and the results were consistent to what has been reported in the literature (Zaida *et al*. 2007). It is known that disordered carbon, in general becomes less reactive as heat treatment temperature increased (Blake *et al*. 1967). The results shown in Figure 4.24 confirm this observation. These was expected because as heat treatment temperature increases, the volatile matter decreases

while fixed carbon increases (Figure 4.1), and consequently result in the decrease in char combustion reactivity as shown in Figure 4.24.

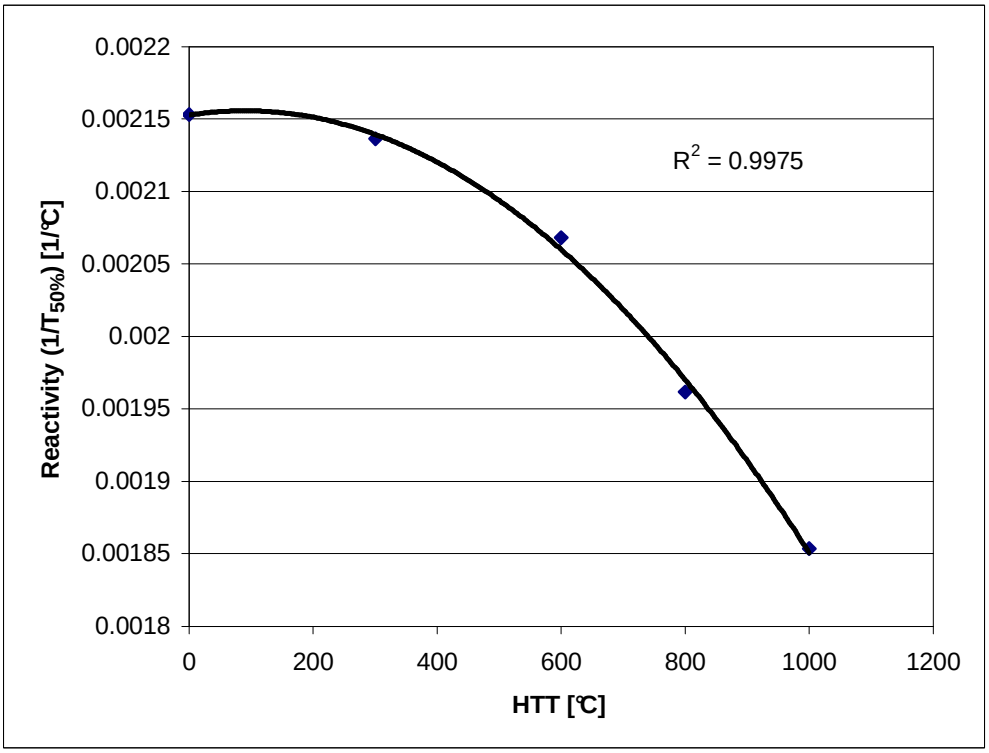

Figure 4.24: Reciprocal temperature for 50% conversion ($1/T_{50\%}$) as a measure of combustion reactivity versus heat treatment temperature.

4.7 Correlations between coal petrography, micro Raman spectroscopy (MRS) and Thermogravimetric analysis (TGA).

4.7.1 Correlations between Raman spectroscopy (D and G bandwidth) and coal petrography (through reflectance measurements).

Attempts were made to find correlations between results obtained from reflectance measurements (mean vitrinite reflectance and mean total reflectance) and MRS parameters (D1 and G bandwidths) (Figure 4.25). It was found that the reflectance measurements (MVR and MTR) correlated with Raman parameters (D1 and G bandwidth). Previous studies of G band reduction of Raman spectra of coals have observed that the G bandwidth can be correlated to mean vitrinite reflectance measurement (Beny-Bassez and Rouzaud, 1985), which is consistent to the results obtained in this study (Figure 4.25 (c)). Johnson *et al*. (1986) studied the characterization of coal chars by Raman spectroscopy, X-ray diffraction and reflectance measurements, where they found no correlations between reflectance and Raman measurements. The results obtained in this study show good correlation between the two parameters (D1 and G bandwidth and reflectance measurements) as illustrated in Figure 4.25 and Table E.1-E.4 (Appendix E). This means that the reflectance measurements can be used as an early indicator of changes in coal when heated, and the correlations enhance the understanding of char structural change during coal combustion.

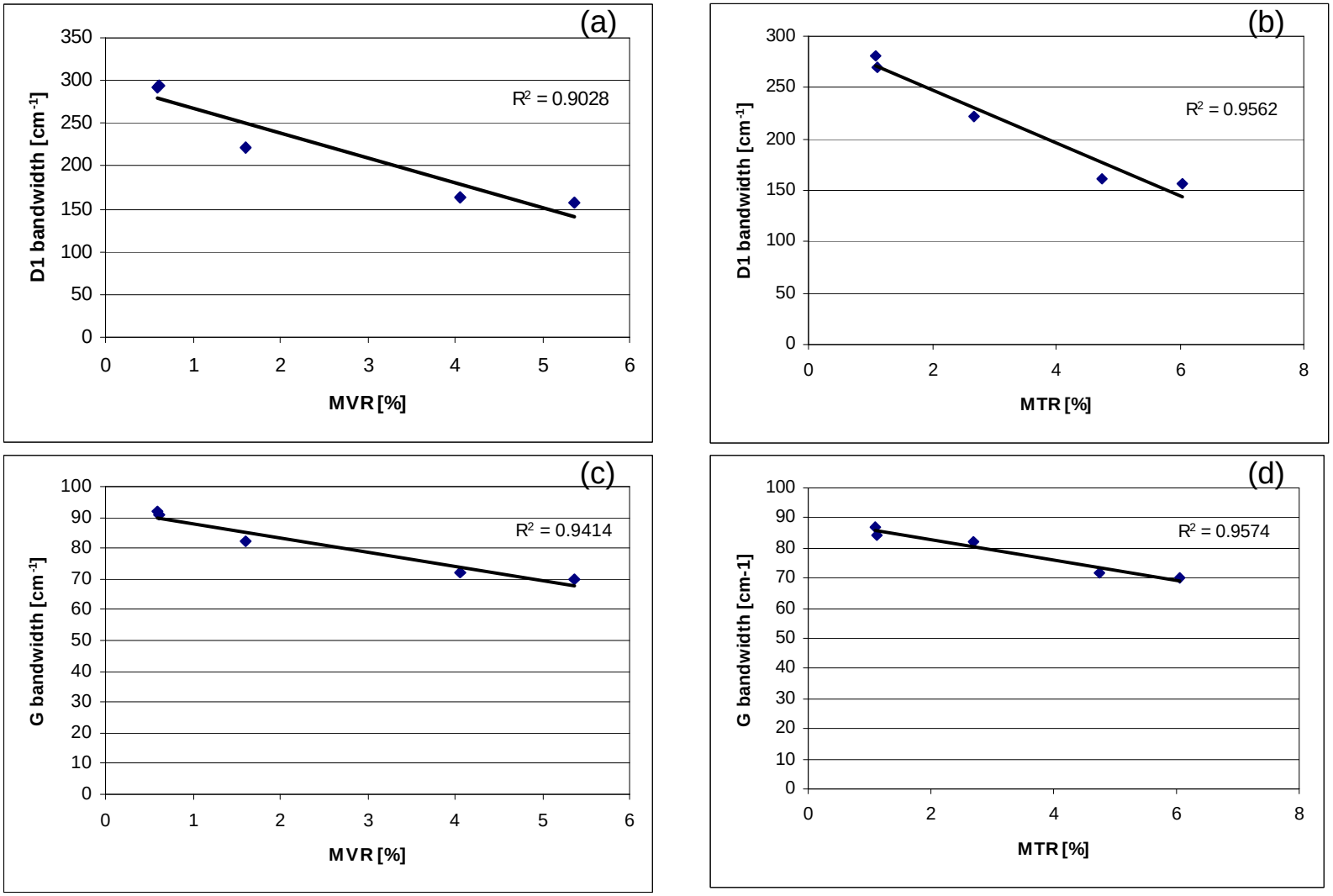

Figure 4.25: (a) D1 bandwidth correlated with mean vitrinite reflectance; (b) D1 bandwidth correlated with mean total reflectance; (c) G bandwidth correlated with mean vitrinite reflectance; (d) G bandwidth correlated with mean total reflectance.

4.7.2 Correlations between Raman spectroscopy (D and G bandwidth) and coal petrography (through % char petrographic count).

The results of D1 and G bandwidth were also correlated with percentage char morphology count obtained from petrography. This was attempted by identifying the reciprocal of D1 and G bandwidth from MRS and percentages of porous and dense char particles determined petrographically. Results are shown in Figure 4.26, where good correlations were obtained through the D1 bandwidth with porous and dense chars (correlation coefficients better than 0.91 and 0.99 respectively) (Figure 4.26 (a) and (b)). The reciprocal of G bandwidth versus % of porous particles/and dense particles did not show good correlation as the plots had lower correlation coefficients to be 0.85 and 0.68 (Figure 4.26 (a) and (b) respectively) (Tables E.5 and E.6 in Appendix E). Since the G band is a graphitic character caused by C-C vibration in the aromatic layers, while the D1 band originates from imperfections in-plane located between the basic structural units (graphene layers). Then at low temperature (below 1000°C), pyrolysis would mostly influence D1 band than G band as shown in Figure 4.17 and 4.18, the influence on D1 bandwidth was more significant than G bandwidth. These resulted on better correlation of Raman spectroscopy and petrography through D1 bandwidth. The correlations confirm the strong connection between char structure and char morphology (determined through petrographic count), and enhance the understanding of coal combustion.

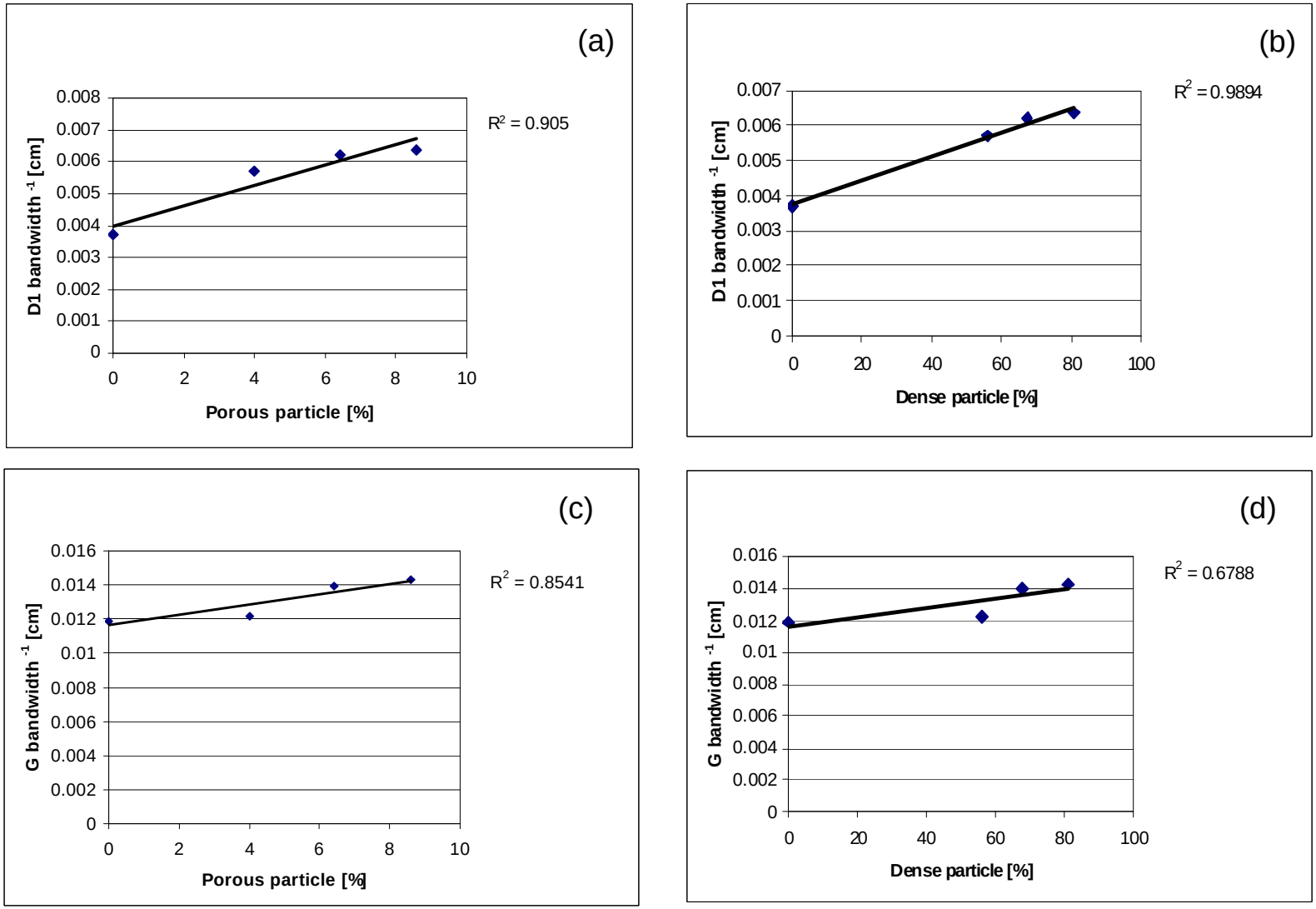

Figure 4.26: (a) Reciprocal of D1 bandwidth correlated with % porous particles; (b) reciprocal of D1 bandwidth correlated with % dense particles; (c) reciprocal of G bandwidth correlated with % porous particle; (d) reciprocal of G bandwidth correlated with % dense particle.

4.7.3 Correlating combustion reactivity (from TGA) with reflectance measurements

Attempts were also made to find the correlation between the TGA combustion reactivity and the reflectance measurements (MVR and MTR). This was attempted through the plot of $1/T_{50\%}$ versus MVR or MTR (Appendix E.3). It was found that the combustion reactivity showed a good correlation with both MVR and MTR with correlation coefficients of 0.96 and 0.91 respectively (Figure 4.27 (a) and (b). The trend of decrease in combustion reactivity with the increase of rank was observed, which agrees with most of the previous work (Morgan and Roberts, 1987; Jenkins *et al*. 1973). The trend shown in Figure 4.27 (a) could be due to the chemical properties of vitrinite varying in a systematic way with rank (Tang *et al*. 2005a, 2005b). Similar observation was also found by Thomas and co-workers (Thomas *et al*. 1991, 1989a, 1989b) on the investigation of Australian coals, where they found the combustion reactivity to correlate well with coal rank (vitrinite reflectance and elemental carbon). The correlations confirm the strong connection between char reactivity and reflectance, and enhance the understanding of coal combustion.

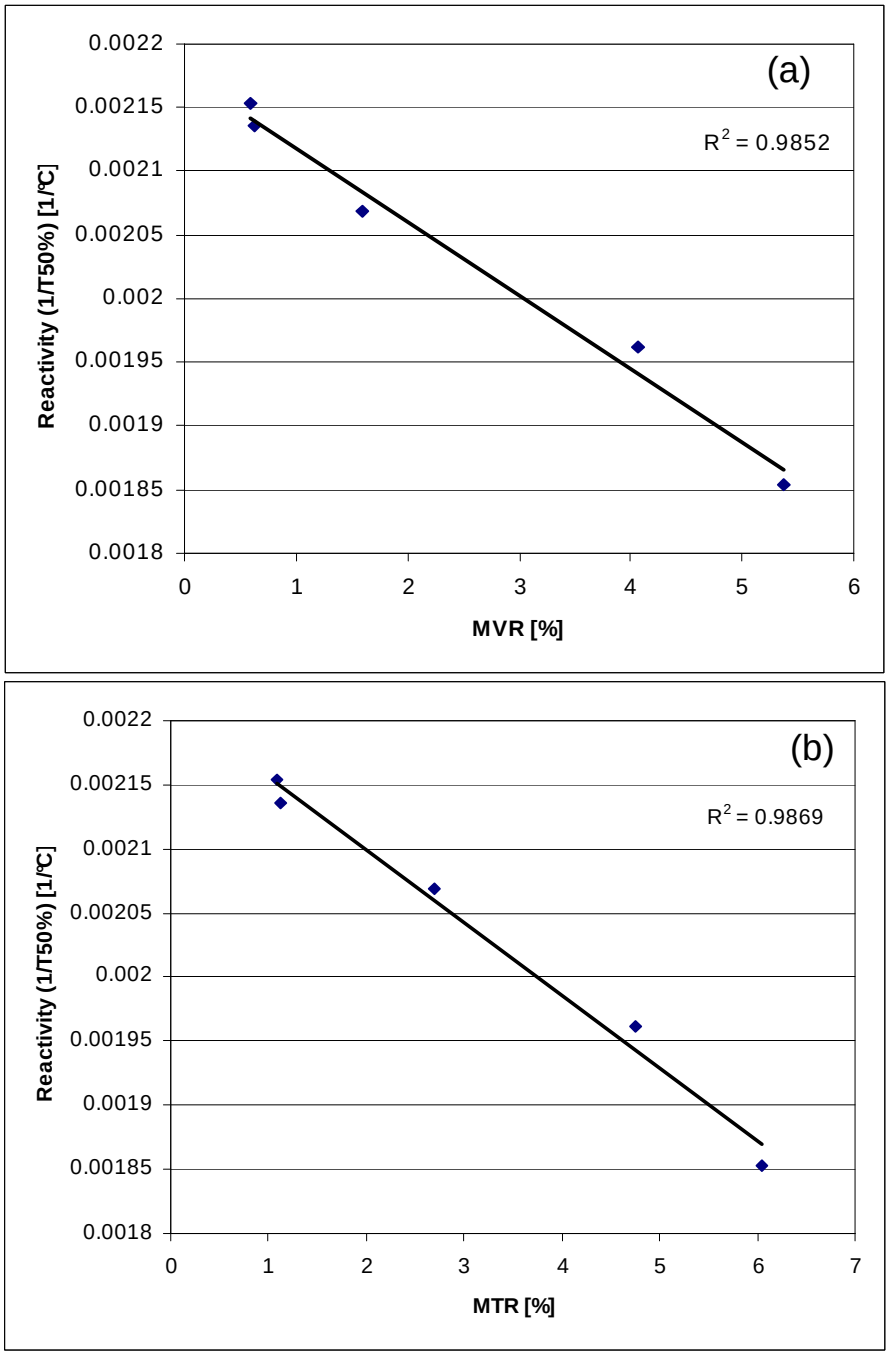

Figure 4.27: (a) The combustion reactivity ($1/T_{50\%}$) correlated with rank (mean vitrinite reflectance); (b) the combustion reactivity ($1/T_{50\%}$) correlated with rank (mean total reflectance)

4.7.4 Correlating combustion reactivity (from TGA) with structure (from MRS)

Attempts were also made to find the correlation between the TGA combustion reactivity and the char structure. This was attempted through the plot of $1/T_{50\%}$ versus the D1 and G bandwidth (Appendix E.4). Good correlations were found between combustion reactivity and D1 and G bandwidth measured from MRS, as shown by the plots with the correlation coefficients of 0.91 and 0.94 (Figures 4.28 (a) and (b) respectively). The correlations confirm the strong connection between char reactivity and char structure, and enhance the understanding of coal combustion.

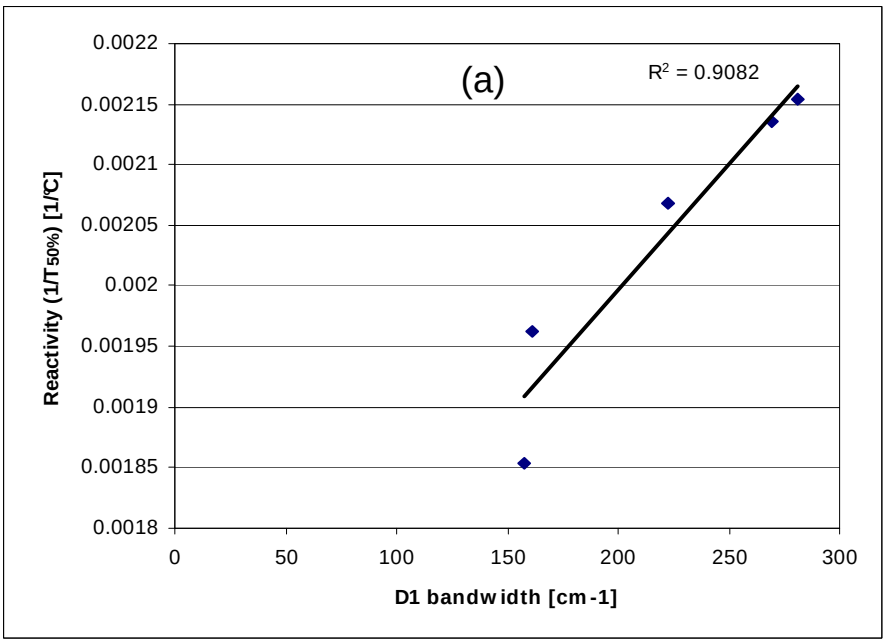

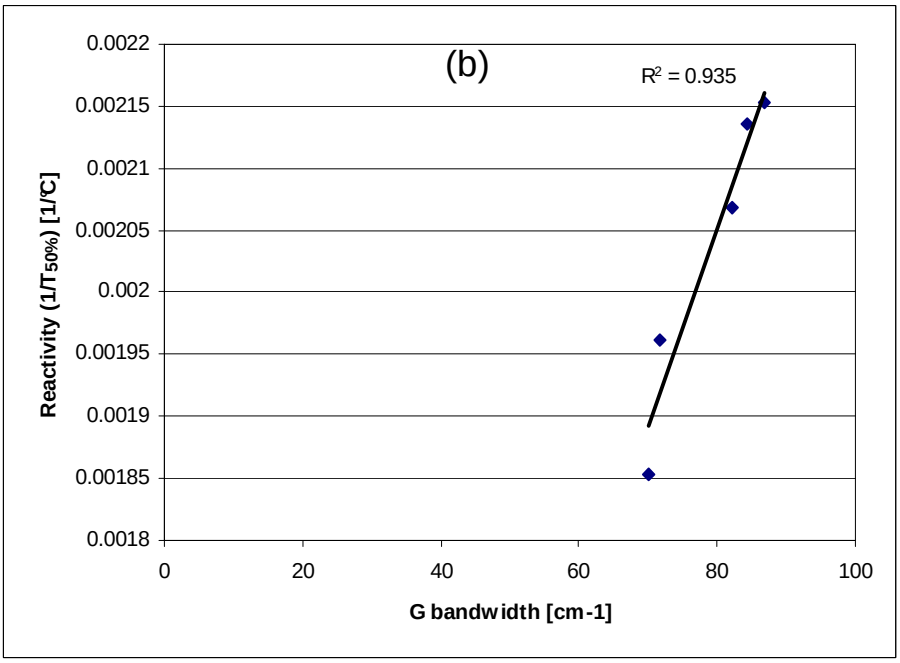

Figure 4.28: (a) The combustion reactivity ($1/T_{50\%}$) correlated with D1 bandwidth; (b) the combustion reactivity ($1/T_{50\%}$) correlated with G bandwidth.

4.8 Summary

The chapter presented the results obtained from different techniques, which included proximate analysis, coal petrography, PXRD, MRS and TGA. The results from these techniques showed the effect of heat treatment temperature on the char structural evolution and the reactivity during combustion. In conclusion, correlations were drawn between some of these techniques. Reflectance measurements showed good correlations with Raman parameters (D1 and G bandwidth), which led to the conclusion that the best correlation between Raman spectroscopy and coal petrography was through reflectance measurements. Figure 4.26 shows that the correlation between Raman spectroscopy and coal petrography can be obtained not only through reflectance measurements and D1 and G bandwidth, but also through % char petrographic counts and D1 and G bandwidth. The combustion reactivity results (from TGA) was also correlated with the first-order Raman bandwidth (D1 and G bandwidth) measurements, which contradicts the findings by Zaida *et al*. (2007) as illustrated in Figures 4.28 above.

CHAPTER 5

5.1 General conclusions

The dissertation presents the results for the characterization of typical Witbank coal and its respective chars derived from the same parent coal prepared at different temperatures (300°C-1400°C). Raman spectroscopy, petrography, TGA and XRD were the key characterisation tools applied. The following conclusions have been made from this investigation:

(1) (a) It was found that the reflectance measurement increases with heat treatment temperature (from parent coal up to char 1000°C) which is attributed to increasing anisotropy resulting from changing mutual orientation of the aromatic layers. The reflectance results are presented in Appendix B (Table B1).

(b) The reflectance measurements of the parent coal and low temperature chars prepared at 300 and 600°C seemed to show a minor increase of MVR and MTR. This might be due to the fact that at these temperatures, the samples are dominated by macerals found in the parent coal. There was major increase in MVR & MTR between 600°C and at 800°C. This might be because the particles were experiencing a marked devolatilisation with complete conversion of all macerals. These samples consisted of a large fraction of dense char originating from the inertinite particles.

(c) It can be concluded from this study that the reflectance measurements should not only be done on vitrinite reflectance and vitrinite chars, but it should also be done by considering all macerals and their respective chars as there were better correlations between MVT, MTR and Raman spectroscopy. These might be taken as an advantage to South African coals, especially Witbank coals, since they are rich in inertinite macerals.

(2) It was found petrographically that the parent coal (Witbank coal) was rich in inertinite particles, low vitrinite content and very low liptinite content. This resulted in a high percentage of inert/dense chars at high temperature (for example 80.8% at 1000°C). Such particles showed little or no porosity, with no apparent softening on charring,

largely retaining their original coal macerals shape and form. In terms quantitative analysis, chars prepared at 300°C was found to have almost the same composition as the parent coal as illustrated in Table 4.3.3 and 4.3.4. The difference between the parent coal and the chars prepared at 300°C was determined through reflectance (rank) analysis.

(3) XRD results confirmed the presence of graphite-like structures to a small degree. This was evident by the positions at the (002) band that corresponds to the position of graphite band. The results also showed that the coal and the chars investigated contained aliphatic side chains which were indicated by gamma bands, which tend to disappear as the heat treatment temperature increased. The gamma band can be associated with disorder in the structure.

(4) MRS spectra were measured in the first-order region in the range 800-2000cm^{-1}. Three bands were observed for the parent coal, which included the G band at ~1590-1603cm^{-1}, D1 band at ~1343-1355cm^{-1} and D3 band at ~1507-1557cm^{-1}. There was an additional band (D4 band at ~1200-1232cm^{-1}) on char particle Raman spectra which was associated with reactive sites being created in chars. It was found that sp2-sp3 bondings were created in dense chars (originating from inertinite particles), with an initial heat treatment temperature, and the sp2-sp3 bondings were known to be consumed later at high temperature. This was because inertinite particles are carbon-rich, creating sp2-sp3 bonding by annealing aromatic structures. Earlier consumption of sp2-sp3 bondings were observed in porous chars from the start, because they were vitrinitic in origin and contain more reactive sites (more oxygen-rich and easier consumption of Sp2-Sp3 bonding from the start). The D1 bandwidth was found to decrease from 281cm^{-1} for the parent coal to 157cm^{-1} for the 1000°C char and could be associated with a reduction of disorder in coal and chars. The G bandwidth was also found to decrease from 87cm^{-1} for the parent coal to 70cm^{-1} for the 1000°C char, which was consistent with the growth of crystallites as charring temperature increased. In conclusion, MRS proves to be a useful technique for obtaining information on the crystalline and molecular structure of coal and chars.

(5) TGA experiments confirmed the significant influence of heat treatment temperature on the char samples. It was found that combustion reactivity of coal and chars could

be measured with the help of sample temperature at 50% conversion ($T_{50\%}$). The combustion reactivity was found to decrease with increase in heat treatment temperature, as expected.

(6) Reflectance measurements were found to correlate with Raman D1 and G bandwidth, as well as combustion reactivity. Raman D1 and G bandwidth were found to correlate with percentage char obtained from petrography. It can be concluded from this study that the best correlation between Raman spectroscopy and coal petrography is through reflectance measurement and Raman D1 and G bandwidth. Reflectance measurement was also found to correlate with combustion reactivity as proposed by various researchers (Thomas *et al.*, 1991, 1989a, 1989b). A good linear correlation was found between Raman D1 and G bandwidth and combustion reactivity. This correlation confirms the strong connection between char structure and its reactivity and illustrates the advantage of Raman spectroscopy with respect to other structural analyses.

Results obtained from this study answer the questions presented in Chapter 1 (Section 1.3) and also proves the hypothesis presented in Section 1.6. The results presented in this study shows that Raman spectroscopy provides good correlations with coal petrography, and the correlations were drawn through D1 and G bandwidths and reflectance measurements as well as through percentage dense and porous chars obtained. Raman spectroscopy provided better correlations with combustion reactivity as well as with petrography. It was found that the use of Raman spectroscopy in conjunction with petrography enables a better understanding of the behaviour of char during combustion. This would assist in solving problems associated with coal utilization including suitability for combustion, gasification and liquefaction.

5.2 Recommendations (Future work)

The study was conducted on parent coal and its respective chars up to 1000°C in the PBBR, and chars prepared in the DTF at 1400°C. The chars prepared in the different reactors show to have different characteristics in terms of quantitative composition determined petrographically. It was recommended that a reactor be obtained/sourced that could operate above 1000°C to make chars at much higher temperatures using the same parent coal sample in order to confirm the findings reported by various workers (Russell *et al*. 1999; Davis *et al*. 1995; Khan, 1987; Smith, 1978). This would eliminate the discrepancies raised in this dissertation for Witbank coal. Goodarzi (1984) has shown that as heat treatment temperature increases above 1000°C, the reflectance measurement decreases slightly. It would be very interesting to investigate whether this would be applicable to the Witbank char samples.

Research shows that the second-order Raman spectrum can be used to characterise disorder in carbon materials (Zaida *et al*. 2007); however it has not been used extensively. The main features in the spectrum are at 2730 and 2940cm^{-1}, where the former is the second-order of the disorder-induced band D (Chieu and Dresselhaus, 1982). Additional bands are located at about 2450 and 3250cm^{-1} (Nemanich and Solin, 1979). The second-order Raman spectra are in part due to structural disorder and are expected to be more sensitive to disorder changes. Since the current study focused on the first-order Raman spectroscopy on the range 800-2000cm^{-1}, it would be interesting to extend the study to the second-order Raman spectroscopy to investigate the behaviour of coal and char, and to try to correlate the results with coal petrography and combustion reactivity.

Research shows that the results for pyrolysis of chars generated over 1000°C indicate that the higher the temperatures and heating rates, the lower the reactivity of the chars (Russell *et al*. 1999; Davis *et al*. 1995). This was being attributed to the increased devolatilization rates, enhanced thermal annealing and decreased concentration of active sites. It would be interesting to confirm such findings as well.

REFERENCES

Alonso, M.J.G., Borrego, A.G., Álvarez, D., Parra, J.B., Menéndez, R., 2001a. Influence of pyrolysis temperature on char optical texture and reactivity. Jour. Anal. Appl. Pyrolysis 58-59, pp. 887-909.

Alonso, M.J.G., Borrego, A.G., Álvarez, D., Menéndez, R., 2001b. A reactivity study of chars obtained at different temperatures in relation to their petrographic characteristics. Fuel Proc. Tech. 69, pp. 257-272.

Alonso, M.J.G., Borrego, A.G., Álvarez, D., Menéndez, R., 1999. in: Li, B.Q., Lin, Z.Y., (Eds.), Prospects for coal science in the 21st century, Shanxi Science and Technology press, pp. 535-538.

Alvarez, D., Borrego, A.G., Menendez, R., Bailey, J., 1998. An unexpected trend in the combustion behavior of hvBb coals as shown by the study of their chars. Energy Fuels 12, pp. 849-855.

Alvarez, A.G., Molina-Sabio, M., Rodriguez-Reinoso, F., 1998. An X-ray scattering investigation of carbonization of olive stones. Carbon 36, pp. 67-70.

Ashu, J.T., Nsakala, N.Y., Mahajan, O.P., Walker, P.L., 1978. Enhancement of char reactivity by rapid heating of precursor coal. Fuel 57, pp. 250-251.

Bailey, J.G., 1989. in proceedings, 'Macerals '89' Symposium, CSIRO Division of Coal Technology, North Ryde, NSW, pp. 6.1-6.11.

Bailey, J.G., Tata, A., Diesel, C.F.K., Wall, T.F., 1990. A char morphology system with applications to coal combustion. Fuel 69, pp. 225-239.

Bar-ziv, E., Zaida, A., Salatino, P., Senneca, O., 2000. Diagnostics of carbon gasification by Raman microprobe spectroscopy, In; Proceedings of the Combustion Institutes; 28, pp. 2369-2374.

Basca, W.S., Lannin, J.S., Papas, D.L., Cuomo, J.J., 1993. Raman scattering of laser-deposited amorphous carbon. Phys. Rev. B 47, pp. 10931-10934.

Bend, S.L., Edwards, I.A.S., Marsh, H., 1992. The influence of rank upon char morphology and combustion. Fuel 72, pp. 493-501.

Bend, S.L., Edwards, I.A.S., Marsh, H., 1991. Coal provincialism, coal characterization and char formation. Fuel 70, pp. 1147-1150.

Bend, S.L., Edwards, I.A.S., Marsh, H., 1989. Petrographic characterization of coals to relate to combustion efficiency. In Proceedings of the 1989 International Conference on Coal Science 23–27 October, NEDO, Tokyo, Japan, NEDO, pp. 437-440.

Benfell, K.E., 2001. Assessment of char morphology in high-pressure pyrolysis and combustion. Doctoral Thesis. The University of Newcastle. Australia.

Bengtsson, M., 1987. Combustion behaviour for a coal containing a high proportion of pseudovitrinite, Fuel 15, pp. 201-212.

Bengtsson, M., 1986. Combustion behaviour for a range of coals of various origins and petrographic composition. The Royal Institute of Technology, Stockholm, Sweden, Ph.D Thesis.

Beny-Bassez, C., Rouzaud, J.N., 1985. Characterization of carbonaceous materials by correlated electron and optical microscopy and Raman microspectroscopy. Scanning Electron Microscopy 1, pp. 119-132.

Berkowitz, N., 1985. The chemistry of coal. Amsterdam, New York, Publisher.

Berry, J., 1981. Petrography: the science of coal marketing. Coal mining and processing. February, 1981, pp. 23-35.

Beyssac, O., Coffe´, B., Petitet, J-P., Froigneux, E., Moreau, M., Rouzaud, J.N., 2003. On the characterization of disordered and heterogeneous carbonaceous materials by Raman spectroscopy. Spectrochim Acta A 59, pp. 2267-2276.

Bhatia, S.K., Perlmutter, D.D., 1980. A random pore model for fluid-solid reactions: I. Isothermal, kinetic control. American Institute of Chemical Engineers (AIChE) J. 26, pp. 379-386.

Blake, J.H., Bopp, G.R., Jones, J.F., Miller, M.G., Tambo, W., 1967. Aspects of the reactivity of porous carbons with carbon dioxide. Fuel 46, pp115-125.

Blayden, H.E., Gibson, J., Riley, H.L.,1944. An X-ray study of the structure of coals, cokes and chars. In: Conference on ultrafine structure of coals and cokes, London: British Coal Utilisation Research Association (BCURA).

Borrego, A.G., Alvarez, D., Menéndez, R., 1997. Effects of inertinite content in coal on char structure and combustion. Energy Fuels 11, pp. 702-708.

Boshoff, H.P., Bergh, C.E., Kruszewska, K.J., 1991. Analyses of coal product samples of producing South African collieries. CSIR Bulletin 105. Pretoria, South Africa.

Brocksiepe, H., 1971. Products of wood pyrolysis. In Chemische Technologie, Part III, ed. K. Winacker & Kiiehler, L. Carl Hanser, Munich.

Brown, S.D.M., Jorio, A., Dresselhaus, M.S., Dresselhaus, G., 2001. Observations of the *D*-band feature in the Raman spectra of carbon nanotubes. Phys. Rev. B 64, pp. 73403-1 – 73403-4.

Brown, H.R., Taylor, G.H., and Cook, A.C., 1971. Prediction of coal strength from the rank and petrographic composition of Australian coals. Fuel, 43 (1), pp. 43-54.

Brown, J.K., 1955. J. Chem. Soc. 744. pp. 752.

Buekens, A. G. & Schoeters, J. G., 1987. Valuable products from the phyrolysis of biomass. In Biomass for Energy and Industry. Proc. 4th European Communities Conference, London, pp. 224-232.

Cadle, A.B., Cairncross, B., Christie, A.D.M., Roberts, D.L., 1993. The Karoo basin of South Africa: type basin for the coal-bearing deposits of southern Africa. International Journal of Coal Geology 23, pp. 117-157.

Cannon, C.G., Sutherland, B.B.G., 1955. Nature 156, pp. 240.

Cai, H.Y., Megaritis, A., Mesenböck, R., Dix, M., Dugwell, D.R., Kandiyoti, R., 1998. Pyrolysis of coal maceral concentrates under pf-combustion conditions (I): changes in volatile release and char combustibility as a function of rank. Fuel 77, pp. 1273-1282.

Cairncross, B., 2001. An overview of the Permian (Karoo) coal deposits of southern Africa. African Earth Sciences 33, pp. 529-562.

Cairncross, B., Stanistreet, I.G., McCarthy, T.S., Ellery, W.N., Ellery, K., Grobicki, T.S.A., 1988. Palaeochannels (stone-rolls) in coal seams from fluvial deposits of the Okavango Delta, Botswana, southern Africa. Sediment. Geol. 57, pp. 107-118.

Cairncross, B., Cadle, A.B., 1988. Depositional paleoenvironments of the coal-bearing Permian Vryheid Formation in the east Witbank Coalfield, South Africa. S. Afr. J. Geol. 91 (1), pp. 1-17.

Chandra, D., Bond, R.L., 1956. Proc. The reflectance of carbonised coals. Int. Comm. Coal Petrology, 2, pp. 47-51.

Chieu, T.C., Dresslhause, M.S., 1982. Raman studies of benzene-derived graphite fibers. Phys. Rev. B 26, pp.5867-5877.

Cho, N.H., Veirs, D.K., Ager, J.W., Rubin, M.D., Hopper, C.B., Bogy, D.B., 1992. Effects of substrate temperature on chemical structure of amorphous carbon films. J. Appl. Phys. 71, pp.2243-2248.

Cloke, M. and Lester, E., 1994. Characterization of coals for combustion using petrographic analysis: a review. Fuel 73, pp. 315-320.

Coal-Maceral Analysis, Australian Standards 2856, 1986. Standards Association of Australia, Sydney, NSW.

Crelling, L.C., Hippo, E.J., Woerner, B.A., West, D.P., 1992. Combustion characteristics of selected whole coals and macerals. Fuel 71, pp. 151-158.

Crelling, J.C., Skorupska, N.M., Marsh, H., 1988. Reactivity of coal macerals and lithotypes, Fuel 67, pp. 781-785.

Cuesta, A., Dhamelincourt, P., Laureyns, J., Martinez-Alonso, A., Tascon, J.M.D., 1998. Comparative performance of X-ray diffraction and Raman microprobe techniques for the study of carbon materials. J. Mater Chem Vol. 8, pp. 2875-2879.

Cuesta, A., Dhamelincourt, P., Laureyns, J., Martinez-Alonso, A., Tascon, J.M.D., 1994. Raman microprobe studies on carbon materials. Carbon 32, pp. 1523-1532.

Cumming, J.W., 1984. Reactivity assessment of coals via a weighted mean activation energy. Fuel 63, pp. 1436-1440.

Cumming, J.W., McLaughlin, 1982. Thermogravimetric behaviour of coal. J. Thermochim. Acta. Vol. 57, pp. 253-272.

Davini, P., Ghetti, P., Bonfanti, L., de Michele, G., 1996. Investigation of the combustion of particles of coal. Fuel 75, pp. 1083-1088.

Davis, K.A., Hurt, R.H., Yang, N.Y.C., Headly, T.J., 1995. Evolution of char chemistry, crystallinity, and ultra-fine structure during pulverised coal combustion. Combust. Flame 100, pp. 31-40.

De Vries, H.A.W., Habets, P.J., Bokhoven, C., 1968. Brennstoff-Chemie 49, pp. 105.

Diessel, C.F.K., Wolff-Fischer, E., 1987. Coal Science and Technology II, Preceding of the 1987 International Conference on Coal Science. Amsterdam: Elsevier, pp 901.

Dillon, R.O., Woollam, J.A., Katkanant, V., 1984. Use of Raman scattering to investigate disorder and crystallite formation in as-deposited and annealed carbon films. Phys. Rev. B29, pp. 3482-3489.

Dippel, B., Heintzenberg, J., 1999. Soot characterization in atmospheric particles from different sources by NIR FT Raman spectroscopy. J Aerosol Sci, 30, pp. 907-908.

Dippel, B., Jander, H., Heintzenberg, J., 1999. NIR FT Raman spectroscopic study of flame soot. Phys Chem Chem Phys, 1, pp. 4707-4712.

(DME) Department: Minerals and Energy South Africa Mineral Economics Directorate (Mineral Bureau), 2004. Operating and Developing coal mines in the republic of South Africa 2003. Directory D2/2004.

Doorn, J.V., Vuurman, M.A., Tromp, P.J.J., Stufkens, D.J., Moulijn, J.A., 1990. Correlation between Raman spectroscopy data and the temperature-programmed oxidation reactivity of coals and carbons. Fuel Process Technol, 24, pp. 407-413.

Emmerich, F.G., 1995. Evolution with heat treatment of crystallinity in carbons. Carbon 33, pp. 1709-1715.

Ergun, S., 1968. Chemistry and Physics of carbon, (Ed P.L. Walker, Jr), Marcel Dekker, New York, Vol 3, pp. 211.

Everson, R.C., Neomagus, H.W.J.P., Kaitano, R., Falcon, R., van Alphen, C., du Cann, V.M., 2008. Properties of high ash char particles derived from inertinite-rich coal: 1. Chemical, structural and petrographic characteristics. Fuel 87, pp. 3082-3090.

Falcon, R., van der Riet, M., 2007. Effect of milling and coal quality on combustion, International Pittsburgh Coal Conference, Sandton, South Africa.

Falcon, R.M.S. & Wagner, N.J., 1995. The Use of Coal Petrography in Determining the Different forms of Weathering and their Applications to Handling, Centinnial Geocongress Extended Abstract, Geological Society of South Africa, vol 2, pp. 1013.

Falcon, R.M.S. & Wagner, N.J. (1994). The Use of Coal Petrography in Determining the Different forms of Weathering and their Applications to Handling, 46th Annual Meeting of the International Committee for Coal and Organic Petrology, White Paper Working Group on Environmental Application of Coal Petrology.

Falcon, R.M.S. & Wagner, N.J. (1994). Internal Report, Falcon Research and Consulting Services.

Falcon, R.M.S., Ham, A.J., 1988. The characteristics of South African coals. Journal of South African Institute of Mining and Metallurgy, Vol. 88, pp. 145-161.

Falcon, R.M.S., 1986. A brief review of the origin, formation and distribution of coal in Southern Africa. In: C.R. Anhaeusser and S. Maske (Editors), Mineral deposits of South Africa, II. Geol. Soc. S. Afr., pp. 1879-1899.

Falcon, R.M.S., Snyman, C.P., 1986. An Introduction to Coal Petrography: Atlas of Petrographic Constituents in the Bituminous Coals of Southern Africa. Geol. Soc. S. Afr., pp 1-27.

Farrell, K., Lu, L., Sahajwalla, V., Harris, D., 1998. The atomic scale structure features of some coals and chars. In: 8th Australian Coal Science Conference, Sydney, Australia: The Australian Institute of Energy.

Faure, K., Willis, J.P., Dreyer, J.C., 1996. The Grootegeluk Formation in the Waterberg coalfield, South Africa: facies, palaeoenvironment and thermal history-evidence from organic and clastic matter. International Journal of Coal Geology 29, pp. 147-186.

Ferrari, A.C., Robertson, J., 2000. Interpretation of Raman spectra of disordered and amorphous carbon. Phys Rev B. Vol. 61, pp. 14095-14100.

Feng, B., Bhatia, S.K., Barry, J.C., 2002. Structural ordering of coal char during heat treatment and its impact on reactivity. Carbon 40, pp. 481-496.

Fischbach, D.B., 1971. In Chemistry and Physics of carbon, (Ed. Walker, Jr, P.L.), Marcel Dekker, New York, Vol 7, pp. 1-105.

Francis, W., 1961. Coal, Coal, Its Formation and Composition. In: Edward Arnold Ltd., London, pp. 806.

Friedal, R.A., Carlson, G.L., 1971. Fuel 51, pp. 194.

Fuwape, J. A., 1996. Effects of carbonisation temperature on charcoal from some tropical trees. Bioresource Technology 57, pp. 91-94.

Gavalas, G.R., 1980. A random capillary model with application to char gasification at chemically controlled rates. AIChE J. 26, pp. 577-585.

Ghetti, P., Robertis, U.D., D'Antone, S., Villani, M., Chiellini, E., 1985. Coal combustion: Correlation between surface area and thermogravimetric analysis data. Fuel 64, pp. 950-955.

Ghosh, T.K., 1968. A study on the optical and chemical characters of some coals carbonised in the laboratory. Economic geology, 63, pp. 182-187.

Goodarzi, F., Murchison, D.G., 1972. Optical properties of carbonised vitrinites. Fuel 51, pp. 322-328.

Goodarzi, F., 1984. Optical properties of high-temperature heat-treated vitrinites. Fuel 63, pp. 820-826.

Green, P.D., Johnson, C.A., Thomas, K.M., 1983. Applications of laser Raman microprobe spectroscopy to the characterization of coals and cokes. Fuel 62, pp. 1013-1023.

Gromulski, J. and Sieurin, J., 1983. Paper to International Flame Research Foundation Conference.

Hagelskamp, H.H.B., Snyman, C.P., 1988. On the origin of low-reflecting inertinites in coals from the Highveld coalfield, South Africa. Fuel 67, pp. 307-313.

Hippo, E., Walker, P.L., 1975. Reactivity of heat-treated coals in carbon dioxide at 900°C. Fuel 54, pp. 245-248.

Hippo, E.J., Jenkins, R.G., Walker, P.L., 1979. Enhancement of lignite char reactivity to steam by cation addition. Fuel 58, pp. 338-344.

Hirsh, P.B., 1954. X-Ray Scattering from Coals. Proc Roy Soc, A226, pp. 143.

Hoffman, O. & Fitz, A., 1968. Batch retort pyrolysis of solid municipal wastes. Environ. Sci. Technol., 2(II), pp. 1023-1026.

Hurt, R.H., Dudek, D.R., Longwell, J.P., Sarofim, A.F., 1988. The phenomenon of gasification-induced carbon densification and its influence on pore structure evolution. Carbon 26, pp. 433-449.

Hurt, R.H., Davis, K.A., Yang, N.Y.C, Headly, T.J., Mitchell, G.D., 1995. Residual carbon from pulverised coal fired boilers: 2. Morphology and physicochemical properties. Fuel 74, pp. 1297-1306.

ISO 7404-3 (1994). Methods for the petrographic analysis of bituminous coal and anthracite. Part 3: Method of determining maceral group composition.

ISO 7404-2 (1985). Methods for the petrographic analysis of bituminous coal and anthracite. Part 2: Method of preparing coal samples.

Iwashita, N., Inagaki, M., 1993. Relations between structural parameters obtained by X-ray powder diffraction of various carbon materials. Carbon 31, pp. 1107-1113.

Jawhari, T., Roid, A., Casado, J., 1995. Raman spectroscopic characterization of some commercially available carbon black materials. Carbon 33, pp. 1561-1565.

Jenkins, R.G., Nandi, S.P., Walker, P.L., 1973. Reactivity of heat-treated in air at 500°C. Fuel 52, pp. 288-293.

Johnson, C.A., Patrick, J.W., Thomas, K.M., 1986. Characterization of coal chars by Raman spectroscopy, X-ray diffraction and reflectance measurements. Fuel 65, pp. 1284-1290.

Jones, L.E., Thrower, P.A., 1991. Carbon-carbon composites. Carbon 29, pp. 251

Jones, R.B., McCourt, C.B., Morley, C., King, K., 1985a. Maceral and rank influences on the morphology of coal char, Fuel 64, pp. 1460-1467.

Jones, R.B., McCourt, C.B., Morley, C., King, K., 1985b. Maceral effects on the morphology and combustion of coal char. in Proceedings 1985 International Conference on Coal Science: Sydney, October 28-31, pp. 669-672.

Jones, J.M., Pourkashanian, M., Rena, C.D., Williams, A., 1999. Modelling the relationship of coal structure to char porosity. Fuel 78, pp. 1737-1744.

Kantorovich, I.I., Bar-Ziv, E., 1998. Role of the Pore Structure in the Fragmentation of Highly Porous Char Particles. Combust. Flame 113, pp. 532-541.

Kantorovich, I.I., Bar-Ziv, E., 1997. The effect of microstructural transformation on the evolution of thermal conductivity of highly porous chars during oxidation. Combust. Flame 109, pp. 521-535.

Kantorovich, I.I., Bar-Ziv, E., 1994. Processes in highly porous chars under kinetically controlled conditions: I. Evolution of the porous structure. Combust. Flame 97, pp. 61-78.

Kantorovich, I.I., Bar-Ziv, E., 1994. Processes in highly porous chars under kinetically controlled conditions: II. Pore reactivity. Combust. Flame 97, pp. 79-87.

Katagiri, G., 1996. Raman spectroscopy of graphite and carbon materials and its recent application. Tanso 175, pp. 304-313.

Kawakami, M., Kanba, H., Sato, K., Takenaka, T., Gupta, S., Chandratilleke, R., Sahajwalla, V., 2006. Charactertization of thermal annealing effects on the evolution of coke carbon structure using Raman spectroscopy and X-ray diffraction. Iron and Steel Institute of Japan (ISIJ) International, Vol. 46, pp. 1165-1170.

Kershaw, J.R., Taylor, G.H., 1992. Properties of Gondwana coals with emphasis on the Permian coals of Australia and South Africa. Fuel Processing Technology 31, pp. 127-168.

Khan, M.R., 1987. Significance of char active surface area for appraising the reactivity of low- and high-temperature chars. Fuel 66, pp. 1626-1634.

Koba, K., Ida, S., 1980. Gasification reactivities of metallurgical cokes with carbon dioxide, steam and their mixtures. Fuel 59, pp. 59-63.

Kruszewska, K.J., 2003. Fluorescing macerals in South African coals. International Journal of Coal Geology 54, pp. 79–94.

Laurendeau, N.M., 1978. Heterogeneous kinetics of coal char gasification and combustion. Prog. Energy Combust. Sci. 4, pp. 221-270.

Lee, G.K., Lau, I.T., 1985. Current coal-fired boiler technology in China. Canadian Boiler Society, Annual Technical Meeting, Toronto (Canada).

Lespade, P., Marchand, A., Couzi, M., Cruege, F., 1984. Characterisation de materiaux carbones par microspectrometrie Raman. Carbon 22, pp. 375-385.

Lespade, P., Al-Jishi, R., Dresselhaus, M.S., 1982. Model for Raman scattering from incompletely graphitised carbons. Carbon 20, pp. 427-431.

Lester, E., Cloke, M., 1999. The characterisation of coals and their respective chars formed at 1300°C in a drop tube furnace. Fuel 78, pp. 1645-1658.

Lester, E., Cloke, M., Gibb, W., 1995. Comparison of chars produced in a drop-tube furnace and combustion test facility from coals characterised using image analysis techniques. *In:* 8th International Conference on Coal Science, I. Amsterdam: Elsevier, Coal science and technology 24, September 1995, Oviedo, Spain. pp. 627-630.

Lewis, P.E., Simons, G.A., 1979. Char gasification: Part II. Oxidation results. Combust. Sci. Tech. 20, pp. 117-124.

Li, X., Hayashi, J., Li, C-Z., 2006. FT-Raman spectroscopic study of the evaluation of char structure during the pyrolysis of a Victorian brown coal, Fuel 85, pp. 1700-1707.

Li, F., Lannin, J.S., 1992. Disorder induced Raman scattering of nanocrystalline carbon. Appl. Phys. Lett. 61, pp. 2116-2118.

Lightman, P., Street, P.J., 1968. Microscopical esamination of heat treated pulverised coal panicles. Fuel 47, pp. 7-28.

Lin, Q., Guet, J.M., 1990. Characterisation of coals and macerals by X-ray diffraction. Fuel 69, pp. 821-825.

Linares-Solano, A., Mahajan, O.P., Walker, P.L., 1979. Reactivity of heat-treated coals in steam. Fuel 58, pp. 327-332.

Livneh, T., Bar-ziv, E., Salatino, P., Senneca, O., 2000. Evolution of reactivity of highly porous chars from Raman microscopy. Combust. Sci Technol, 153, pp. 65-82.

Lu, L.M, Sahajwalla, V., Harris, D., 2000. Characteristics of chars prepared from various pulverised coals at different temperatures using drop-tube furnace. Energy & Fuels 14, pp. 869-876.

Lu, L., Sahajwalla, V., Kong, C., Harris, D., 2001. Quantitative X-ray diffraction analysis and its application to various coals. Carbon 39, pp1821-1833.

Marchand, A., 1986. Physico-Chemical and structural characterization of carbons in carbon. Coal gasification-science and Technology 105, (Eds J.L. Figueiredo and J.A. Moulijn), Martinus Nijhoff, pp. 93-136.

Mendez, L.B., Borrego, A.G., Martinez-Tarazona, M.R. Menendez, R., 2003. Influence of petrographic and mineral matter composition of coal particles on their combustion reactivity. Fuel 82, pp. 1875-1882.

Mering, J., Maire, J., 1960. J. Chim. Phys. 57, pp. 803.

Morgan, P.A., Robertson, S.D., Unsworth, J.F., 1986. Combustion studies by thermogravimetric analysis: 1. Coal oxidation. Fuel 65, pp. 1546-1551.

Morgan, M.E., Roberts, P.A., 1987. Coal combustion characterisation studies at the international flame research foundation. Fuel Process. Technol. 15, pp. 173-187.

Murchison, D.G., 1978. Optical properties of carbonised vitrinites, in Karr, C., Jr., ed., Analytical methods for coal and coal products, v. 2: New York, Academic Press, London 2, pp. 415-464.

Nakamizo, M., Kammereck, R., Walker, P.L., 1974. Laser raman studies on carbons. Carbon 12, pp. 259-267.

Nandi, B.N., Brown, T.D., Lee, G.K., 1977. Inert coal macerals in combustion. Fuel 56, pp. 125-130.

Nathan, M.I., Smith, J.E., Tu, K.N., 1974. Raman spectra of glassy carbon. J. Appl. Phys. 45, pp. 2370.

Nemanich, R.J., Solin, S.A., 1979. First and second order Raman scattering from finite size crystals of graphite. Phys. Rev. B 20, pp. 392-401.

Nistor, L.C., Van Landuyt, J., Ralchenko, V.G., Kononenko, T.V., Obraztsova, E.D., Strelnitsky, V.E., 1994. Direct observation of Laser-Induced Crystallization of a-C:H film. Appl. Phys. A 58, pp. 137-144.

O'Brien, G., Jenkins, B., Esterle, J., Beath, H., 2003. Coal characterisation by automated coal petrography. Fuel 82, pp. 1067-1073.

Oka, N., Murayama, T., Matsuoka, H., Yamada, S., Yamada, T., Shinozaki, S., Shibaoka, M., Thomas, C.G., 1987. The influence of rank and maceral composition on ignition and char burnout of pulverised coal, Fuel Process Technol. 15, pp. 213-224.

Patrick, J.W., Shaw, F.W., 1972. Influence of sodium carbonate on coke reactivity. Fuel 51, pp. 69-75.

Petersen, E.E., 1957. Reaction of porous solids. American Institute of Chemical Engineers (AIChE) J. 3, pp. 443-448.

Pinnick, H.T., 1952. J. Chem. Phys. 20, pp. 756

Potgieter-Vermaak, S., Maledi, N., Wagner, N., Van Heerden, J.H.P., Van Grieken, R., Potgieter, J.H., 2010. Raman spectroscopy for the analysis of coal: a review. J. Raman spectrosc. 41.

Pyatenko, A.T., Bukhman, S.V., Lebedinskii, V.S., Nasarov, V.M., and Tolmachev, I. Ya., 1992. Experimental investigation of single coal particle devolatilization by laser heating, Fuel 71, pp. 701-704.

Qui, J.R., Zheng Li, J.R., Zheng, Y., Zheng, C.G., Zhou, H.C., 1999. The influences of mineral behaviour on blended coal ash fusion characteristics. Fuel 78, pp. 963-969.

Quirico, E., Rouzaud, J., Bonal, L., Montagnac, G., 2005. Maturation grade of coals as revealed by Raman spectroscopy: Progress and problems. Spectrochimica Acta Part A 61, pp. 2368-2377.

Radovic, L.R., Karra, M., Skokova, K., Thrower, P.A., 1998. The role of substitutional boron on carbon in carbon oxidation. Carbon 36, pp. 1841-1854.

Radovic, L.R., Walker, P.L., Jr and Jenkins, R.G., 1983a. Effect of lignite pyrolysis conditions on calcium oxide dispersion and subsequent char reactivity. Fuel 62, pp. 209-212.

Radovic, L.R., Walker, P.L., Jr and Jenkins, R.G., 1983b. Importance of carbon active sites in the gasification of coal chars. Fuel 62, pp. 849-856.

Reifenstein, A.P., Kahraman, H., Coin, C.D.A., Calos, N.J., Miller, G., Uwins, P., 1999. Behaviour of selected minerals in an improved ash fusion test: quartz, potassium feldspar, sodium feldspar, kaolinite, illite, calcite, dolomite, siderite, pyrite and apatite. Fuel 78, pp. 1449-1461.

Robertson, J., 1986. "Amorphous carbon". Adv Phys 35, pp. 317-374.

Rosenberg, P., Petersen, H.I., Thomsen, E., 1996a. Combustion char morphology related to combustion temperature and coal petrography, Fuel 75, pp. 1071-1082.

Rosenberg, P., Petersen, H.I., Thomsen, E., 1996b. Combustion char morphology related to combustion temperature and coal petrography, Fuel 9, pp. 739.

Rouzaud J-N, Oberlin, A., Beny-Bassez, C., 1983. Carbon films: structure and microtexture (optical and electron microscopy, Raman spectroscopy). Thin Solid Film 105, pp. 75-96.

Ruland, W., 1968. in Chemistry and Physics of carbon, (Ed P.L. Walker, Jr), Marcel Dekker, New York, Vol 4, pp. 1.

Russell, N.V., Gibbins, J.R., Williamson, J., 1999. Structural ordering in high temperature coal chars and the effect on reactivity. Fuel 78, pp. 803-807.

Sadakata, M., Saito, M., Soutome, T., Murata, H., Ohno, Y., 1989. in extended abstracts, Joint International Conference, Australia/New Zealand and Japanese Sections, The Combustion Institute, Pittsburgh.

Sadezky, A., Muckenhuber, H., Grothe, H., Niessner, R., Po¨schl, U., 2005. Raman microspectroscopy of soot and related carbonaceous materials: spectral analysis and structural information. Carbon 43, pp. 1731-1742.

Salatino, P., Senneca, O., Masi, S., 1999. Assessment of Thermodeactivation during Gasification of a Bituminous Coal Char. Energy Fuels, 13, pp. 1154-1159.

Schapiro, N., and Gray, J., 1964. The use of coal petrography in coke making. J. Inst. Fuel 38, pp. 234.242.

Schoening, F.R.L., 1983. X-ray structure of some South African coals before and after heat treatment at 500 and 1000°C. Fuel 62, pp. 1315-1320.

Schwan, J., Ulrich, S., Batori, V., Ehrhardt, H., Silva, S.R.P., 1996. Raman spectroscopy on amorphous carbon films. J. Appl. Phys. 80, pp. 440-447.

Sekine, Y., Ishikawa, K., Kikuchi, E., Matsukata, M., Akimoto, A., 2006. Reactivity and structural change of coal char during steam gasification, Fuel 85, pp. 122-126.

Sekine, Y., Ishikawa, K., Kikuchi, E., Matsukata, M., 2005. New evaluation method of carbonaceous structure on coal steam gasification. Energy Fuels 19, pp. 326-327.

Senneca, O., Salatino, P., Masi, S., 2005. The influence of char surface oxidation on thermal annealing and loss of combustion reactivity. Proc. Comb. Inst. 30, pp. 2223-2230.

Senneca, O., Salatino, P., Masi, S., 2004. Heat treatment-induced loss of combustion reactivity of a coal char: the effect of exposure to oxygen. Exp. Therm. Fluid Sci 28, pp. 735-741.

Senneca, O., Salatino, P., Masi, S., 1998. Microstructural changes and loss of gasification reactivity of chars upon heat treatment. Fuel 77, pp. 1483-1493.

Sharma, A., Kyotani, T., Tomita, A., 2001. Quantitative evaluation of structural transformations in raw coals on heat treatment using HRTEM technique. Fuel 80, pp. 1467-1473.

Sheng, C., 2007. Char structure characterised by Raman spectroscopy and its correlations with combustion reactivity. Fuel 86, pp. 2316-2324.

Shibaoka, M., Thomas, C.G., Gawronski, E., Young, B.C., 1989. Preceedings of the 1989 International Conference on Coal Science, Tokyo, 2. Amsterdam: Elsevier, pp. 1123.

Shibaoka, M., 1969. Fuel 47, pp. 285-295.

Shibaoka, M., Thomas, C.G., Oka, N., Matsuoka, H., Murayama, T., Tamaru, K., 1985. The Influence of Rank and Macerals Composition of Pulverised coal, Inter. Conf. on Coal Science, Sydney, pp. 665-668.

Shim, H-S., Hurt, R.H., 2000. Thermal annealing of chars from diverse organic precursor under combustion-like conditions. Energ Fuels 14, pp. 340-348.

Shim, H., Hurt, R.H., Yang, N.Y.C., 2000. A methodology for analysis of 002 lattice fringe images and its applications to combustion-derived carbons. Carbon 38, pp. 29-45.

Skoruspka, N.M., Sanyal, A., Hesselman, G.J., Crelling, J.C., Edwards, I.A.S., Marsh, H., 1987. International Conference on Coal Science (Eds Moulijin, J.A., Nater, K.A., Chermin, H.A.G), Elsevier, Amsterdam, pp. 827.

Skoruspka, N.M., 1987. PhD Thesis University of Newcastle upon Tyne.

Smith, K.L., Smoot, L.D., Fletcher, T.H., 1993. in: L.D. Smoot (Ed.), Fundamentals of coal combustion for clean and efficient use, Elsevier, Amsterdam, pp. 131-298.

Smith, D.A.M., Whittaker, F.R.L.G., 1986. The coalfields of Southern Africa: an introduction. In: Anhaeusser, C.R., Maske, S. (Eds.), Mineral Deposits of Southern Africa, vol. II. Geol. Soc. S. Afr., Johannesburg, pp. 1875-1878.

Smith, W.H., Roux, H.J., Steyn, J.G.H., 1983. The classification of coal macerals and their relation to certain chemical and physical parameters of coal. Special publication of Geological Society of South Africa. 7, pp. 111-115.

Smith, S.E., Neavel, R.C., Hippo, E.J and Miller, R.N., 1981. DTGA combustion of coals in the Exxon coal library. Fuel 60, pp. 458-462.

Smith, I.W., 1978. The intrinsic reactivity of carbons to oxygen. Fuel 57, pp. 409-414.

Smith, A.H.V., 1972a. Coal petrography as a guide to carbonization. Paper presented at Chief Scientists' Conference, National Coal board, Yorkshire Region, May, pp. 1-12.

Smith, A.H.V., 1972b. Applications of coal petrology. Paper presented at Chief Scientists' Conference National Coal board, Yorkshire Region, May, pp. 25-40.

Smoog, M.D., 1992. Correlation of coal combustion in a drop tube furnace to a full size boiler. Eskom Report TRR/P92/027.

Snow, C.W., Wallace, D.R., Lyon, L.L., Cracker, G.R., 1960. Proc. 4th Conf. on Carbon, Pergamon Press, New York, pp. 79.

Snyman, C.P., Botha,W.J., 1993. Coal in South Africa. Journal of African Earth Sciences 16, pp. 171–180.

Soladade, L.E.B., Mahajan, O.P., Walker, P.L., 1978. On the high reactivity of American lignite chars. Fuel 57, pp. 56-57.

Solin, S.A., Kobliska, R.J., 1974. Proc. 5th Int. Conf. on amorphous liquid semiconductors, Taylor and Francis, Landon, pp. 1251.

Steyn, J.G.D. and Smith, W.H., 1977. Coal petrography in the evaluation of South African coals. Coal, Gold and Base minerals, 25 (9), pp. 107-117.

Suuberg, E.M., 1990. Fundamental Issues in Control of Carbon Gasification Reactivity, in: J. Lahaye, P. Ehrburger (Eds.), Series E. Applied Sciences, 192, Kluwer Academic Publishers, pp. 269-305.

Tang. L., Gupta, R., Sheng, C., Wall, T., 2005a. The char structure characterisation from the coal reflectogram. Fuel 84, pp. 1268-1276.

Tang, L.G., Gupta, R.P., Sheng, C.D., Wall, T.F., 2005b. The estimation of char reactivity from coal reflectogram. Fuel 84, pp. 127-134.

Taylor, G.H., Mackowsky, M-Th., and ALPERN, B., 1967. The behaviour of inertinite during carbonisation. Fuel 46, pp. 431-440.

Thomas, C.G., Shibaoka, M., Gawronski, E., Gosnell, M.E., Phong-anant, D.D., 1993a. Reactive (fusible) inertinite in pulverised fuel combustion: 2. Determination of reactive (fusible) inertinite, Fuel 72, pp. 913-919.

Thomas, C.G., Gosnell, E., Gawronski, E., Phong-anant, D., Shibaoka, M., 1993b. The behaviour of inertinite macerals under pulverised fuel (pf) combustion conditions. Org Geochem. 20, pp. 779-788.

Thomas, C.G., Shibaoka, M., Gawronski, E., Gosnell, M.E., Phong-anant, D., 1991a. in Preceding of the International Conference on Coal Science, Newcastle upon Tyne, UK, September, pp. 48.

Thomas, C.G., Shibaoka, M., Gawronski, E., Gosnell, M.E., Phong-anant, D., 1991b. in Precedings of the 1991 Conference on Coal Science, Butterworth-Heinemann, Oxford, pp. 424.

Thomas, C.G., Holcombe, D., Shibaoka, M., Young, B.C., Gawronski, E., Brunckhorst, L.F., 1989a. In Preceding of the International Conference on Coal Science, Tokyo, September 1989, pp. 257.

Thomas, C.G., Shibaoka, M., Gawronski, E., Gosnell, M.E., Phong-anant, D., Brunckhorst, L.F., Salehi, M.E., 1989b. In preceedings of the International conference on coal science, Tokyo, September 1989, pp. 213.

Tomita, A., Mahajan, O.P., Walker, P.L., 1977. Reactivity of heat-treated coals in hydrogen. Fuel 56, pp. 137-144.

Tsai, C., Scaroni, A.W., 1987. Reactivity of bituminous coal chars during the initial stage of pulverised-coal combustion. Fuel 66, pp 1400-1406.

Tsu, R., González, J., Hernädez, I., Luengo, C.A., 1977. Solid State Commun. 24, pp. 809.

Tuinstra, F. and Koenig, J.L., 1970. Raman spectrum of graphite. J. Chem Phys. Fuel 53, pp. 1126-1130.

Unsworth, J.F., Barratt, D.J., Roberts, P.T., 1991. Coal quality and combustion performance. Amsterdam: Elseviser.

Van der Riet M., 1995. Coal combustion. In: Proceedings of the 1st coal science and technology indaba, Johannesburg, South Africa. Fossil Fuel Foundation of South Africa.

Van Doorn, J., Vuurman, M.A., Tromp, P.J.J., Stufkens, D.J., Moulijn, J.A., 1990. Corelation between Raman spectroscopic data and the temperature-programmed oxidation reactivity of coals and carbons. Fuel Process Technol 24, pp. 407-413.

Van Niekerk, D., Pugmire, R.J., Solum, M.S., Painter, P.C., Mathews, J.P., 2008. Structural characterization of vitrinite-rich and inertinite-rich Permian-aged South African bituminous coals. International Journal of Coal Geology 76, pp. 290-300.

Vidano, R., Fischbach, D.B. 1978. New lines in the Raman spectra of carbons and graphite. J Am. Ceram. Soc. 61 (1-2), pp. 13-17.

Vidano, R.P, Fischbach, D.B. 1981. Solid State Commun. 39, pp. 341.

Wagner, N.J., 2008. The characterization of weathered discard coals and their behaviour during combustion. Fuel 87, pp. 1687-1697.

Wagner, N.J., 1998. The effect of Weathering on stored discard coals and the impact on combustion. Ph.D Thesis Vol 1&2, University of the Witwatersrand.

Wagner, N.J., Hlatshwayo, B., 2005. The occurrence of potentially hazardous trace elements in five Highveld coals, South Africa. International Journal of Coal Geology 63, pp.228-246.

Wagoner, C.L. and Duzy, A.F., 1976. ASME paper 67-WA/FU-4.

Wagoner, C.L. and Winegartner, E.C., 1973. Further development of the burning profile. J. Eng. Power. Vol. 95, pp. 119-123.

Walker, S., 2000. Major coalfields of the world. IEA Coal Research, London. Pp. 131.

Walker, P.L., Jr and Mahajan, O.P., 1978. Analytical Methods for Coal and Coal Products (Ed. C. Karr), Vol. I, Academic Press, New York, pp. 125 and 163.

Walker, P.L., Jr, Rusinko, F., Jr and Austin, L.G., 1959. Gas Reactions of Carbon. in Advances in Catalysis**,** Vol.11, Academic Press, New York, pp. 138

Weiss, Y., Bar-Ziv, E., 1993. Further development of the electrodynamic chamber for studying single-particle oxidation and nonuniform shrinkage of char particles. Combust. Flame 95, pp. 362-373.

White, A., Davies, M.R., Jones, S.D., 1989. Reactivity and characterization of coal maceral concentrates. Fuel 68, pp. 511-519.

Yamauchi, S., Kurimoto, Y., 2003. Raman spectroscopic study on pyrolyzed wood and bark of Japanese cedar: temperature dependence of Raman parameters. J. Wood Sci. 49, pp. 235-240.

Yoshida, A., Kaburagi, Y., Hishiyama, Y., 2006. Full width at half maximum intensity of the G band in the first order Raman spectrum of carbon material as a parameter for graphitization. Carbon 44, pp. 2333-2334.

Zaida, A., Bar-Ziv, E., Radovic, L.R., Lee, Y-J., 2007. Further development of Raman Microprobe spectroscopy for characterization of char reactivity. Proceedings of the combustion institute; 31, pp. 1881-1887.

Zaida, V., Bar-Ziv, E., Radovic, L.R., Lee, Y-J., 2006. Further development of Raman microprobe spectroscopy for characterization of char reactivity, In: proceedings of the combustion institute; 31, pp. 1873-1880.

Zerda, T.W., Xu, W., Zerda, A., Zhao, Y., Von Dreele, R.B., 2000. High pressure Raman and neutron scattering study on structure of carbon black particles. Carbon 38, pp. 355-361.

Zhang, X., Dukhan, D., Kantorovich, I.I., Bar-Ziv, E., 1998. The Thermal Conductivity and Porous Structure of Char Particles. Combust. Flame 113, pp. 519-531.

Zimmerman, R.E., 1979. Evaluating and testing the Coking Properties of Coal. Miller Freeman Publications, Inc., San Francisco, pp. 365.

APPENDICES

APPENDIX A: Proximate analysis

Proximate analyses were conducted using thermogravimetric analysis (TGA) in order to obtain the percentage coal properties such as moisture, volatile matter, fixed carbon and ash. TGA results are presented in Figure A.1 below showing different regions on the sketch, whereby first region represents moisture loss, followed by volatile matter in the second region. The third region represents the fixed carbon, and what remains after complete combustion is ash in the fourth region. The percentage coal properties were determined by calculating the change in weight percent (Δ weight %) on each region as shown in Figure A.1 below. The results obtained from proximate analysis in coal and chars are presented in Table A.1 and A.2.

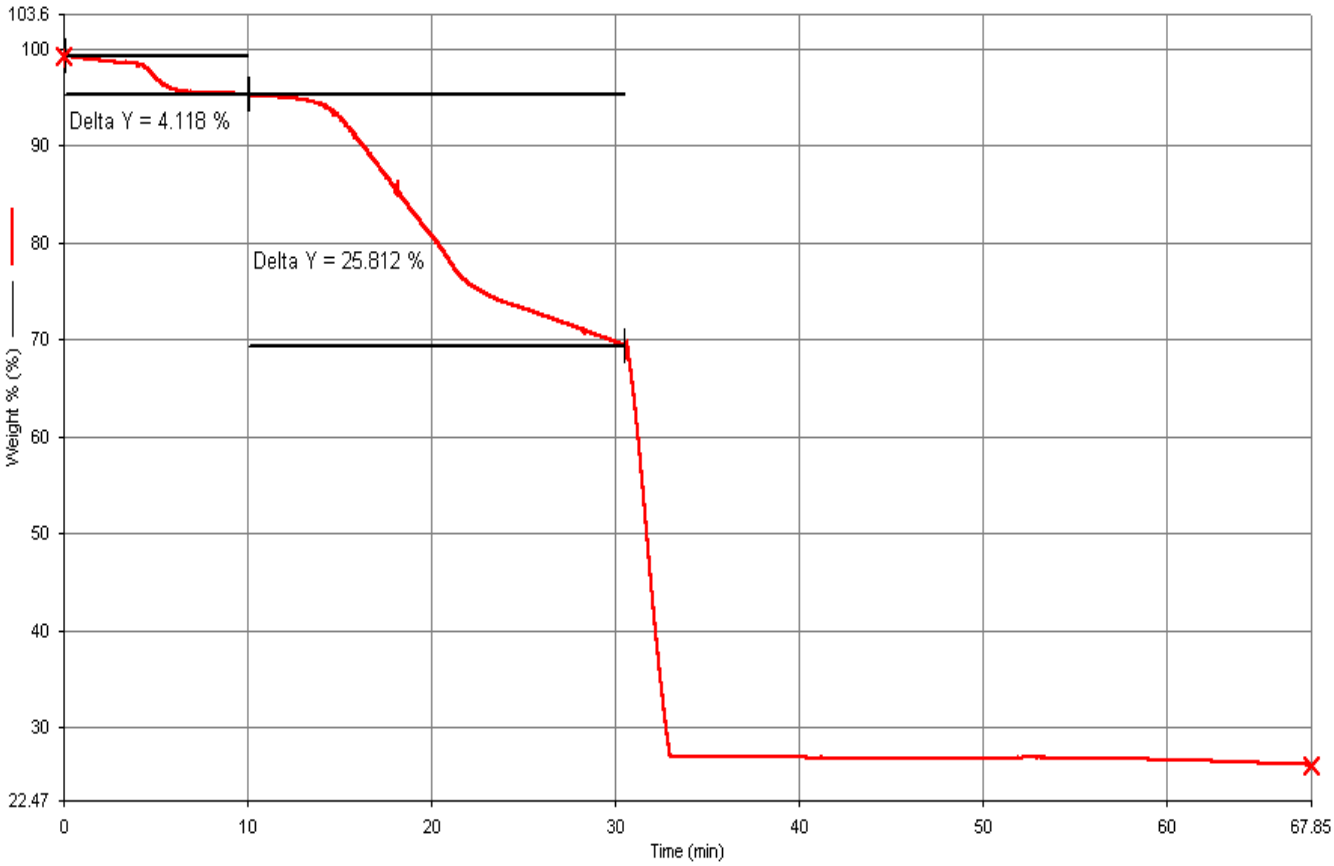

Figure A.1: Proximate analysis result showing Weight loss in percentage against time.

Table A.1: Proximate analyses PBBR chars

Sample	Moisture [%]	Volatile matter [%]	Ash [%]	Fixed carbon [%]
Parent coal	4.105	27.029	26.34	42.5
Char 300℃	2.388	27.026	27.725	42.9
Char 600℃	1.017	20.457	34.02	44.5
Char 800℃	3.48	13.485	33.951	49.1
Char 1000℃	3.209	12.254	34.091	50.4

Table A.2: Proximate analyses DTF chars

Sample no:	Moisture	Volatile matter	Ash	Fixed carbon
1	0.941	10.261	23.638	65.6
2	0.443	13.621	36.378	49.6
3	0.224	11.966	38.771	49.0
4	0.492	11.493	40.497	47.5

APPENDIX B: Petrography results

B.1 Rank (reflectance) and count

Table B.1: The table of Mean Vitrinite Reflectance (MVR / %), Mean Total reflectance (MTR /%) and total chars count.

Sample name	Reflectance [%]		Porous char [%]	Dense char [%]
	MVR	MTR		
Parent coal	0.59	1.09	0	0
Char 300°C	0.62	1.12	0	0
Char 600°C	1.60	2.69	4.0	56.0
Char 800°C	4.06	4.75	6.4	67.4
Char 1000°C	5.38	6.05	8.6	80.8

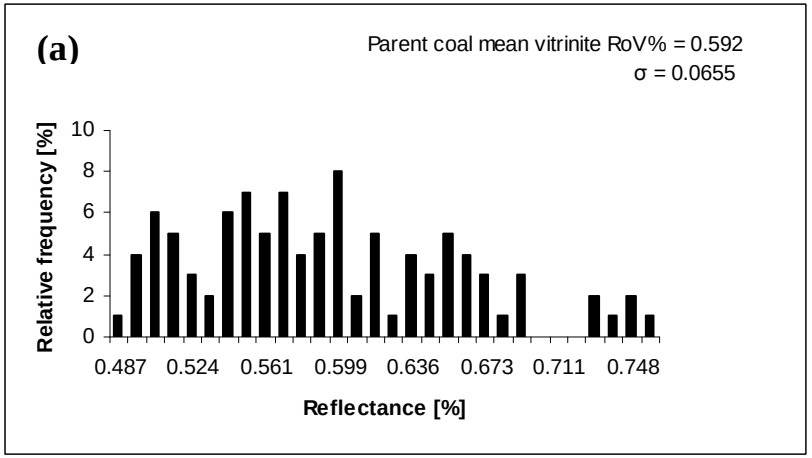
(a)
Parent coal mean vitrinite RoV% = 0.592
σ = 0.0655
Relative frequency [%]
0
2
4
6
8
10
0.487 0.524 0.561 0.599 0.636 0.673 0.711 0.748
Reflectance [%]

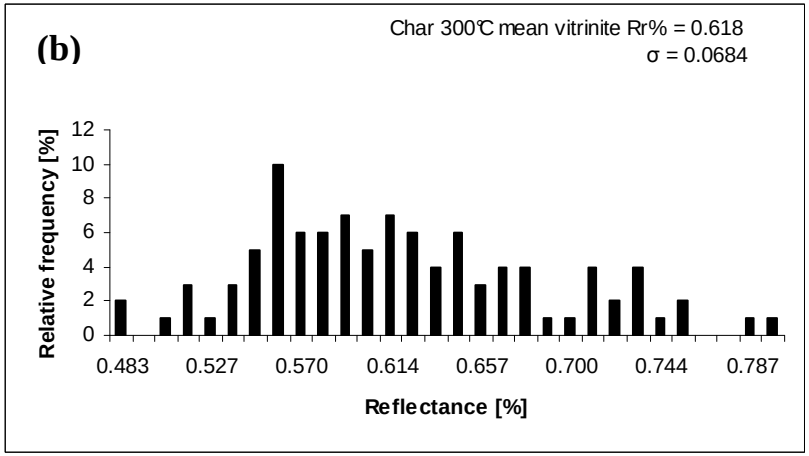
(b)
Char 300℃ mean vitrinite Rr% = 0.618
σ = 0.0684
Relative frequency [%]
0
2
4
6
8
10
12
0.483 0.527 0.570 0.614 0.657 0.700 0.744 0.787
Reflectance [%]

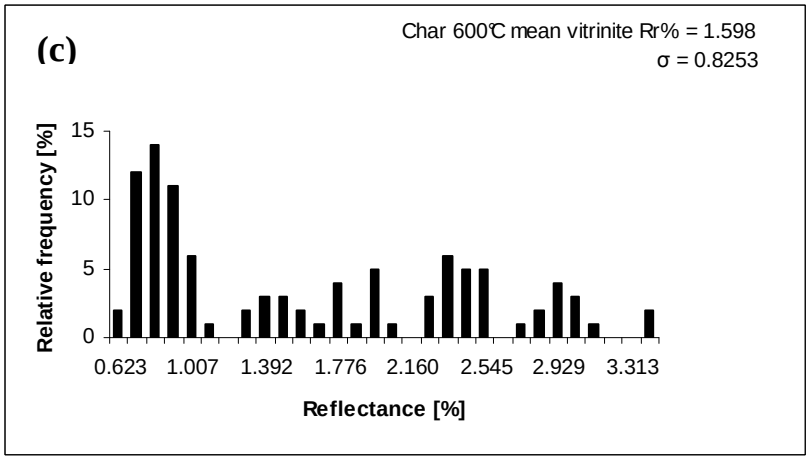
(c)
Char 600℃ mean vitrinite Rr% = 1.598
σ = 0.8253
Relative frequency [%]
0
5
10
15
0.623 1.007 1.392 1.776 2.160 2.545 2.929 3.313
Reflectance [%]

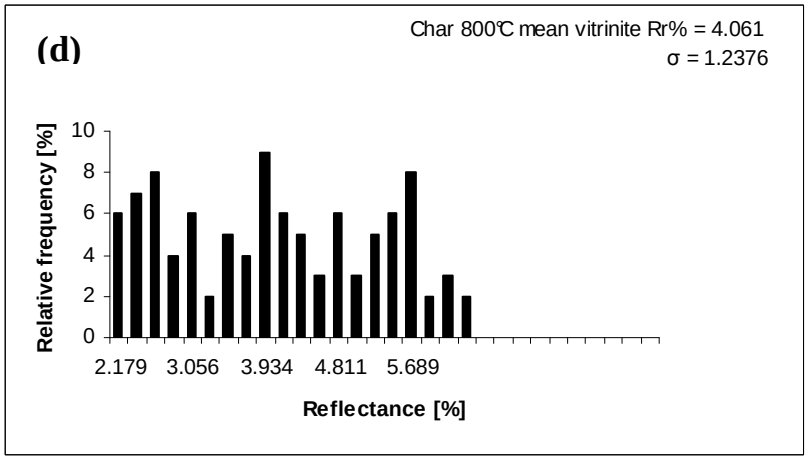
(d)
Char 800℃ mean vitrinite Rr% = 4.061
σ = 1.2376
Relative frequency [%]
0
2
4
6
8
10
2.179 3.056 3.934 4.811 5.689
Reflectance [%]

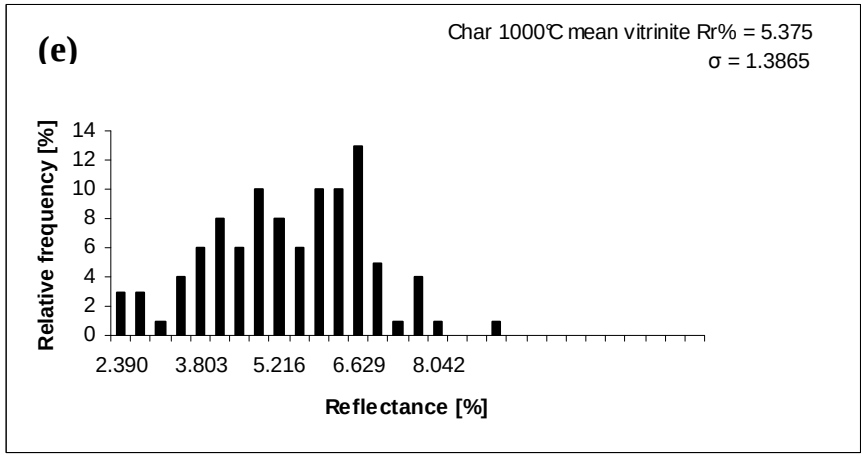

Figure B.1: Reflectance measurements on vitrinite particles on parent coal (MVR) (a) and the resultant chars derived from vitrinite particle at different temperatures (300-1000°C) (b)-(e).

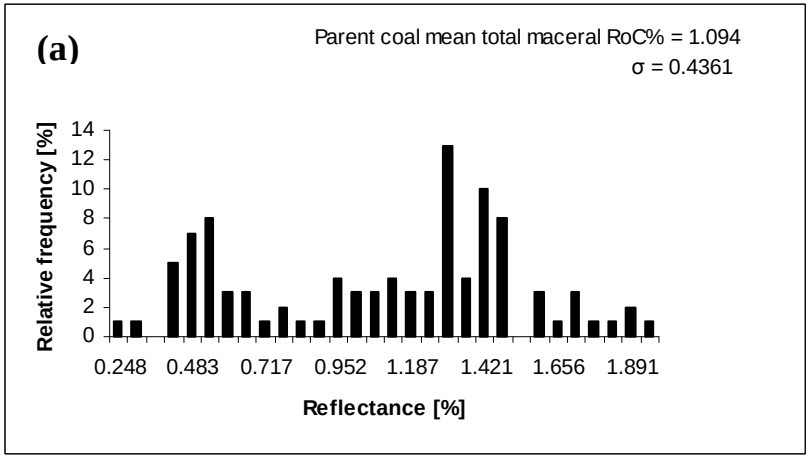
(a)
Parent coal mean total maceral RoC% = 1.094
σ = 0.4361
Relative frequency [%]
0
2
4
6
8
10
12
14
0.248
0.483
0.717
0.952
1.187
1.421
1.656
1.891
Reflectance [%]

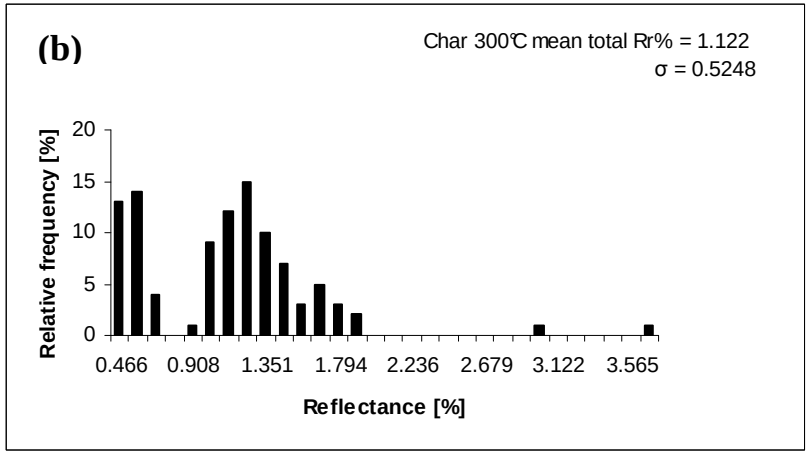
(b)
Char 300℃ mean total Rr% = 1.122
σ = 0.5248
Relative frequency [%]
0
5
10
15
20
0.466
0.908
1.351
1.794
2.236
2.679
3.122
3.565
Reflectance [%]

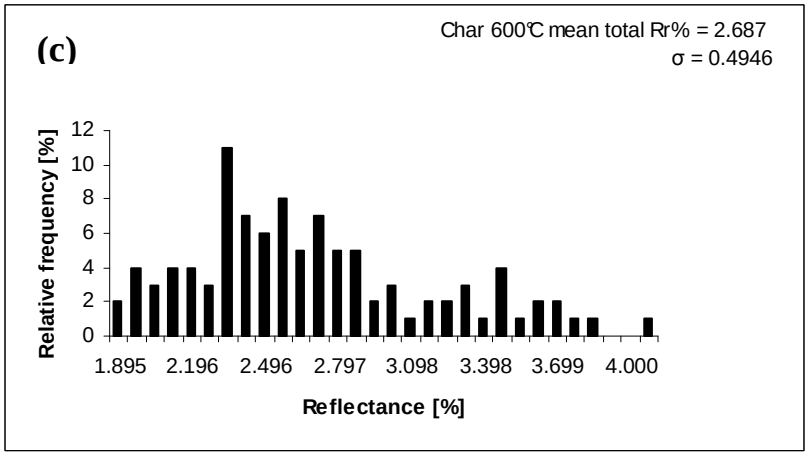
(c)
Char 600℃ mean total Rr% = 2.687
σ = 0.4946
Relative frequency [%]
0
2
4
6
8
10
12
1.895
2.196
2.496
2.797
3.098
3.398
3.699
4.000
Reflectance [%]

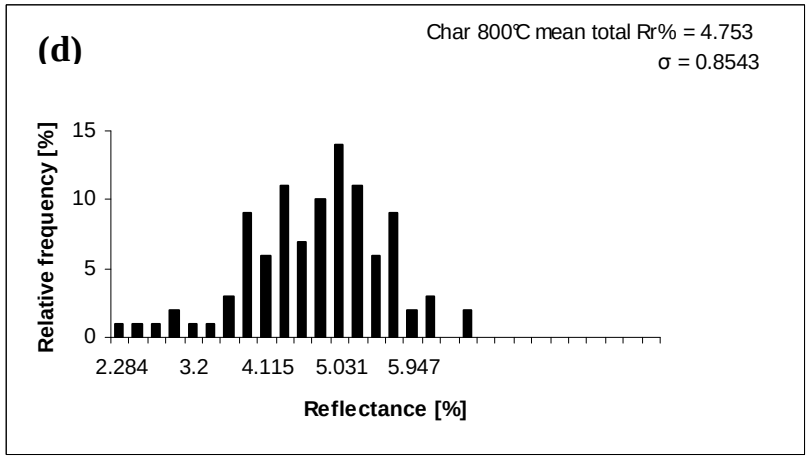
(d)
Char 800℃ mean total Rr% = 4.753
σ = 0.8543
Relative frequency [%]
0
5
10
15
2.284
3.2
4.115
5.031
5.947
Reflectance [%]

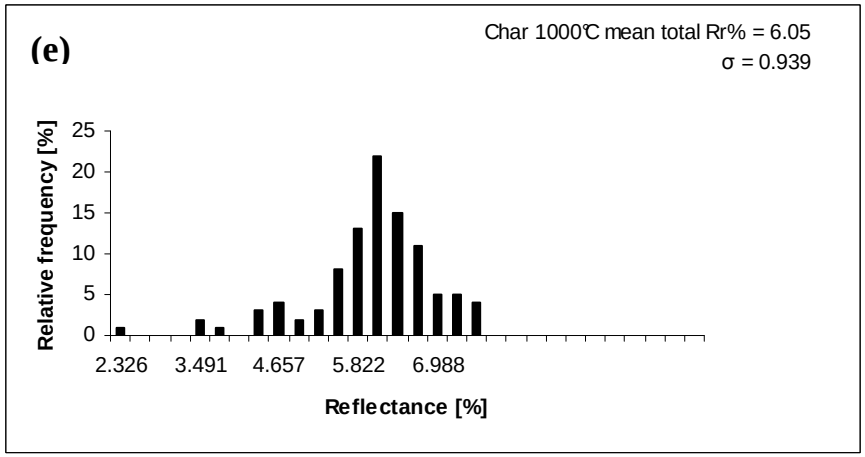

Figure B.2: Reflectance measurements of total coal macerals on parent coal (MTR) (a) and the resultant chars at different temperatures (300-1000°C) (b)-(e).

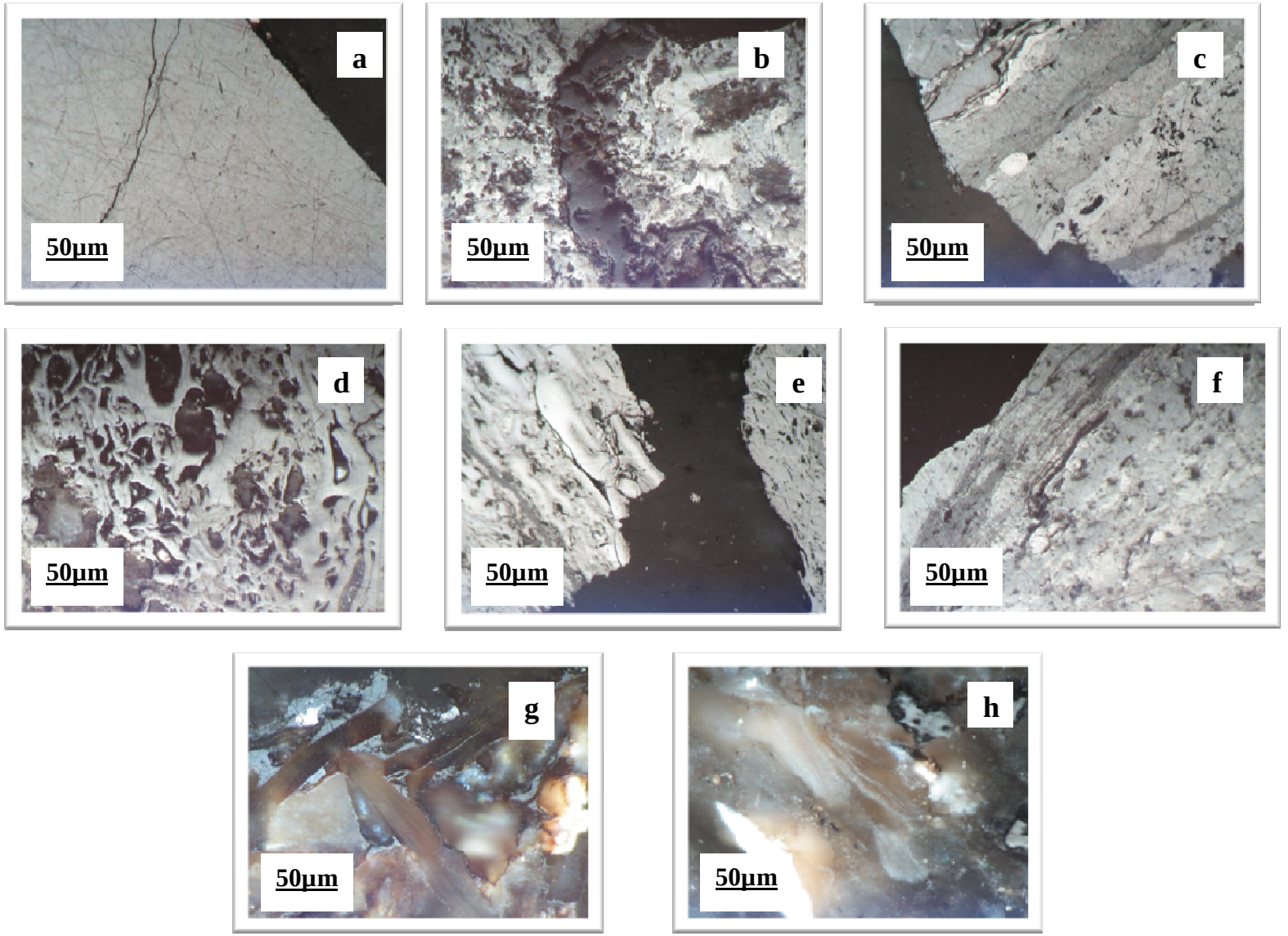

Figure B.3: Examples of different particles found in parent coal (oil immersion lense, X500, reflected light) with a scale of 50 µm as described in Table 4.2: **(a)**, vitrinite particle with a crack on it; **(b)**, liptinite particle which is dark grayish; **(c)**, semifusinite particle which is banded; **(d)** and **(e)**, are fusinite particles showing some wholes and high reflectance; **(f)**, inertodetrinite with minor vitrinite towards left; **(g)** and **(h)**, are examples of some minerals found in parent coal.

APPENDIX C: Raman spectroscopic data

C.1: Calculations of root mean square (RMS), mean/average and standard deviation.

These were obtained by curve fitting each spectrum using the OPUS software program following the procedures outlined on Sadezky *et al.* (2005), Dippel *et al*. (1999), Jawhari *et al*. (1995), Cuesta *et al*. (1994), and Nistor *et al*. (1994). Raman bands were added to each individual spectrum depending on the number of bands available. For example, in coal spectrum (Jawhari *et al*., 1995; Cuesta *et al*., 1994), three bands were added, while four bands were added to char spectrum (Dippel *et al*., 1999) (Figure C.1). The mixture of Lorentzian and Gaussian functions was employed on the curve fitted spectra. The OPUS program contains an auto-fit which is used to calculate the RMS for each spectrum. Mean and standard deviation were calculated by the summation of all the information (band positions, bandwidth/FWHM, Intensity ratios and integral) obtained from each spectrum on each sample. The results are presented below in Table C.1-C.4 below.

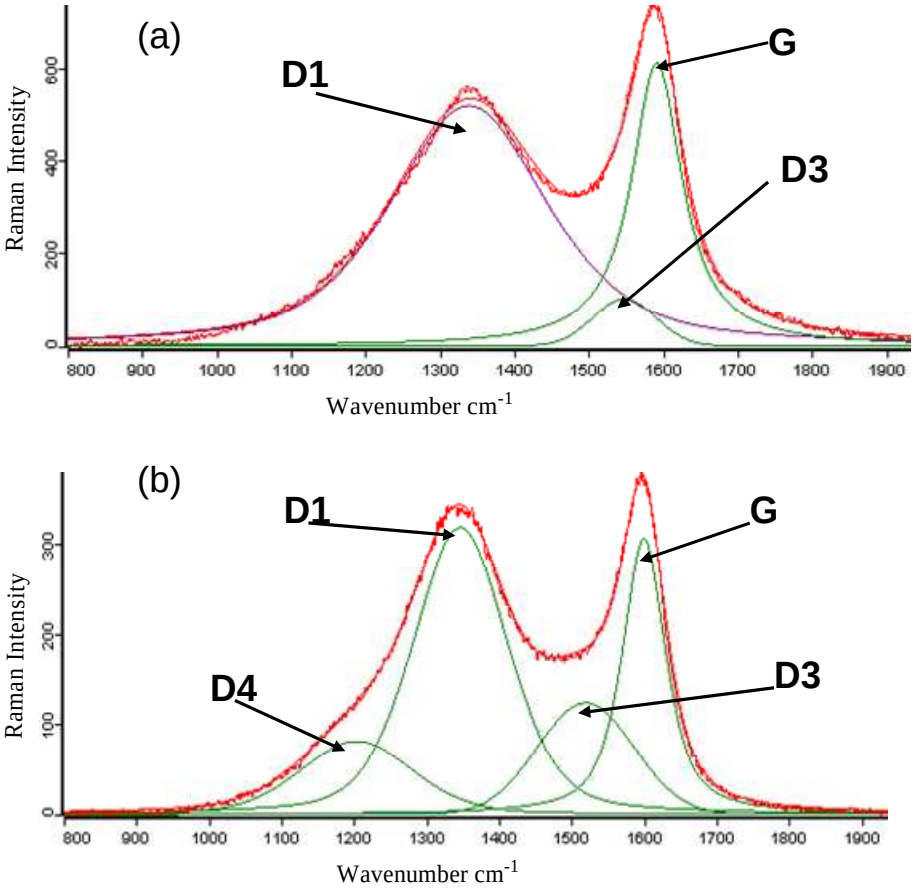

Figure C.1: First order region Raman spectra of coal (a) and char 1000°C (b).

Table C.1: Summarised results from micro Raman Spectroscopy (MRS) (PBBR chars), vitrin = Vitrinite, inert = Inertinite.

Sample and Raman bands	Band position (cm^{-1})								Intensity ratios		Full width at Half maximum (cm^{-1})	
	Lowest-highest		Lowest-Highest		Average/ mean		Standard deviations					
									I_D/I_G	I_D/I_G		
Parent coal	Vitrin	vitrin	inert	inert	Vitrin	Inert	vitrin	inert	vitrin	inert	vitrin	inert
D1	1353	1364	1338	1354	1359	1346	3.0	3.9	0.96	0.90	292	268
D3	1550	1568	1545	1568	1560	1557	4.0	6.8	0.36	0.25	91	92
G	1591	1597	1593	1596	1595	1594	1.6	0.8			92	81
Char 300°C	Vitrin	vitrin	inert	inert	Vitrin	Inert	vitrin	inert	vitrin	inert	vitrin	inert
D1	1354	1367	1337	1356	1359	1343	2.8	3.1	0.98	0.88	295	257
D3	1554	1565	1536	1567	1561	1554	3.0	7.8	0.37	0.22	92	93
G	1592	1598	1590	1597	1595	1593	1.4	1.5			91	81
Char 600°C	Porous	porous	dense	dense	porous	dense	porous	dense	porous	dense	porous	dense
D4	1217	1266	1185	1268	1235	1225	16.8	17.4	0.27	0.23	210	210
D1	1350	1362	1334	1370	1355	1354	4.5	8.4	0.63	0.73	166	179
D3	1490	1525	1470	1544	1505	1508	11.4	17.9	0.17	0.18	149	136
G	1588	1593	1587	1597	1590	1591	1.8	2.6			81	84
Char 800°C	Porous	porous	dense	dense	porous	dense	porous	dense	porous	dense	porous	dense
D4	1188	1256	1186	1253	1206	1207	23.2	19.6	0.23	0.25	165	166
D1	1338	1355	1337	1364	1343	1344	5.1	5.2	0.84	0.86	163	159
D3	1492	1518	1465	1535	1510	1510	8.6	15.0	0.28	0.30	151	157
G	1588	1602	1587	1600	1596	1596	3.9	3.5			72	71
Char 1000°C	Porous	porous	dense	dense	porous	dense	porous	dense	porous	dense	porous	dense
D4	1184	1223	1186	1218	1200	1201	10.0	7.1	0.24	0.24	180	185
D1	1338	1354	1343	1365	1349	1349	3.2	3.0	1.15	1.10	158	156
D3	1514	1542	1511	1545	1529	1527	6.9	6.0	0.42	0.42	156	157
G	1597	1603	1599	1608	1602	1602	1.6	1.6			70	70

Table C.2: Summarised results from micro Raman Spectroscopy (MRS) in PBBR chars.

Sample and Raman bands	Band position (cm^{-1})				Intensity ratios	Full width at Half maximum (cm^{-1})	Integral	RMS error	Stdev RMS error
	Lowest-highest		Average/ mean	Standard deviations					
					I_D/I_G				
Parent coal									
D1	1345	1359	1352 ± 3	5.3	0.956 ± 0.04	281 ± 8	160703	8.63	1.8
D3	1555	1566	1559 ± 2	3.9	0.324 ± 0.06	91 ± 1	13606		
G	1593	1595	1594 ± 1	0.8		87 ± 2	64503		
Char 300°C									
D1	1342	1359	1348 ± 3	7.6	0.913 ± 0.05	270 ± 6	181943	10.58	2.5
D3	1554	1561	1556 ± 2	3.2	0.268 ± 0.03	93 ± 4	14005		
G	1593	1595	1594 ± 1	0.9		84 ± 3	75066		
Char 600°C									
D4	1199	1281	1238 ± 8	5.3	0.234 ± 0.03	189 ± 21	56265	11.07	0.1
D1	1335	1364	1351 ± 3	3.5	0.802 ± 0.12	176 ± 4	184467		
D3	1505	1478	1529 ± 22	27.8	0.215 ± 0.06	135 ± 7	21255		
G	1587	1594	1591 ± 1	1.6		82 ± 2	111452		
Char 800°C									
D4	1206	1208	1207 ± 7	0.5	0.239 ± 0	165 ± 12	34497	7.31	0.01
D1	1343	1344	1343 ± 2	0.3	0.848 ± 0.09	161 ± 4	126014		
D3	1510	1510	1510 ± 7	0.2	0.288 ± 0.04	154 ± 11	31979		
G	1596	1596	1596 ± 1	0.1		72 ± 5	80514		
Char 1000°C									
D4	1200	1202	1200 ± 4	0.6	0.240 ± 0	183 ± 14	15737	3.01	0.05
D1	1348	1350	1349 ± 3	0.1	1.123 ± 0.01	157 ± 3	66631		
D3	1527	1531	1528 ± 1	0.9	0.421 ± 0	157 ± 1	21247		
G	1601	1602	1602 ± 0	0.2		70 ± 1	29935		

Table C.3: Summarised results from micro Raman Spectroscopy (MRS) (DTF chars), vitrin = Vitrinite, inert = Inertinite.

Sample and Raman bands	**Band position (cm^{-1})**								**Intensity ratios**		**Full width at Half maximum (cm^{-1})**	
	Lowest-highest		**Lowest-Highest**		**Average/ mean**		**Standard deviations**					
Sample 1									**I_D/I_G**	**I_D/I_G**		
Char 1400°C	porous	porous	dense	dense	porous	dense	porous	dense	porous	dense	porous	dense
D4	1182	1259	1172	1332	1208	1223	15.8	20.8	0.17	0.19	219	225
D1	1348	1359	1351	1357	1355	1354	2.81	1.73	1.16	1.25	165	146
D3	1501	1540	1524	1552	1531	1535	6.21	6.39	0.38	0.39	154	153
G	1596	1605	1602	1605	1603	1604	1.60	0.71			77	73
Sample 2												
Char 1400°C	porous	porous	dense	dense	porous	dense	porous	dense	porous	dense	porous	dense
D4	1185	1334	1195	1333	1217	1243	22.4	31.0	0.19	0.22	229	250
D1	1347	1359	1350	1357	1355	1353	2.1	1.4	1.21	1.20	163	141
D3	1520	1558	1526	1556	1536	1538	6.9	7.5	0.44	0.40	154	152
G	1596	1605	1602	1605	1603	1604	1.4	0.9			75	71
Sample 3												
Char 1400°C	porous	porous	dense	dense	porous	dense	porous	dense	porous	dense	porous	dense
D4	1175	1273	1183	1331	1209	1225	15.7	28.7	0.21	0.22	222	234
D1	1351	1359	1348	1358	1356	1354	1.9	1.7	1.25	1.24	163	144
D3	1522	1555	1527	1554	1538	1538	6.8	6.5	0.47	0.44	163	161
G	1599	1605	1602	1605	1604	1604	1.1	0.7			75	71
Sample 4												
Char 1400°C	porous	porous	dense	dense	porous	dense	porous	dense	porous	dense	porous	dense
D4	1172	1243	1193	1297	1201	1221	15.5	22.4	0.17	0.22	210	231
D1	1351	1361	1351	1362	1356	1356	2.2	2.4	1.30	1.25	172	150
D3	1525	1561	1527	1556	1541	1540	9.6	5.2	0.48	0.47	159	162
G	1601	1605	1603	1606	1603	1604	1.3	0.8			75	72

Table C.4: Summarised results from micro Raman Spectroscopy (MRS) in DTF chars.

Sample and Raman bands	Band position (cm^{-1})				Intensity ratios	Full width at Half maximum (cm^{-1})	Integral	RMS error	Stdev RMS error
	Lowest-highest		Average/ mean	Standard deviations					
Sample 1					I_D/I_G				
Char 1400°C									
D4	1206	1239	1216 ± 3	7.3	0.178 ± 0	222 ± 9	6590	2.17	0.1
D1	1353	1356	1355 ± 9	0.8	1.204 ± 0	156 ± 1	37046		
D3	1527	1539	1533 ± 2	1.8	0.384 ± 0.01	153 ± 3	8679		
G	1602	1605	1603 ± 0	0.3		75 ± 4	14170		
Sample 2									
Char 1400°C									
D4	1211	1273	1230 ± 1	13.0	0.209 ± 0	240 ± 7	9817	2.27	0.1
D1	1352	1356	1354 ± 5	0.9	1.208 ± 0	152 ± 2	41988		
D3	1535	1539	1537 ± 7	1.0	0.420 ± 0	153 ± 1	10904		
G	1602	1604	1603 ± 1	0.3		73 ± 1	15943		
Sample 3									
Char 1400°C									
D4	1205	1234	1217 ± 4	8.0	0.212 ± 0.02	228 ± 10	8490	2.17	0.02
D1	1353	1356	1355 ± 6	0.9	1.246 ± 0	154 ± 1	39155		
D3	1537	1539	1538 ± 3	0.01	0.457 ± 0	162 ± 3	11259		
G	1603	1604	1604 ± 0	0.01		73 ± 1	14199		
Sample 4									
Char 1400°C									
D4	1201	1222	1211 ± 3	9.9	0.196 ± 0	221 ± 5	6303	2.08	0.07
D1	1355	1357	1356 ± 7	0.2	1.279 ± 0	161 ± 3	35111		
D3	1539	1542	1540 ± 2	0.3	0.478 ± 0	161 ± 1	9529		
G	1603	1605	1604 ± 0	0.5		74 ± 2	11706		

C.2 Curve fitting of spectra obtained from particles charred at 600°C.

Sample charred at 600°C was found to have significant amount of macerals being mixed with chars. Two types of curve fitting were applied on different spectra obtained from different particles. Maceral spectra at 600°C were fitted following the procedure applied on parent coal spectra. This includes the bands D1 at 1350cm^{-1}, D3 at 1530cm^{-1} and G at 1592cm^{-1}. The overall D1 bandwidth was obtained to be 272cm^{-1}. The char spectra were fitted with four bands; which include D1 band at 1350cm^{-1}, D3 at 1530cm^{-1}, D4 at 1200cm^{-1} and G at 1592cm^{-1}. The overall D1 bandwidth was obtained to be 176cm^{-1}. The overall D1 bandwidth of particles at 600°C was obtained to be 222cm^{-1}.

APPENDIX D: Reactivity

Table D.1: Reactivity at 20% and 50% conversion on PBBR chars.

Sample name	**T (20%) [°C]**	**T (50%) [°C]**	**Reactivity ($1/T_{20\%}$) [1/°C]**	**Reactivity ($1/T_{50\%}$) [1/°C]**
Parent coal	399.75	464.38	0.002502	0.002153
Char 300°C	399.69	468.08	0.002502	0.002136
Char 600°C	420.27	483.48	0.002379	0.002068
Char 800°C	439.52	509.76	0.002275	0.001962
Char 1000°C	471.68	539.52	0.002120	0.001853

Table D.2: Reactivity at 20% and 50% conversion on DTF chars.

Sample name	**T (20%) [°C]**	**T (50%) [°C]**	**Reactivity ($1/T_{20\%}$) [1/°C]**	**Reactivity ($1/T_{50\%}$) [1/°C]**
1	-	-	-	-
2	518.41	582.88	0.001929	0.001716
3	522.52	552.61	0.001914	0.001810
4	501.65	565.85	0.001993	0.001767

The reactivity on Sample 1 could not be calculated due to the sharpness on the point of the decomposition as indicated in Figure 4.21, which could be attributed to the experimental errors of the TGA equipment.

APPENDIX E: Correlation tables

E.1: Correlation between Raman spectroscopy and coal petrography through reflectance and bandwidth measurements.

Table E.1: Mean Vitrinite Reflectance (MVR) and D1 bandwidth measured from Raman spectroscopy.

Sample name	**MVR [%]**	**D1 bandwidth [cm^{-1}]**
Parent coal	0.592	292
Char 300°C	0.618	295
Char 600°C	1.598	222
Char 800°C	4.061	163
Char 1000°C	5.375	157

Table E.2: Mean Total Reflectance (MTR) and D1 bandwidth measured from Raman spectroscopy.

Sample name	**MTR [%]**	**D1 bandwidth [cm^{-1}]**
Parent coal	1.094	281
Char 300°C	1.122	270
Char 600°C	2.687	222
Char 800°C	4.753	161
Char 1000°C	6.05	157

Table E.3: MVR and G bandwidth measured from Raman spectroscopy.

Sample name	**MVR [%]**	**G bandwidth [cm^{-1}]**
Parent coal	0.592	92
Char 300°C	0.618	91
Char 600°C	1.598	82
Char 800°C	4.061	72
Char 1000°C	5.375	70

Table E.4: MTR and D1 bandwidth measured from Raman spectroscopy.

Sample name	MTR [%]	G bandwidth [cm^{-1}]
Parent coal	1.094	87
Char 300°C	1.122	84
Char 600°C	2.687	82
Char 800°C	4.753	72
Char 1000°C	6.05	70

E.2: Correlation between Raman spectroscopy and coal petrography through counts and bandwidth.

Table E.5: Petrographic counts and Raman D1 bandwidth.

Sample name	Porous [%]	Dense [%]	D1 bandwidth [cm^{-1}]
Parent coal	0	0	281.0935
Char 300°C	0	0	269.5724
Char 600°C	4.0	56.0	175.8526
Char 800°C	6.4	67.4	161.3135
Char 1000°C	8.6	80.8	157.3208

Table E.6: Petrographic counts and Raman G bandwidth.

Sample name	Porous [%]	Dense [%]	G bandwidth [cm^{-1}]
Parent coal	0	0	86.90844
Char 300°C	0	0	84.2558
Char 600°C	4.0	56.0	82.11838
Char 800°C	6.4	67.4	71.63294
Char 1000°C	8.6	80.8	70.08748

E.3: Correlation between reactivity (measure by TGA) and reflectance measurements of coal and chars.

Table E.7: Reactivity and reflectance measurements (MVR and MTR).

Sample name	**Reflectance [%]**		**$1/T_{20\%}$ [1/°C]**	**$1/T_{50\%}$ [1/°C]**
	MVR	**MTR**		
Parent coal	0.592	1.094	0.002502	0.002153
Char 300°C	0.618	1.122	0.002502	0.002136
Char 600°C	1.598	2.687	0.002379	0.002068
Char 800°C	4.061	4.753	0.002275	0.001962
Char 1000°C	5.375	6.05	0.002120	0.001853

E.4: Correlation between reactivity (measure by TGA) and Raman bandwidth (D1 and G bandwidth).

Table E.8: Reactivity and Raman D1 bandwidth.

Sample name	**$1/T_{20\%}$ [1/°C]**	**$1/T_{50\%}$ [1/°C]**	**D1 bandwidth [cm^{-1}]**
Parent coal	0.002502	0.002153	281.0935
Char 300°C	0.002502	0.002136	269.5724
Char 600°C	0.002379	0.002068	222.1446
Char 800°C	0.002275	0.001962	161.3135
Char 1000°C	0.002120	0.001853	157.3208

Table E.9: Reactivity and Raman G bandwidth.

Sample name	**$1/T_{20\%}$ [1/°C]**	**$1/T_{50\%}$ [1/°C]**	**G bandwidth [cm^{-1}]**
Parent coal	0.002502	0.002153	86.90844
Char 300°C	0.002502	0.002136	84.2558
Char 600°C	0.002379	0.002068	82.11838
Char 800°C	0.002275	0.001962	71.63294
Char 1000°C	0.002120	0.001853	70.08748